



**Cooperative Institute for Marine and Atmospheric Studies**  
Rosenstiel School of Marine and Atmospheric Science  
University of Miami  
4600 Rickenbacker Causeway, Miami, FL 33149

January 30, 2013

Philip L. Hoffman  
Cooperative Institutes Program Director  
NOAA Office of Ocean and Atmospheric Research  
1315 East West Highway #11342 R/LCI  
Silver Spring, Maryland 20910

Ref: Project Progress Report for Reporting Period: January 1, 2012 – December 31, 2012  
NA08OAR4320889 – “Shadow Award” – (7/1/08—6/30/13)

There are nine research projects (with seven different principal investigators) included in this progress report. All were funded through more than one amendment to the single Shadow Award. Subaccounts were created and work was initiated only when the funds were actually received by CIMAS. Individual projects will be completed on or before the end of the Shadow Award performance period. All have been reporting to and been regularly reviewed by the program managers of the funding NOAA competitive program and what is included herein is primarily what has been already submitted to and approved by the funding program manager. These projects fall under Task III. Task III funds activities of University scientists on projects carried out in close collaboration with NOAA scientists. The indirect cost rate for Task III is currently 40%. The projects all fall under the same scope of work and under the six research themes (see below) described in the Cooperative Agreement accepted on December 1, 2001. All research carried out under these themes is specifically linked to the NOAA Strategic Plan and to its Goals.

**Theme 1: Climate Variability**

Investigate the dynamics of the ocean and the atmosphere and the ways in which they interact on interannual and longer-scales and the link to climate variations.

**Theme 2: Fisheries Dynamics**

Enhance our understanding of fisheries and ecosystem dynamics so as to improve the management of fisheries and marine protected species.

**Theme 3: Regional Coastal Ecosystem Processes**

Carry out research on the ecological health of coastal ocean ecosystems in the Southeast U.S so as to lead to better management strategies.

**Theme 4: Human Interactions with the Coastal Environment**

Study human interactions and impacts on the coastal environment so as to provide a scientific basis for environmental decision-making.

**Theme 5: Air-Sea Interactions and Exchanges**

Understand the energy exchanges and interactions between the atmosphere and the oceans and the consequent effects on atmospheric and ocean mixing and circulation.

**Theme 6: Integrated Ocean Observations**

Study the integration of modeling and physical measurements in the ocean and the atmosphere so as to achieve optimal designs of observing systems.

If you require additional information about this progress report, do not hesitate to contact me.

A handwritten signature in cursive script, reading "Peter B. Ortner".

Peter B. Ortner  
CIMAS Director

# Understanding Discrepancies between Satellite-Observed and GCM-Simulated Precipitation Change in Response to Surface Warming

**Principal Investigator:** B.J. Soden (UM/RSMAS); G. Vecchi (NOAA/GFDL)

**NOAA Funding Unit:** OGP

**NOAA Technical Contact:** James Todd

## Activity:

Future substantial changes in the global water cycle are an expected consequence of a warming climate; this is based upon understanding of the governing physical processes and projections made by sophisticated models of the Earth's climate system. Monitoring changes in tropical precipitation is a vital step toward building confidence in regional and large-scale climate predictions and the associated impacts on society.

A number of robust large-scale responses of the hydrological cycle have been identified in models, relating primarily to increases in low-level moisture with temperature, a consequence of the Clausius-Clapeyron equation. Improving confidence in climate projections demands the use of observations, sampling the many aspects of the global energy and water cycles, to evaluate the relevant processes simulated by models. It is important to establish causes of disagreement, for example relating to observing system deficiencies or inadequate representation of forcing and feedback processes in models. There is observational evidence of increased tropical monthly-average moisture and precipitation and an amplification of extreme precipitation events in response to atmospheric as well as a contrasting precipitation response over wet and dry regions of the tropics. While observed precipitation responses appear larger than those simulated by models it is unclear whether this relates to model deficiency, inadequacy in the observing system or is a statistical artifact of the relatively short satellite record.

In Allan et al. (2010) and Chung et al. (2010) we examine current changes in tropical precipitation and its extremes, and the radiative feedbacks which govern them. In particular we addressed the questions: (1) What are current trends in tropical mean precipitation? (2) Are the wet regions becoming wetter at the expense of the dry regions? (3) Is there an intensification in extreme precipitation with warming in models and observations over the period 1979-2008? (4) How consistent are observed and model-simulated rates of radiative feedbacks?

Current changes in tropical precipitation from satellite data and climate models were assessed. Increased precipitation in moist, ascending regions and reductions in drier descending branches of the large-scale circulation, previously identified, were sensitive to the reanalysis products used to define these regions. To avoid homogeneity issues with reanalysis fields, wet and dry regions of the tropics were defined as the highest 30% and lowest 70% of monthly precipitation values. Observed tropical ocean trends in the wet regime (1.8%/decade) and the dry regions (-2.6%/decade) for the Global Precipitation Climatology Project (GPCP) over the period including Special Sensor Microwave Imager (SSM/I) data (1988-2008) were of smaller magnitude than when including the entire time-series (1979-2008) and in closer agreement with model simulations than previous comparisons. Analyzing changes in extreme precipitation using daily data within the wet regions we found that SSM/I observations indicate an increased frequency of the heaviest 0.2% of events of approximately 60% per K warming. This is at the upper limit of the model simulations which display a substantial range in responses.

However, we find that the radiative feedback processes which govern variations in clear-sky longwave damping are highly consistent between observations and models.

**Publications:**

Allan, R.P., B.J. Soden, V.O. John, W. Ingram and P. Good, 2010: Current changes in tropical precipitation, *Environ. Res. Lett.*, submitted.

Chung, E., D. Yeomans, B.J. Soden, 2010: An assessment of climate feedback processes using satellite observations of clear-sky OLR, *Geophys. Res. Lett.*, **37**, L02702, doi:10.1029/2009GL041889.

# Role of Diabatic Heating Profiles in MJO Simulation and Prediction

**Principal Investigator:** Chidong Zhang

**NOAA Funding Unit:** OGP

**NOAA Technical Contact:** Jin Huang

## Results and Accomplishments:

This year, the diagnostic work focused on comparing diabatic heating profiles in CFS hindcasts (CFHS) to their skills. From the hindcast data we have, we first identified 72 cases in which CFS 21-day hindcasts were initiated in MJO phases 2 and 3 (MJO convection centers located over the Indian Ocean). These 72 cases include days when MJO events were present and days when there was no MJO, i.e., the magnitude of the RMM index of Wheeler and Hendon (2004) was less than one standard deviation. For each case, we calculated forecast skill through the 21 days using the RMM index. The forecast skills of the 72 cases were then divided into terciles. The top tercile (higher hindcast skills) is labeled as the best cases (BEST). The bottom tercile (lower hindcast skill) is labeled as the worst cases (WORST). Diabatic heating (Q1), OLR, and zonal wind over the Indian Ocean and Maritime Continents produced by CFHS from BEST and WORST were compared to each other and to the CFS reanalysis (CFSR). The main results are:

- 1) In general, Q1 in the CFHS behaves similarly in BEST and WORST. There is no obvious eastward propagation in Q1 (and OLR) in most cases in both terciles. If there is an MJO event that moves eastward in CFSR, the CFHS skill drops substantially. Most days with MJO events are in WORST. The CFHS skill is higher in BEST simply because there is no MJO signal in that tercile.
- 2) Vertical structures of Q1 in CFHS are similar in BEST and WORST. Most discrepancies in Q1 between CFHS and CFSR are in its location and amplitude. But there is evidence that CFHS produces too much upper-level heating and insufficient low-level heating.
- 3) The problem in Q1 produced by CFHS can be summarized in Figure 1. This figure was generated by first making composites for BEST and WORST terciles for both CFHS and CFSR, and then calculate the difference (BEST – WORST composites) for CFHS (right column) and CFSR (left). The top row is 3-day hindcast and the bottom is 21-day hindcast with 3-day increments in between. It is evident that there is an eastward movement in CFSR Q1 in WORST but not in BEST, manifested by the negative values of Q1 difference in the left column. This eastward movement consists of two parts. One is an eastward expansion of the convective area, the other is an eastward penetration of low-level heating that gradually deepens. The eastward movement in CFHS Q1 is absent, even though there is one time attempt for CFHS to develop an eastward penetration of low-level heating eastward (at hindcast day 15).
- 4) Another obvious difference in CFHS between BEST and WORST is in 850 hPa zonal wind . Equatorial 850 hPa westerly anomalies exist over the western Indian Ocean in CFSR in both BEST and WORST. In CFHS, there are westerly anomalies over the Indian Ocean in BEST (mostly in the southern hemisphere though) but they are absent in WORST (Fig. 2). Low-level westerlies are known to advect dry air into convective areas and either terminate deep convection, or push it eastward and initiate an MJO event. The low hindcast skill of CFHS during an active MJO event might be in its

inability of producing low-level westerlies. This may be related to the inadequate low-level heating in CFSH.

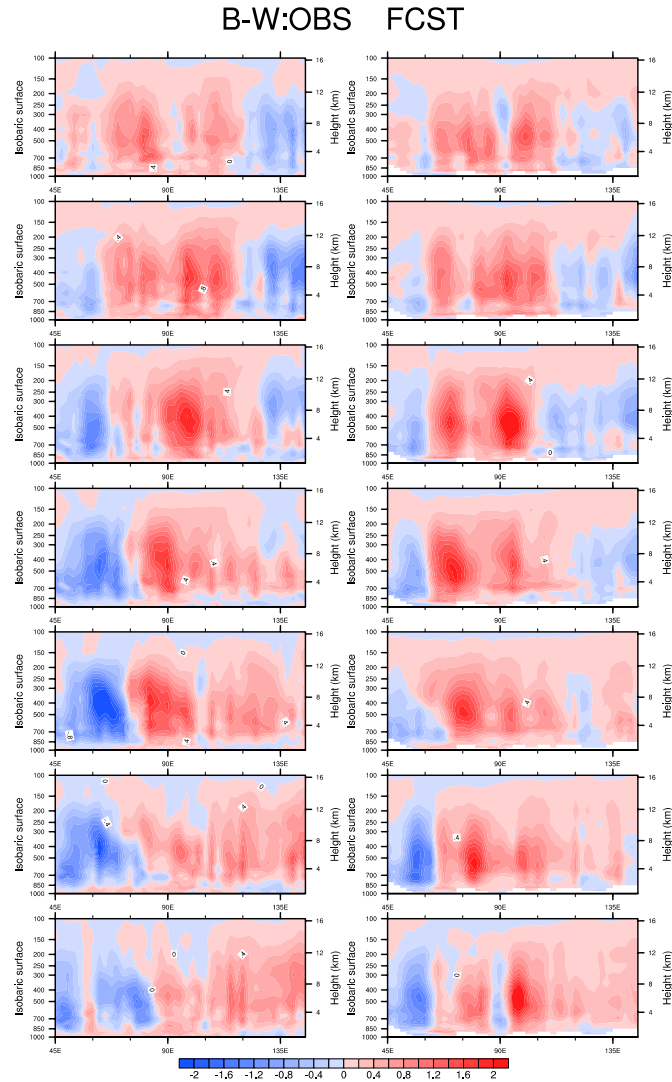


**Figure 1:** Differences in composite Q1 between BEST and WORST terciles for CFSR (left column) and CFSH (right) from 3 (top) to 21 (bottom) days after the initiation time with 3-day increment in between.

5) The same procedure was followed for MJO phases 4 and 5 (convection center located over the Maritime Continents). In this case, the difference between BEST and WORST in CFSH is much more obvious. As for MJO phases 2 and 3, there is an eastward expansion in Q1 from the Indian Ocean to the Maritime Continents in WORST but not in BEST in CFSR (Fig. 3, left column). This occurs in WORST of CFSH but not persistently (right column). It is also clear that CFSH produces too much heating over the eastern Indian Ocean in WORST, which tends to be stationary instead of eastward moving.

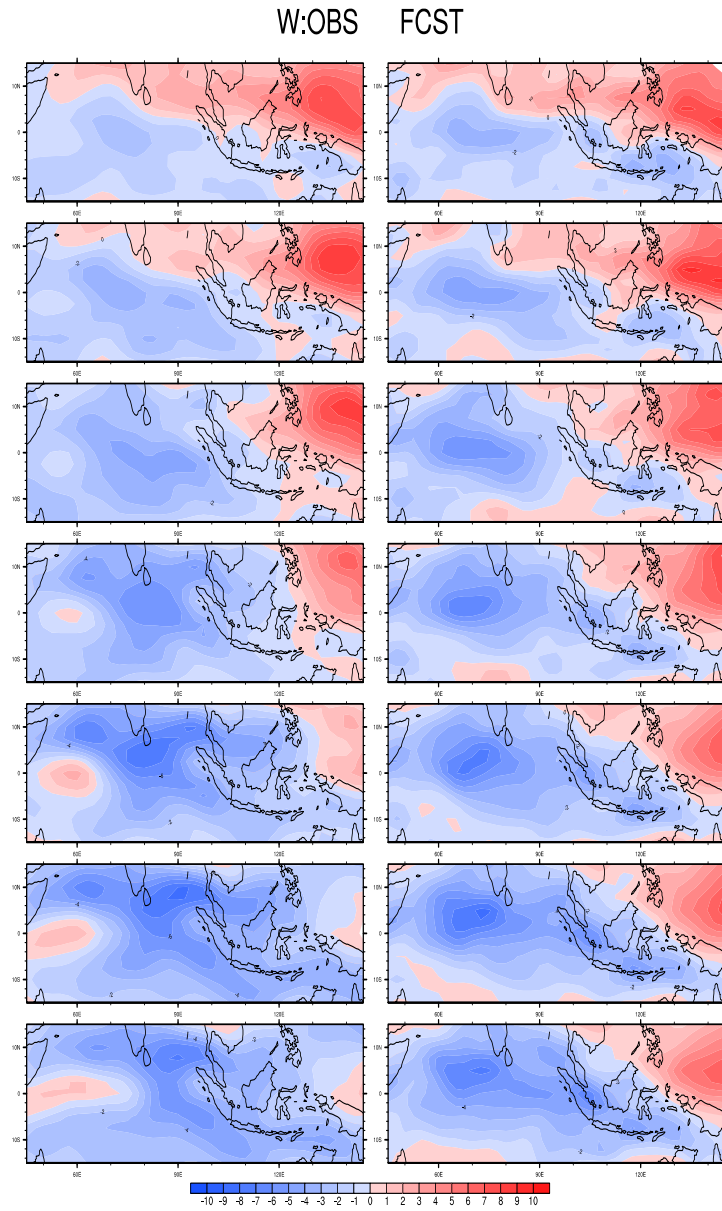


**Figure 2:** Composite 850 hPa zonal wind in WORST terciles for CFSR (left column) and CFSH (right) from 3 (top) to 21 (bottom) days after the initiation time with 3-day increment in between.

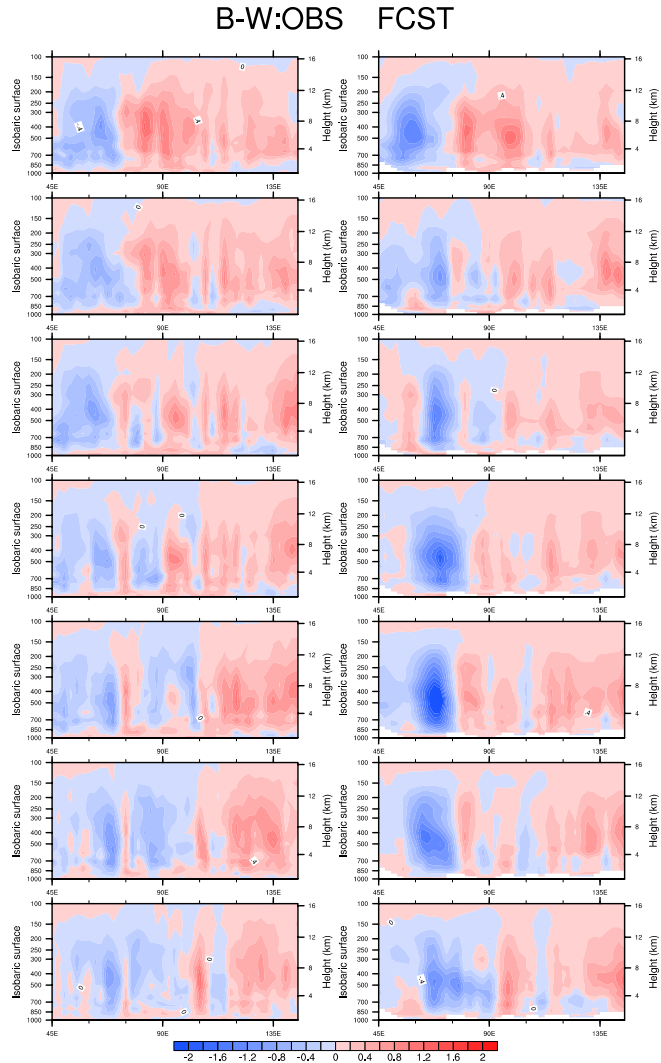


**Figure 3:** Same as Fig. 1 but for MJO phases 4 and 5.

The modeling work focused on using NCAR WRF with humidity nudging to correct its dry biases and enhance its capability of reproducing the MJO. The main results are:

6) WRF failed to reproduce the MJO no matter what parameterization package was used. We have exhausted all options available for WRF. Heating profiles produced by different cumulus parameterization schemes and their combinations with different boundary layer scheme vary substantially (Fig. 4). So heating profiles alone cannot explain the failure of WRF in simulating the MJO.

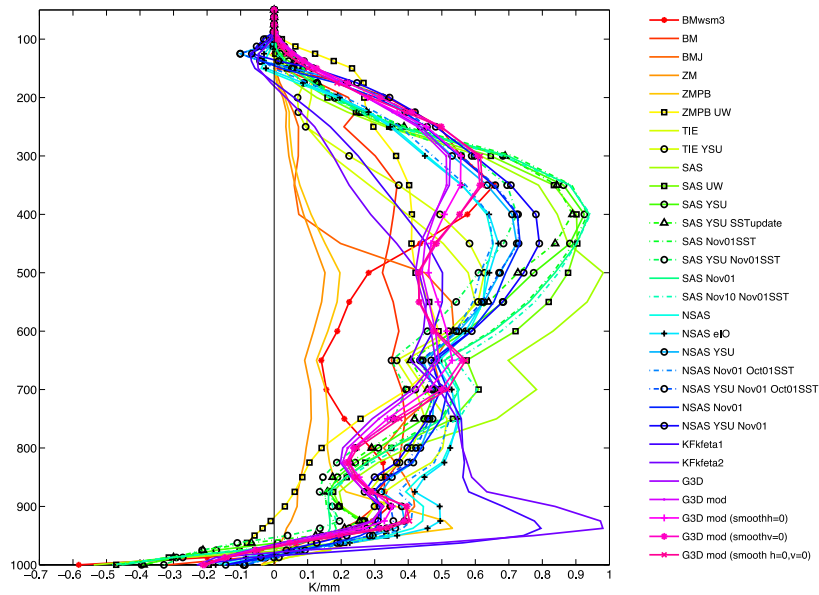


**Figure 4:** Heating profiles produced by various combinations of cumulus and boundary layer parameterization schemes in WRF.

7) Among all parameterization schemes used, the Betts-Miller (BM) scheme produces the best mean state. So we decided to use this scheme for humidity nudging experiments. When humidity from the ERA-Interim (ERA-Interim) reanalysis was used to correct dry biases in WRF + BM in the nudging experiment, WRF can produce eastward propagation in rainfall (Fig. 5, right panel), which is completely missing without nudging (Fig. 5, middle).

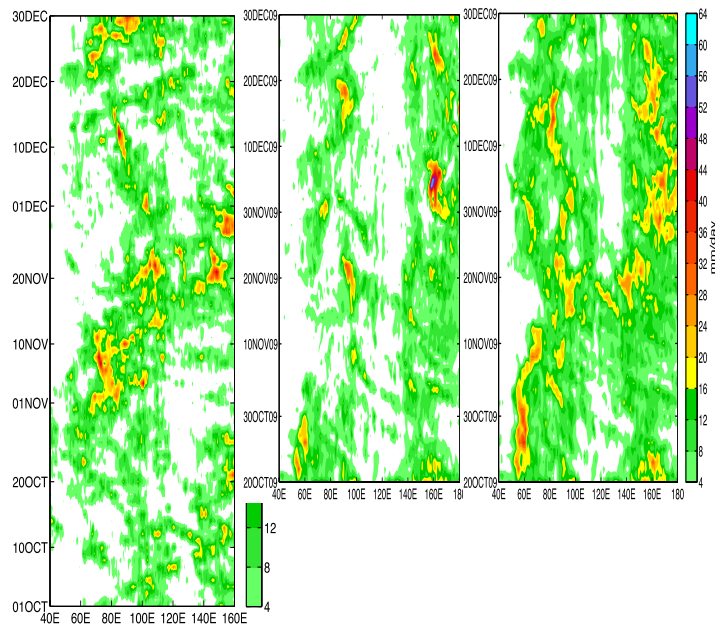


**Figure 5:** Longitude-time plots of rainfall from (left) TRMM, (middle) control run of WRF (without nudging), and (right) WRF with humidity nudging.

8) The differences between the heating profiles in the control run (without nudging, no MJO signals in rainfall) and the nudging run (with MJO signals in rainfall) are evident (Fig. 6) in several aspects. Heating in the nudging run is more organized and occupies larger area (lower panel), whereas it is more scattered in the control run (upper panel). Heating in the nudging run is stronger than in the control run. There is a strong cooling immediately above the boundary layer from time to time in the control run (and in its zonal mean), but not in the nudging run. This cooling is due mainly to longwave radiation in the absence of shallow convection in a very dry (and biased) environment in the control run. When the dry bias is corrected in the nudging run, low-level heating becomes possible, which replaces the low-level cooling.

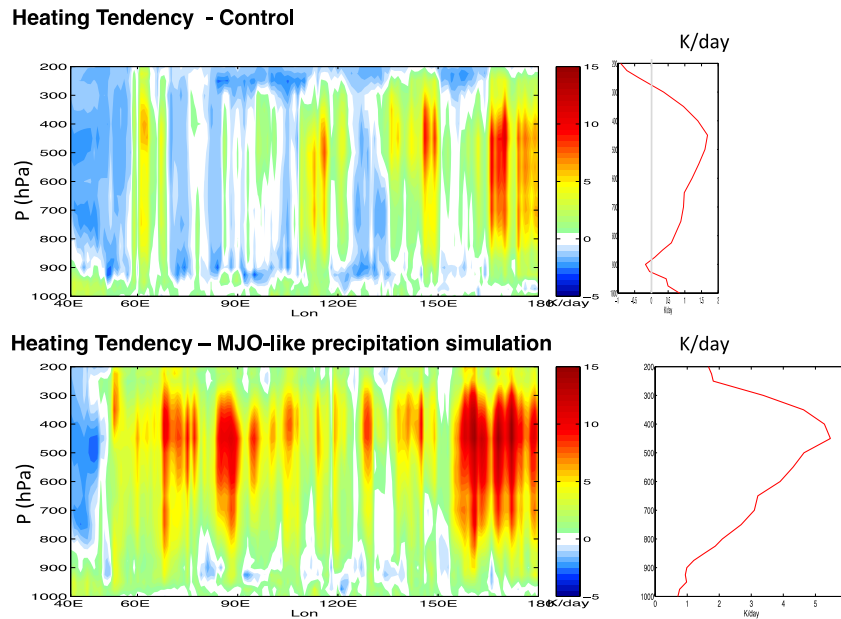


**Figure 6:** A snapshot of (left columns) longitudinal distribution of heating profiles in WRF control run (upper panel) and nudging run (lower), and (right) their zonal (40 – 180E) means.

9) We have made many other runs to test the sensitivity of MJO simulations by WRF to humidity by varying nudging strategy (vertical levels, zonal wavenumbers, etc.). The general conclusions are: Low and middle level humidity is more important than upper-level humidity to MJO simulations. Zonal mean humidity is necessary but insufficient for correction the dry biases for MJO simulations. The main eastward propagation signal of the MJO comes from zonal wavenumber one humidity. But zonal wavenumbers 2 and 3 are also important to realistic MJO simulations. The dry biases in WRF mainly come from its inability to pump moisture from the boundary layer into the lower troposphere and insufficient surface evaporation.

### Highlights of Accomplishments:

- A lack of low-level heating appears to be the main deficit in both CFS and WRF that are at least partially responsible for their failure of producing MJO signals.
- The reason for the lack of low-level heating in CFS might be the inherited vertical structure of diabatic heating produced by its cumulus scheme. The reason in WRF is its dry biases in the lower troposphere.

- The consequence of insufficient low-level heating in CFS is the absence of low-level westerlies that advect dry air into convection centers and push them move eastward during MJO initiation. Without the low-level westerlies, convection become stationary and there is no MJO initiation.
- In WRF, even the low-level westerlies are produced, the dry biases prevent shallow convection from developing into organized convective systems that are needed for MJO initiation.

In summary, the role of the vertical structure of diabatic heating in MJO simulations and hindcast/forecast will have to be understood together with other variables key to the MJO dynamics.

### **Publications**

Chattopadhyay, R., A. Vintzileos, and C., Zhang, 2012: A Description of the Madden Julian Oscillation Based on Self Organizing Map. *J. Climate*, conditionally accepted.

Chattopadhyay, R., C. Zhang, and A. Vintzileos, 2012: Representation of diabatic heating profiles in CSF hindcast. *Clim. Dyn.*, in preparation.

Ulate, M., C. Zhang, J. Dudhia, 2012: Moisture bias and its effect on MJO simulations by WRF. *Mon. Wea. Rev.*, in preparation.

**Budget for Coming year (2013) \$0.0**

### **Future Work**

A no-cost extension was requested to complete the proposed work. The replacement of Dr. Rajib Chattopadhyay, the postdoctoral associate who had worked on this project but left early this year for another position. The planned cloud-resolving simulations needed to be completed, which was delayed because of a gap of computing resources at NCAR. We expect to conclude this project by June 2013.

The remaining funds will be used to partially support the new postdoctoral associate, who has been recruited with joint funding from this and another grants.

## **Evaluation and Improvement of Ocean Model Parameterizations for NCEP Operations (FINAL REPORT)**

**Project Personnel:** Lynn K Shay (PI, UM/RSMAS); George Halliwell (Co-PI, NOAA/PhOD); Hyun-Sook Kim (NCEP Collaborator)

**NOAA Funding Unit:** USWRP Joint Hurricane Testbed

**NOAA Technical Contact:** Dr. Jiann-Gwo Jiing

**Goal:** The long term goal of this NOAA Joint Hurricane Testbed (JHT) grant is to evaluate and improve ocean model parameterizations in NOAA National Centers for Environmental Prediction (NCEP) coupled hurricane forecast models in collaboration with the NOAA Tropical Prediction Center (TPC) and NOAA/NCEP Environmental Modeling Center (EMC). This effort targets the Joint Hurricane Testbed programmatic priorities **EMC-1** and **EMC-2** along with hurricane forecaster priorities **TPC-1** and **TPC-2** that focus on improving intensity forecasts through evaluating and improving oceanic boundary layer performance in the coupled model and improving observations required for model initialization, evaluation, and analysis. This project will be conducted under the auspices of the Cooperative Institute of Marine and Atmospheric Science program, and addresses **CIMAS Theme 2 and 3: Tropical Weather and Sustained Coastal and Ocean Observations and NOAA Strategic Goal 3: Weather and Water (local forecasts and warnings)**.

Specific objectives of this grant are:

- i) optimizing spatial resolution that will permit the ocean model to run efficiently as possible without degrading the simulated response;
- ii) improving the initial background state provided to the ocean model;
- iii) improving the representation of vertical and horizontal friction and mixing;
- iv) generating the realistic high-resolution atmospheric forcing fields necessary to achieve the previous objectives; and
- v) interacting with NOAA/NCEP/EMC in implementing ocean model code and evaluating the ocean model response in coupled hurricane forecast tests.

**Summary of Progress and Recommendations:** This effort has proceeded along two closely related tracks: (1) evaluation of ocean model performance; and, (2) the preparation and analysis of the *in-situ* ocean observations required to perform these careful evaluations. The Hybrid Coordinate Ocean Model (HYCOM) is chosen as the primary ocean model because it is being evaluated as the ocean model component of the next-generation coupled hurricane forecast model at NOAA/NCEP/EMC. It also contains multiple choices of numerical schemes and subgrid-scale parameterizations, making it possible to isolate model sensitivity to individual processes and devise strategies to improve model representation of these processes. Results from our model evaluation during Hurricane Ivan (2004) were recently published (Halliwell *et al.*, 2011), leading to a specific list of model recommendations. Reference experiments have also been performed for Hurricanes Katrina and Rita (2005).

A key result of our prior work is that accurate ocean model initialization with respect to both the location of ocean features and the upper-ocean temperature and salinity (density) profiles within them is the most important factor influencing the quality of SST and intensity forecasts from coupled models. The initialization errors and biases encountered in our previous work produced large SST forecast errors that made it impossible to quantitatively estimate optimum values of ocean model and surface flux parameterizations. As a result, the modeling effort over the prior year has primarily focused on improving ocean model initialization and developing useful metrics to evaluate model

performance. Multiple ocean analysis products produced by operational forecast centers that use HYCOM and other model types have been evaluated for overall accuracy, and also to quantify the impact of targeted airborne ocean observations on the accuracy of initial ocean fields. The accuracy of velocity shear profiles produced by HYCOM, which are critically important for simulating entrainment cooling of SST, has been further evaluated against the measurements available during Hurricane Ivan.

What separates this modeling study from others is a fairly complete analysis of experimental data sets. This observational effort has included processing the *in-situ* Acoustic Doppler Current Profiler (ADCP) data from Ivan (provided by the U.S. Naval Research Laboratory). It also included moored observations during Katrina and Rita (data courtesy of Bureau of Ocean Energy Management Regulation and Enforcement (BOEMRE: formerly Minerals Management Service-MMS), and the NOAA Hurricane Research Division (HRD) Intensity Fluctuation Experiments (IFEX) 2005 observations for pre- and post Rita (Rogers *et al.*, 2006; Jaimes and Shay, 2009, 2010). In addition, oceanic and atmospheric profiler measurements were acquired during hurricanes Gustav and Ike in 2008 in and over the Gulf of Mexico. In all of these cases, satellite observations (altimetry and SST) have been obtained and Ocean Heat Content (OHC) maps have been produced following the Shay and Brewster (2010) approach. The effort to improve ocean model initialization during the previous year was significantly enhanced by the large set of ocean observations in the Gulf of Mexico collected in response to the Deepwater Horizon oil spill. Since early May of 2010, both Shay and Halliwell redirected part of their work toward observational and modeling efforts in response to the spill, which included the acquisition of multiple synoptic maps of upper-ocean temperature, salinity, and velocity profiles deployed from NOAA WP-3D aircraft. These repeat flights in conjunction with other *in-situ* observations provide an unprecedented dataset for evaluating existing analysis products for ocean model initialization.

Based on our work over the prior year, we conclude that data-assimilative ocean model analysis products will achieve sufficient accuracy to replace the existing operational feature-based initialization procedure. Model evaluation conducted in the Gulf of Mexico demonstrates that the Navy global HYCOM analysis is presently the optimum choice to provide initial fields for ocean model initialization. The large negative temperature bias present in the Navy HYCOM products that we documented in prior reports and publications has been substantially corrected by employing a different vertical projection procedure to estimate synthetic temperature and salinity profiles from satellite altimetry for assimilation. By contrast, significant problems were encountered in the NOAA/EMC HYCOM-based RTOFS Atlantic Ocean analysis, and also in the existing operational feature-based initialization procedure. As discussed later in this report, the Navy will soon release a HYCOM reanalysis product using this latest forecast system, which will enable us to revisit historical storms with improved initial fields. We further determined that assimilation of P-3 synoptic ocean profiles in the eastern Gulf of Mexico reduced upper-ocean temperature RMS errors by ~30% and remaining biases by ~50%. Given the improvement achieved in this particular case, research on the optimum use of targeted aircraft observations to improve ocean model initialization must continue. Finally, our research demonstrates the critical importance of using three-dimensional ocean models that include the impact of ocean dynamics on the magnitude and pattern of SST cooling. Results supporting these conclusions are summarized in the remainder of this report.

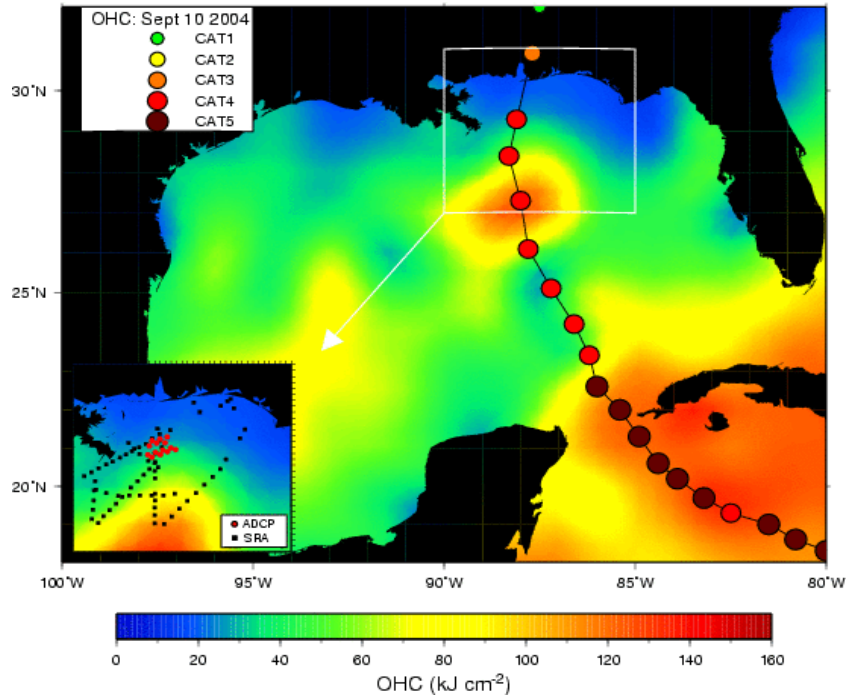


**Figure 1:** OHC map and inset showing NRL mooring locations (red) and SRA wave measurements (black) relative to Ivan's storm track and intensity. The OHC pattern shows the WCR encountered by Ivan prior to landfall. The cooler shelf water ( $\text{OHC} < 20 \text{ kJ cm}^{-2}$ ) resulted from the passage of Frances two weeks earlier

**Current Profiler Analysis During Ivan:** Hurricane Ivan passed directly over 14 ADCP moorings (Figure 1) that were deployed from May through Nov. 2004 as part of the NRL *Slope to Shelf Energetics and Exchange Dynamics (SEED)* project (Teague *et al.*, 2007). These observations enable the simulated ocean current (and shear) response to a hurricane over a continental shelf/slope region to be evaluated. These profiler measurements provide the evolution of the current (and shear) structure from the deep ocean across the shelf break to the continental shelf. The current shear response, estimated over 4-m vertical scales, is shown in Figure 2 based on objectively analyzed data from these moorings. The normalized shear magnitude forced by Ivan is a factor of four times larger over the shelf (depths < 100 m) compared to normalized values over the deeper part of the mooring array (500 to 1000 m). The current shear rotates anticyclonically (clockwise) in time, consistent with the forced near-inertial response (periods slightly shorter than the local inertial period). In this measurement domain, the local inertial period is close to the 24 hr diurnal tide period. By removing the weaker tidal currents and digitally filtering the records, the analysis revealed that the predominant response was due to forced near-inertial motions. These motions have the characteristic time scale for the phase of each mode when the wind stress scale ( $2R_{\text{max}} \sim 64 \text{ km}$  in Ivan during time of closest approach) exceeds the deformation radius associated with the first baroclinic mode ( $\approx 30$  to  $40 \text{ km}$ ). This time scale increases with the number of baroclinic modes because phase speeds decrease with increasing mode number (Shay *et al.*, 1998). The resulting vertical energy propagation from the OML into the ocean interior is associated with the predominance of the anticyclonic (clockwise) rotating energy with depth and time that is about four times larger than the cyclonic (counterclockwise) rotating component.

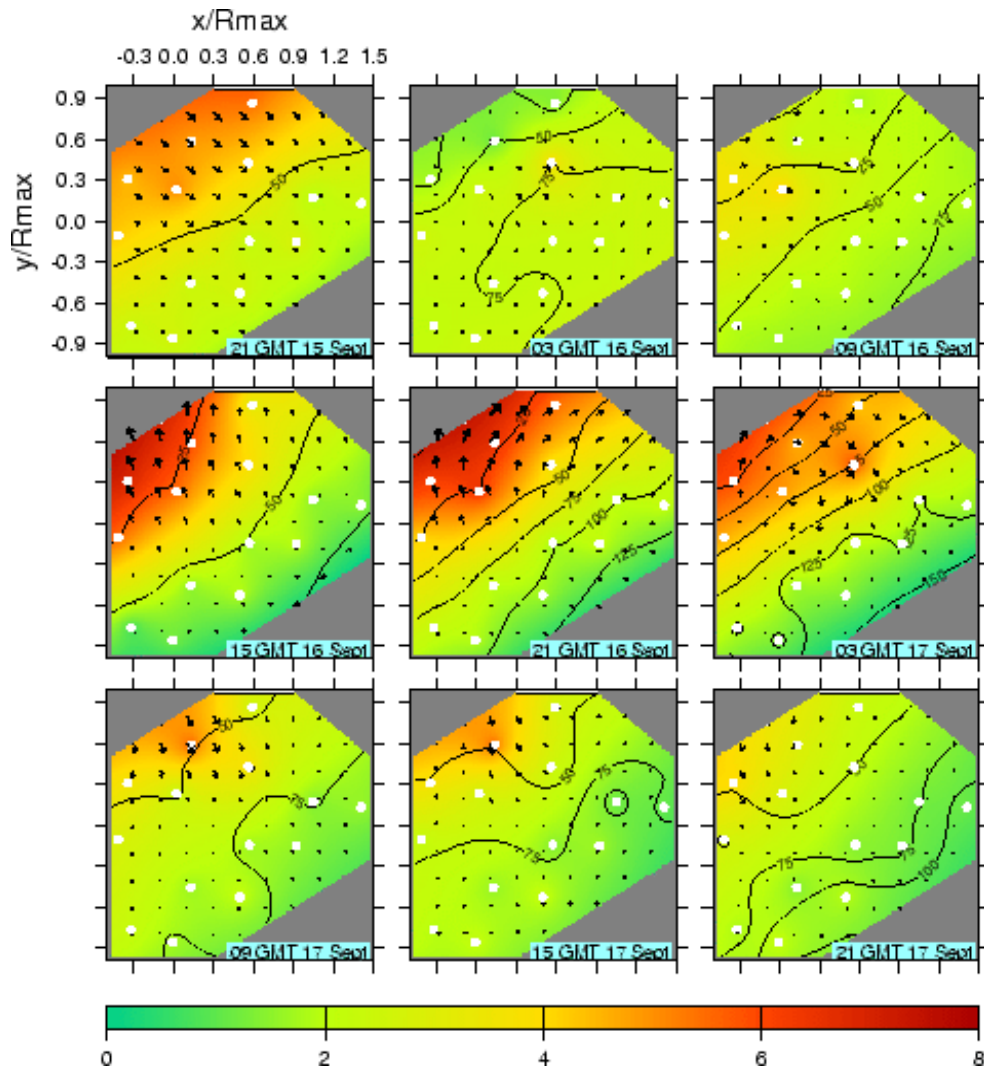


**Figure 2:** Spatial evolution of the rotated current shear magnitude normalized by observed shears from the ADCP measurements (white dots) normalized by observed shears in the LC of  $1.5 \times 10^2 \text{ s}^{-1}$  (color) during Ivan starting at 2100 GMT 15 Sept every 6 hours. Black contours (25-m) represent the depth of the maximum shears. Distances are normalized by  $R_{max}$  (32 km for Ivan).

Observed current shear profiles were estimated over 4-m vertical scales for each time sample following hurricane passage at mooring 9 (Figure 3). The shear magnitudes are typically two to three times larger than observed in the Loop Current (e.g., during Lili’s passage). This is not surprising since the SEED ADCP measurements were acquired in the Gulf Common Water (Nowlin and Hubertz, 1972), and they are similar to the shear documented during hurricane Gilbert’s passage where up to  $3.5^\circ\text{C}$  cooling was observed in the Gulf Common Water. In the near-inertial wave wake (Shay *et al.*, 1998), the key issue is how much of the current shear is associated with near-inertial wave processes. Compared to the Gulf Common Water, the presence of warm and cold eddies significantly impact these levels of near-inertial wave (and shear) activity (Jaimes and Shay, 2010).

## Shear at MS9

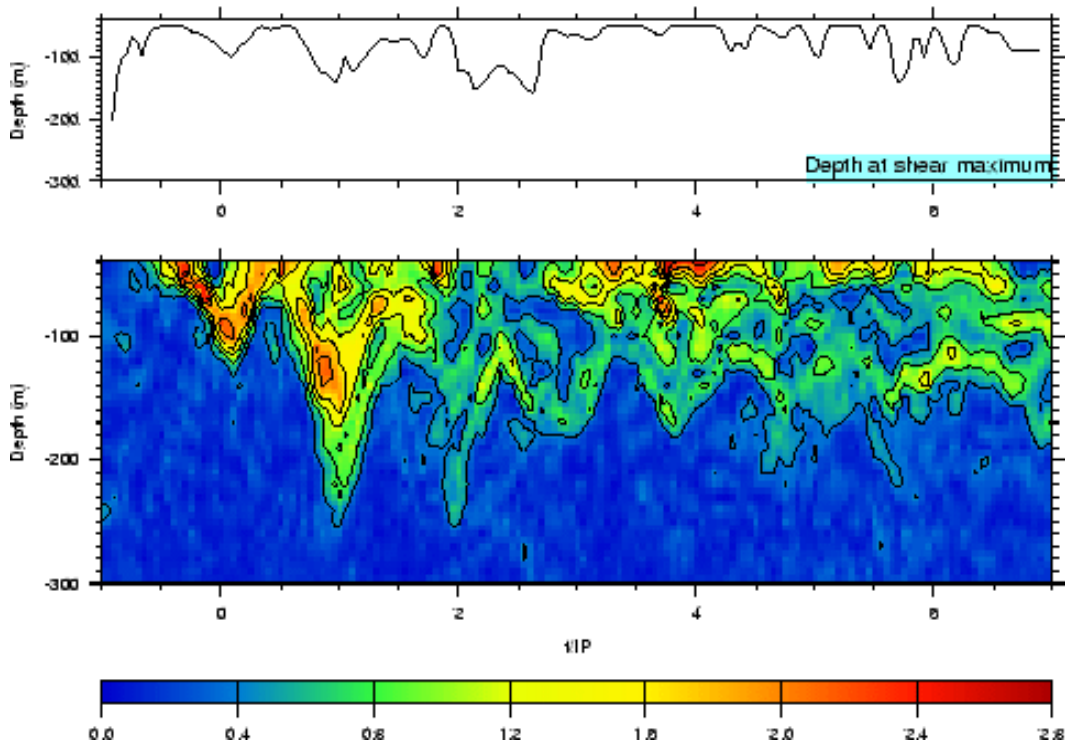


**Figure 3:** Time series (normalized by inertial period) of observed current shear magnitudes (colored contours) and the respective depths (m) of maximum current shears observed at Mooring 9 ( $1.5 R_{max}$  to the right of the Ivan) relative to the time of the closest approach. Shears are normalized by a value of  $1.5 \times 10^{-2} s^{-1}$  that have been observed in the LC (Shay and Uhlhorn, 2008).

**Comparison of Model and Observed Current Shear:** At SEED mooring 9, velocity shear magnitude profiles from a control experiment are compared to shear profiles from alternate experiments that each varies a single attribute (Figure 4). These observations and simulations suggest that vertical energy propagates out of the surface mixed layer and into the thermocline consistent with surface intensified flows (Jaimes and Shay, 2010). The closest visual agreement exists between observed shear and simulated shear from the control experiment that used KPP vertical mixing and the Donelan *et al.* (2004) wind stress drag coefficient. Velocity shears produced by two different vertical mixing models (Mellor-Yamada and GISS) and by two different choices of wind stress drag coefficient (Powell *et al.*, 2003; Large and Pond capped at high wind speed) produced less realistic shear responses in comparison to observations. These latest results agree with the recommendations of the Ivan analysis in Halliwell *et al.* (2011) as listed in Table 1. We are in the process of making additional comparisons for all the ADCP records during storm forcing. The importance of the impact of vertical mixing and wind stress drag coefficient on shear evolution and the resulting entrainment of cold water into the mixed layer (and hence SST cooling rate) cannot be overstated.

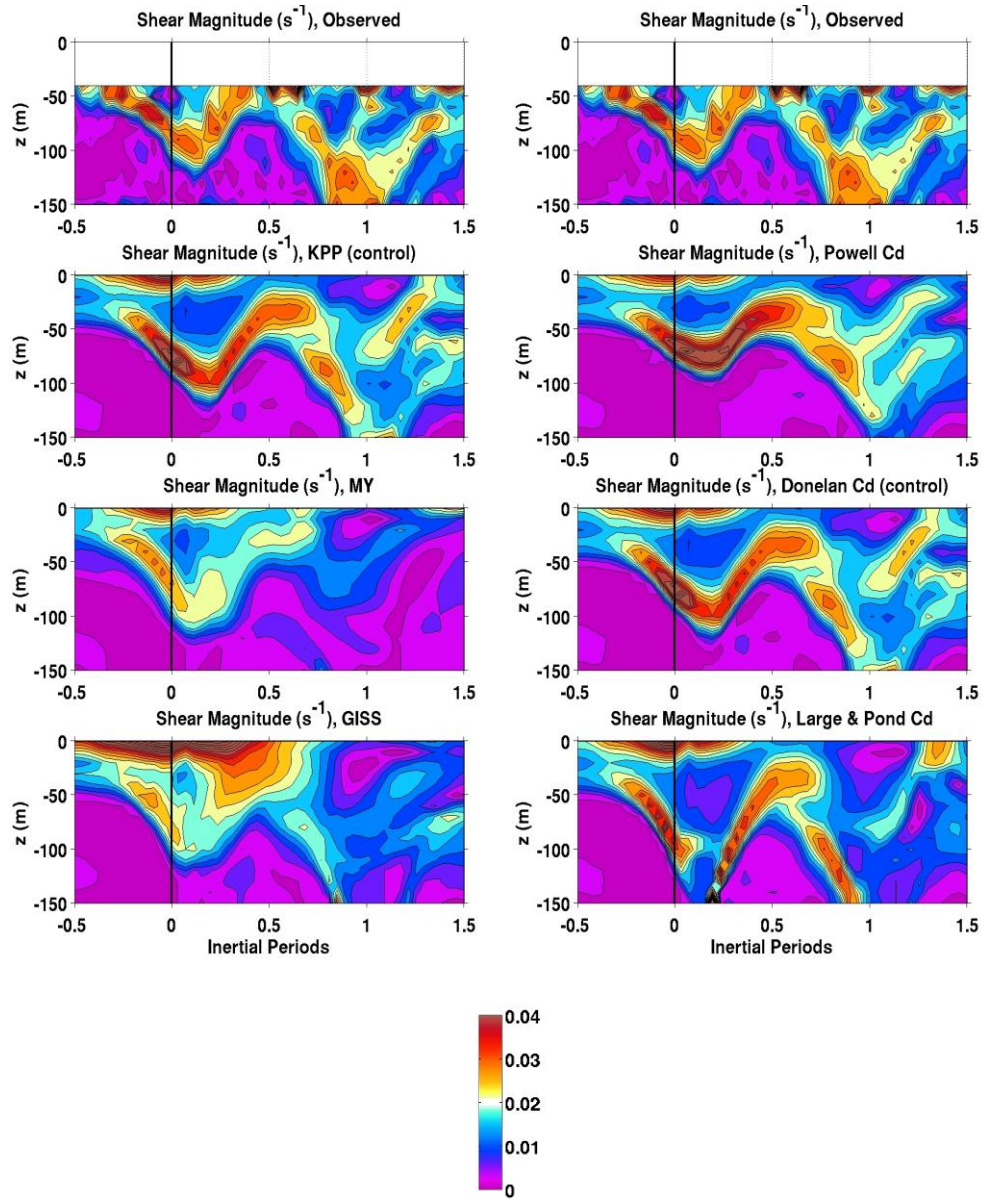


**Figure 4:** Time series of the magnitude of vertical shear ( $s^{-1}$ ) comparing observations from SEED mooring 9 (top left and top right) to three vertical mixing choices (left) and three wind stress drag coefficient choices (right). The combination of KPP mixing and Donelan et al. drag coefficient parameterizations produce the most realistic shear structure and maximum OML depth.

**Table 1:** Recommendations to improve upper-ocean forecasts during tropical cyclones based on analysis of the simulated ocean response to Hurricane Ivan in the Gulf of Mexico (Halliwell *et al.*, 2011). **Analysis of Feature-Based Initialization:** A major goal of this project is to interact with the HWRF developers at EMC and URI to evaluate the performance of ocean models to be used in the next-generation HWRF model and to improve the performance of the ocean model. As part of this effort, URI provided feature-based initialization fields to G. Halliwell initially to be used to initialize HYCOM in a POM-HYCOM comparison study. By inspecting these fields, we discovered a problem that will impact the pattern and rate of SST cooling in the vicinity of the Loop Current and warm eddies as represented by the feature-based algorithm (Falkovich *et al.*, 2005).

Model Attribute	Recommendations
Horizontal resolution	$\approx 10$ km adequately resolves horizontal structure of response forced by eye/eyewall
Vertical resolution	$\approx 10$ m in the OML is adequate to resolve vertical structure of shear
Vertical mixing	KPP outperformed the other models; MY, GISS produce slower cooling, larger heat flux, less-accurate shear representation
$C_D$	Donelan, Large & Pond capped, Jarosz <i>et al.</i> (values between 2.0 and $2.5 \times 10^{-3}$ at high wind speed) produce most realistic results
$C_{EL}$ , $C_{ES}$	Little SST and velocity sensitivity but large heat flux sensitivity. Need heat flux observations to evaluate
Atmospheric forcing	Must resolve inner-core structure ( $\leq 10$ km horizontal resolution)
Outer model (assimilative vs. non-assimilative)	Accurate initialization is the most important factor to accurately forecast velocity and SST evolution in the GOM and NW Caribbean
Ocean dynamics (1-D vs. 3-D)	3-D required (second most important factor in the GOM)

The primary problem is described as follows: Baroclinic fronts slope in the wrong direction with increasing depth. This situation is illustrated by initial HYCOM fields prior to hurricane Ivan produced from the feature-based product and spun up for several inertial periods to approximately achieve geostrophic balance. Figure 5 shows the SSH pattern in the Gulf of Mexico, highlighting the LC Path and the detached warm ring. The subsurface structure of these features is investigated along the two sections shown in Figure 5. A meridional cross-section of zonal velocity through the warm ring (Figure 6) reveals that the diameter of the ring *increases* with increasing depth instead of decreasing as expected. Similarly, a zonal cross-section of meridional velocity across the Loop Current north of the Yucatan Channel (Figure 6) demonstrates that the core of maximum velocity shifts *westward* with increasing depth instead of eastward as expected. In both of these sections, the model interfaces below the near-surface level-coordinate domain follow isopycnals and demonstrate that the fronts (large horizontal density gradient and vertical shear) slope in the wrong direction with increasing depth. There is also a problem in blending the ring with the background ocean structure that is caused by a large vertical density jump near 650 m depth in the ring interior.

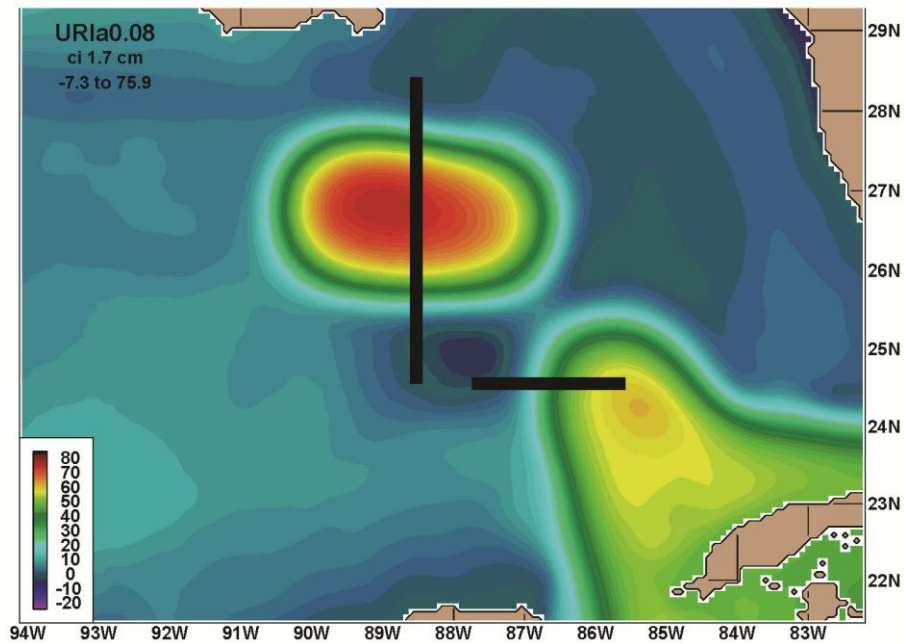


**Figure 5.** Pre-Ivan initial SSH map derived from the feature-based ocean model initialization product. The two cross-sections presented in Figure 6 are illustrated with black bars.

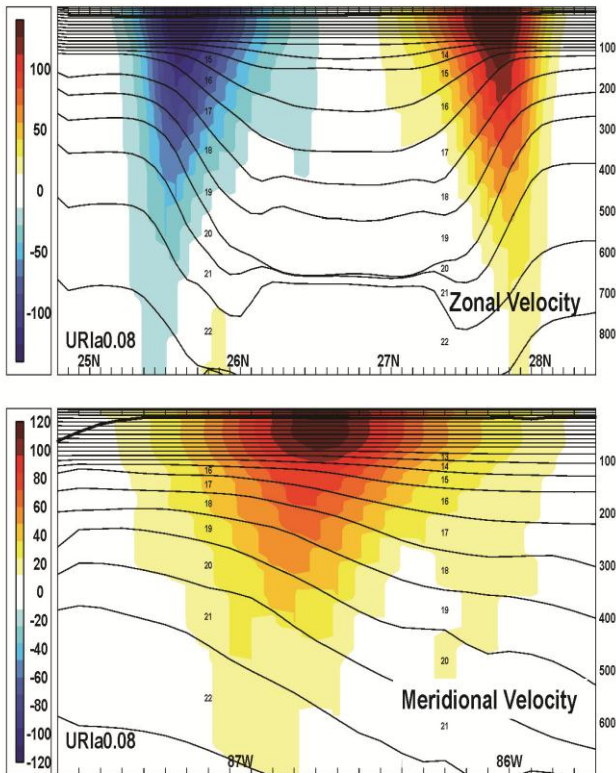


**Figure 6:** Pre-Ivan velocity cross-sections: (top) zonal velocity from a meridional section through the detached ring and (bottom) meridional velocity from a zonal section across the Loop Current. The locations of these two cross-sections are illustrated in Figure 5.

**DeepWater Horizon Oil Spill:** The effort to improve ocean model initialization has been significantly enhanced by the extensive observational dataset collected in response to the Deepwater Horizon oil spill. Shay was responsible for flying nine missions from the NOAA WP-3D research aircraft to

sample the Loop Current and adjacent eddies over the eastern Gulf of Mexico by deploying AXBTs, AXCPs and AXCTDs and GPS sondes (~666 profilers) in support of oil spill forecasting (see Figure 7, Table 2) (Shay *et al.*, 2011). Much of this sampling grid was over the BOEMRE moorings deployed in support of the Loop Current Dynamics Study. Although the short-term effect of this emergency effort was to delay our underway analysis of storms other than Ivan (Katrina, Rita, Frances, Gustav, Ike), the repeated aerial sampling over the eastern GOM in conjunction with other observations provided an unprecedented dataset for evaluating ocean model products initialization. Furthermore, the emergency aircraft sampling revealed significant problems with many of the AXCP probes and with vendor supplied software and firmware that will lead to improved sampling in the future in support of IFEX and HFIP.

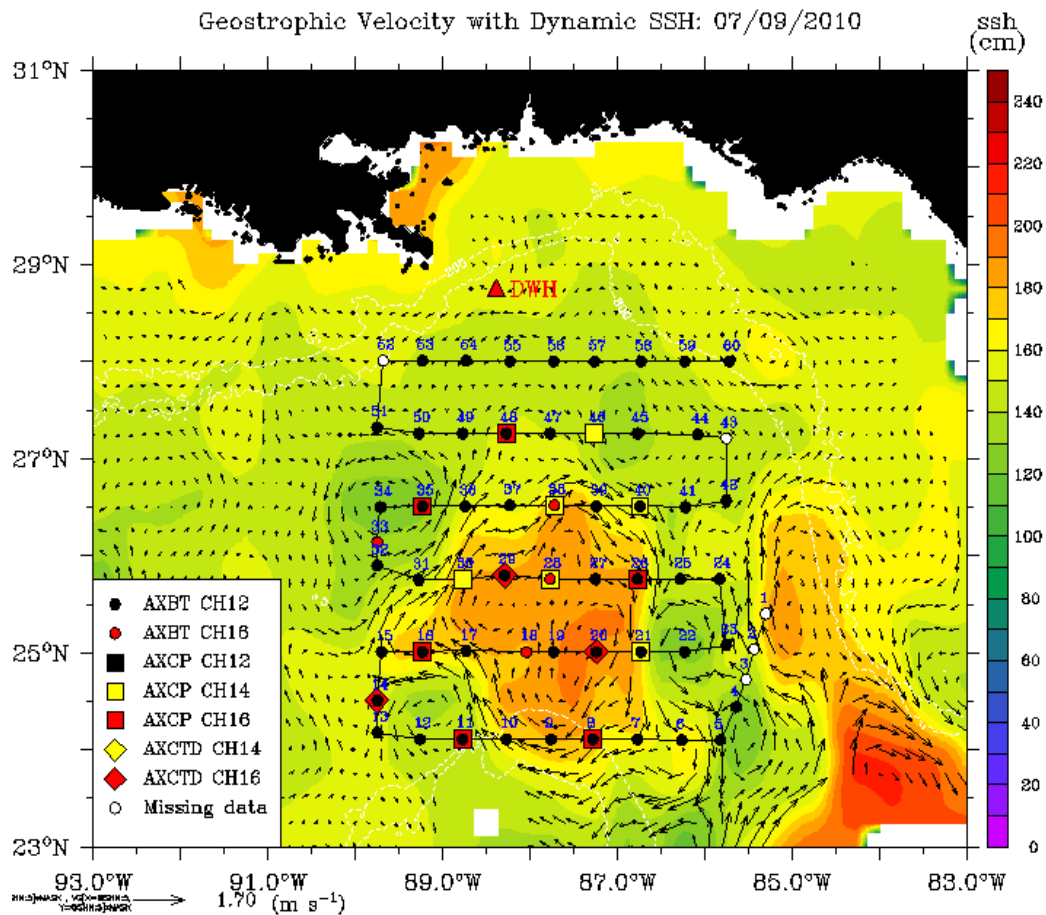


**Figure 7:** NOAA WP-3D mesoscale ocean grid on 9 July 2010 deploying a combination of AXBTs (circles), AXCTDs (diamonds), and AXCPs (squares) superposed on sea surface height (cm: color bar) and surface geostrophic currents based on sea surface slopes (maximum vector is  $1.7 \text{ m s}^{-1}$ ). Notice that warm core eddy (called Franklin) detached from the Loop Current.

**Table 2:** Summary of thirteen NOAA WP-3D aircraft flights on RF-42 in the eastern Gulf of Mexico from 24 to 28°N and 85 to 89°W in support of DWH oil spill that occurred on 20 April 2010 in the northern Gulf of Mexico along the slope of the DeSoto Canyon and IFEX flights . The overall success rate for all probes (in parentheses) was ~83%. This is lower than usual due to manufacturing problems with the AXCPs such as unsealed transmitter boards, agar, and software and firmware problems in the new Mark21/Mark10A software. The number of GPS sondes deployed was 78 (from Shay et al., 2011).

Flight	Event	AXBT	AXCP	AXCTD	TOTAL
100508H	DWH	52 (46)	0	0	52 (46)
100518H	DWH	29 (28)	26 (10)	11 (10)	66 (48)
100521H	DWH	42 (41)	22 (11)	2 (2)	66 (54)
100528H	DWH	41 (37)	22 (12)	2 (1)	65 (50)
100603H	DWH	37 (33)	23 (9)	6 (6)	66 (48)
100611H	DWH	53 (48)	15 (10)	0	68 (58)
100618H	DWH	34 (23)	22 (11)	8 (7)	64 (41)
100625H	DWH	58 (53)	0	6 (6)	64 (59)
100709H	DWH	59 (54)	12 (11)	6 (3)	77 (68)
100724H	<i>T.S. Bonnie</i>	35(33)	0	0	35 (33)
100812H	<i>Test</i>	6 (6)	6 (5)	0	12 (11)
100909H	<i>Pre Matthew</i>	62 (58)	0	20 (17)	82 (75)
100924H	<i>Pre Matthew</i>	30 (30)	10 (5)	20 (20)	60 (55)
Total		538(490)	158 (84)	81 (72)	777 (646)

Our previous HYCOM evaluation efforts typically revealed large negative temperature biases in the upper ocean prior to nearly all storms (the Ivan bias was relatively small) that led to large overcooling when the model was initialized by these biased fields. The Navy recently changed their vertical T, S projection method from Cooper-Haines to “MODAS Synthetics” derived from their Modular Ocean Data Assimilation System. The P-3 profiles enabled us to quantify the improvement in upper-ocean temperature, and the new projection method was found to greatly reduce the mean bias and also reduce RMS errors by an average of ~50% (Figure 8). These observations also enabled us to evaluate several ocean analysis products for the purpose of ocean model initialization, and the Navy global HYCOM analysis product was determined to be the optimum choice with respect to both bias and RMS error (Figure 8). We conclude that errors and biases have been reduced to the point where data-assimilative ocean analyses should replace the feature-based method of ocean model initialization. By contrast, comparatively large errors and biases were evident in the NOAA/NCEP/EMC HYCOM-based RTOFS Atlantic Ocean analysis. We intend to work closely with EMC to insure that the ocean initialization scheme being implemented and tested for the HYCOM-HWRF coupled forecast model has errors comparable to or smaller than the Navy global HYCOM product.

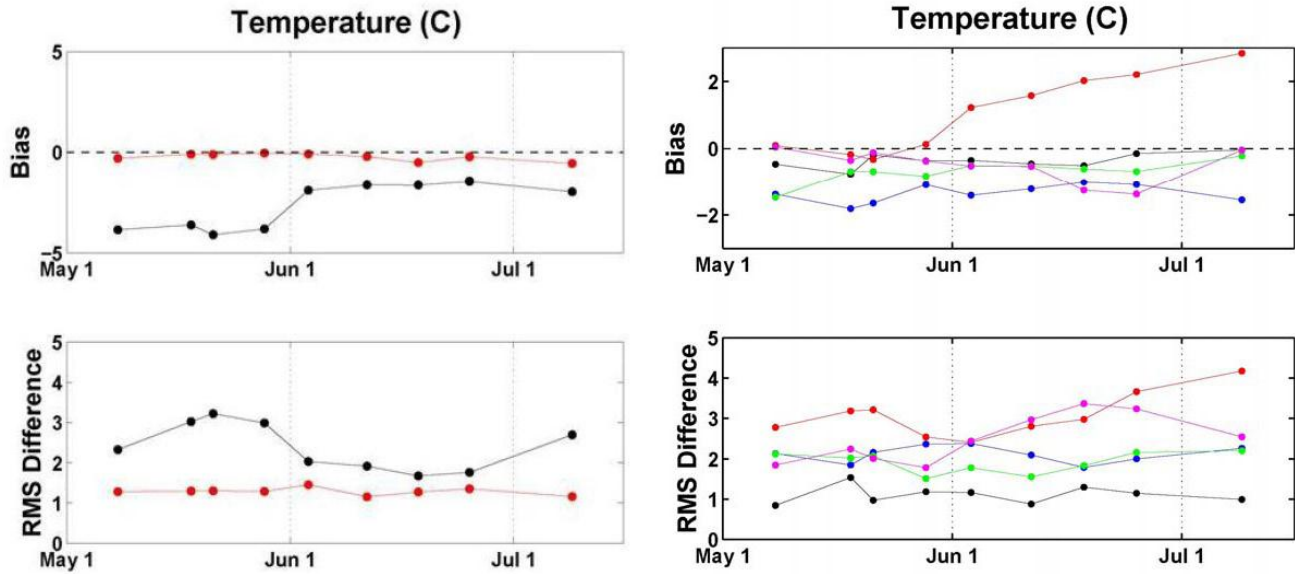


**Figure 8:** Bias (top) and RMS error (bottom) between several ocean model analyses and P3 temperature profiles on nine flight days between 30 and 360 m. The left panels are for two HYCOM Gulf of Mexico analyses, one using the old Cooper-Haines vertical projection of T and S profiles (black) and the other using the new “MODAS Synthetics” method (red). The right panels compare the Navy global HYCOM analysis (black) to four other ocean analyses: NOAA/EMC RTOFS HYCOM (red), NRL IASNFS NCOM (blue), NOAA/NOS NGOM (magenta), and North Carolina State SABGOM ROMS (green).

The DWH oil spill aircraft observations also gave us a chance to perform a preliminary study of the impact that targeted (and gridded) aircraft observations will have on improving ocean model initialization for hurricane forecasting. In collaboration with NRL-Stennis (Ole Martin Smedstad and Pat Hogan), we performed twin Observing System Experiments (OSE) where two data-assimilative analyses were performed in the Gulf of Mexico. The first experiment assimilated all observations while the second denied only the P-3 profiles. The degree to which the upper-ocean temperature distribution was improved is demonstrated by the zonal cross-section across the detaching Eddy Franklin on 21 May 2010 (Figure 9). Denial of the P-3 observations doubled the temperature differences within the central region of the eddy above about 250 m, and also doubled the error along the eastern boundary of the eddy. Assimilation of P-3 profiles apparently improved the location of the eastern boundary of the eddy. The reduction in temperature bias (not included in Taylor diagrams) over all nine P-3 flight days is about 50% on average while the reduction of RMS error is 25 to 30% (not shown).

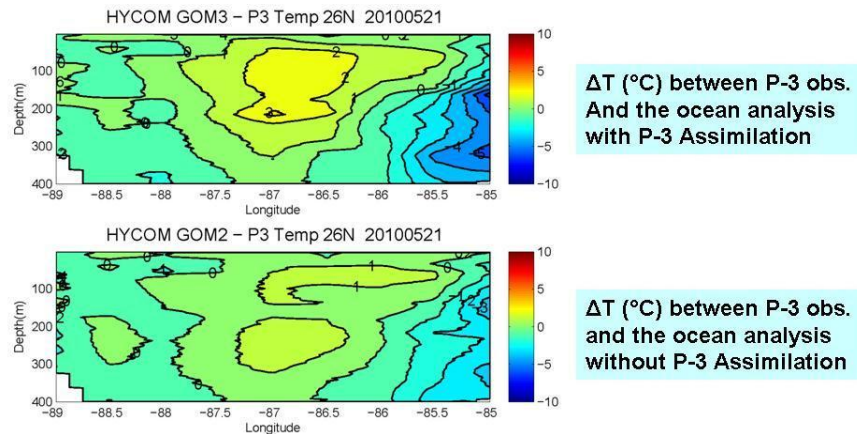


**Figure 9:** Zonal temperature difference sections between P-3 temperature profiles along  $25.5^{\circ}\text{N}$  across the detaching Eddy Franklin on 21 May 2010 and two Gulf of Mexico HYCOM analyses, one that assimilated all observations (top) and one that denied only the P-3 observations (bottom) Assimilation of P-3 observations reduced errors by up to 50% in both the center and eastern boundary of the detaching eddy.

A metric for evaluating ocean model analyses is utilized by comparing differing ocean model analyses to the observations using Taylor (2001) diagrams (Figure 10). These diagrams are first constructed by removing the overall mean from each field, normalizing each field by the variance of the observed field, and then calculating the three different but related metrics represented on this diagram (correlation coefficient, RMS amplitude, and RMS error). Errors are analyzed for two fields over all nine flight days: temperature between depths of 30 and 360 m from the aircraft and model profiles sampled at the same locations; and, horizontal maps of  $H_{20}$  calculated from these model and observed profiles (lower panel of Figure 10). To provide a reference point to assess analysis improvements resulting from data assimilation, a non-assimilative HYCOM experiment was also compared to observations, with the large black circles in the Taylor diagrams demonstrating the poor comparison between this numerical experiment and observations. Comparisons between seven data-assimilative ocean analyses and observations demonstrate that substantial error reductions result from assimilation of these observations, although the levels of error reduction varies among models. The model with the least error reduction (RTOFS-HYCOM: *Mehra and Rivlin* (2008)) is known to have a problem with their version of the model that will be fixed during the next upgrade of the operational system (*H. Tolman*, 2011, personal communication). Four models with intermediate error reduction (SABGOM-ROMS, <http://omgrhe.meas.ncsu.edu/Group/>; IASNFS NCOM (*Ko et al.*, 2008); NOAA/NOS NGOM <http://www.nauticalcharts.noaa.gov/csdl/NGOM.html>; and experiment GoM-HYCOM run for the OSE) did not assimilate the aircraft profiles. The two models that assimilated profile observations (global HYCOM (*Chassignet et al.*, 2007) and experiment P3-GoM-HYCOM) produced the analyses that resulted in the largest error reduction compared to the non-assimilative models, again demonstrating the positive impact of assimilating the aircraft observations. Based on these encouraging results, we recommend that targeted aircraft observations should be used to improve ocean model initialization, and that research should continue to further evaluate the impact of these observations and to devise observing strategies that will maximize this positive impact. These results depend on factors such as the ocean model, data assimilation method, and details of the assimilation cycle such as the observation time windows and whether it is performed in real-time versus delayed reanalysis mode. Further detailed studies must consider these factors and employ observations that were not assimilated (e.g., BOEMRE moorings) to determine the robustness of these conclusions.

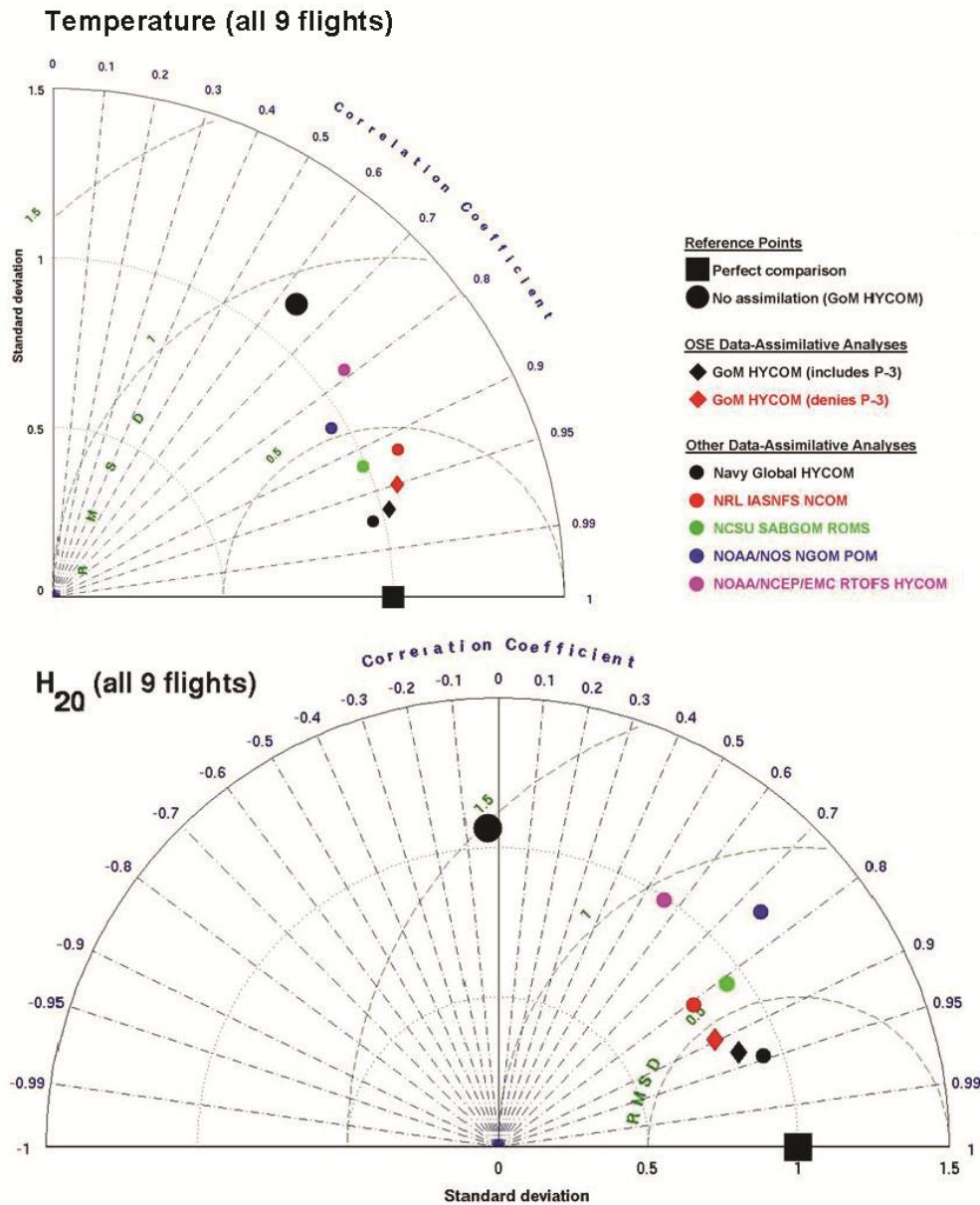


**Figure 10:** Taylor (2001) diagram metrics for (a) temperature ( $^{\circ}\text{C}$ ) between 30 and 360 m depth and (b)  $H_{20}$  (m) comparing several model analyses to the observed fields. A perfect comparison is marked by the large black square. The quality of each analysis field is inversely proportional to the distance from this reference point. The large black circle represents a non-assimilative GoM HYCOM run. Black and red diamonds compare the P3-GoM-HYCOM and GoM-HYCOM experiments performed at NRL for the P-3 OSE. Analyses from several other models are included for comparison. The only two models that assimilated aircraft observations are P3-GoM-HYCOM (black diamond) and global HYCOM (small black circle).

**Katrina and Rita:** Our original goal was to extend the analyses performed for Ivan to other storms, first to Katrina and Rita (2005) and then to Gustav and Ike (2008), to further evaluate model numerics and parameterizations. However, the Navy HYCOM analysis that we intended to use possessed very large cold biases in upper-ocean temperature that prevented accurate SST forecasts due to large overcooling. The bias is illustrated using Ocean Heat Content maps prior to Katrina (Figure 11). The

Navy plans to produce a multi-decadal reanalysis using the updated nowcast-forecast system that reduced the large cold bias as shown in Figure 8 above. This new product was initially intended to be available by the beginning of 2011, so we decided to delay the model evaluation prior to other storms until it became available. Unfortunately, this new analysis was delayed and the product release is now scheduled for early-to-mid 2013. We therefore proceeded with an observational and idealized model study of the impact of ocean features on upper-ocean SST cooling during Katrina and Rita using the predecessor model for HYCOM, the Miami Isopycnic-Coordinate Ocean Model (MICOM) (Jaimes *et al.*, 2011). The decision to use MICOM was made to take advantage of the slab mixed layer model, which permits simplified analyses of mixed layer budgets.

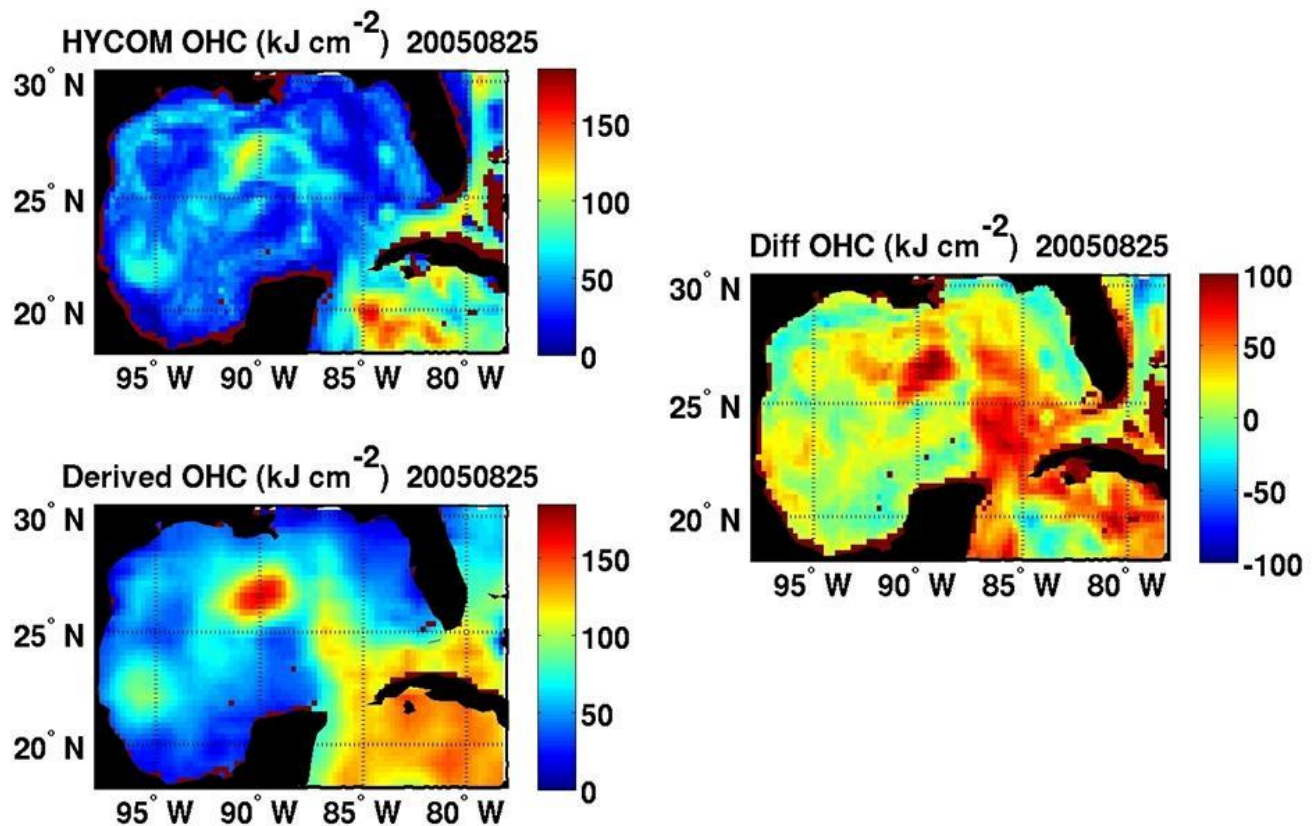


**Figure 11:** Ocean Heat Content relative to the 26°C isotherm prior to Hurricane Katrina on 25 August 2005. The left panels show OHC from the Navy HYCOM analysis (upper left) and derived from satellite altimetry, SST, and climatology (lower left; Mainelli *et al.*, 2008). The right panel shows the difference between the two (derived minus model analysis).

The 3-D upper ocean thermal and salinity structure in the LC system was surveyed with Airborne eXpendable BathyThermographs (AXBT), Current Profilers (AXCP), and Conductivity-Temperature-Depth sensors (AXCTD) deployed from four aircraft flights during September 2005, as part of a joint NOAA and National Science Foundation experiment (Rogers *et al.*, 2006; Shay, 2009). Flight patterns were designed to sample the mesoscale features in the LC system: the LC bulge (amplifying WCE), the WCE that separated from the LC about two days before the passage of Rita, and two CCEs that moved along the LC periphery during the WCR shedding event (Fig. 12). The first aircraft flight was

conducted on 15 Sept (two weeks after Katrina or one week before Rita, i.e. pre-Rita), the second and third flights were conducted during Rita's passage (22 and 23 Sept, respectively), and the final flight was conducted on 26 Sept, a few days after Rita's passage. Pre-Rita and post-Rita (not shown) flights followed the same pattern, while these other Rita flights focused on different regions along Rita's track.

Data acquired during pre-Rita includes temperature profilers from AXBTs, temperature and salinity profilers from AXCTDs, and current and temperature profilers from two AXCPs.

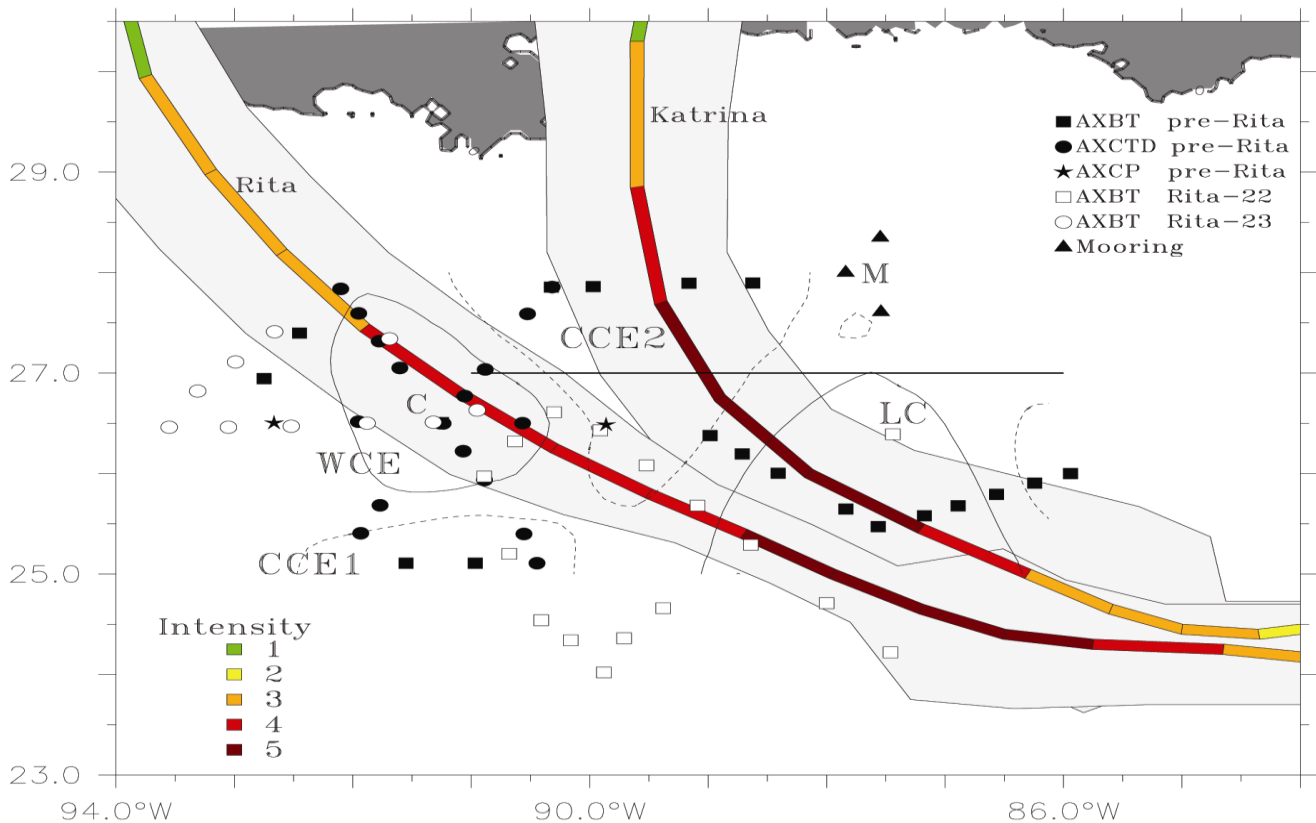


**Figure 12:** Airborne profilers deployed in Sept 2005 relative the track and intensity of Katrina and Rita (colored lines, with color indicating intensity as per the legend) over the LC System. The light-gray shades on the sides of the storm tracks represent twice the radius of maximum winds ( $R_{max}$ ). The contours are envelopes of anticyclonic (solid: WCE and LC) and cyclonic (dashed: CCE1 and CCE2) circulations. A set of AXBTs (not shown) was deployed after hurricane Rita (26 Sept), following a sampling pattern similar to pre-Rita (or post Katrina) (15 September). Point M indicates the position of several BOEMRE moorings used during this study, and Point C represents the drop site for profiler comparison (AXBT versus AXCTD). The transect along 27°N indicates the extent of vertical sections discussed in the text (Jaimes and Shay, 2009).

The combination of these airborne profiles of temperature and salinity measurements with the MMS-sponsored ADCP and CTD moorings were fairly consistent. These continuous measurements of ocean temperatures, salinities (via conductivities), and currents were acquired from the mooring sensors at intervals of 0.5 and 1 hr for CTDs and ADCPs, respectively. Although the moorings were located outside the radius of maximum winds  $R_{max}$  of hurricanes Katrina ( $\sim 4.5 R_{max}$  where  $R_{max} = 47$  km) and Rita ( $\sim 17.5 R_{max}$  where  $R_{max} = 19$  km) (Fig. 12), CCE2 that was affected by Katrina (category 5 status)

propagated over the mooring site  $\approx 2$  days after interacting with the storm. The circulation of the LC bulge that interacted with Rita (category 5 status) extended over the mooring  $\approx 3$  days after having been affected by the storm. Cluster averages of the thermal structure revealed that the LC cooled by  $1^\circ\text{C}$ , the WCE temperature cooled by  $0.5^\circ\text{C}$ , and the eddy shedding region and the CCE cooled by more than  $4.5^\circ\text{C}$  (Jaimes and Shay, 2009). These profiles will represent a challenge for the model especially placing the oceanic features in the correct position as suggested by the Ivan model analyses (Halliwell *et al.*, 2011).

Jaimes and Shay (2010) analyzed the contrasting thermal responses during and subsequent to Katrina and Rita by estimating the energetic geostrophic currents in these oceanic features. Increased and reduced oceanic mixed layer (OML) cooling was measured following the passage of both storms over cyclonic (CCE) and anticyclonic (WCE) geostrophic relative vorticity  $\zeta_g$ , respectively (Fig. 13). Within the context of the storms' near-inertial wave wake in geostrophic eddies, ray-tracing techniques in realistic geostrophic flow indicate that hurricane forced OML near-inertial waves are trapped in regions of negative  $\zeta_g$ , where they rapidly propagate into the thermocline. These anticyclonic-rotating regimes coincided with distribution of reduced OML cooling, as rapid downward dispersion of near-inertial energy reduced the amount of kinetic energy available to increase vertical shears at the OML base. By contrast, forced OML near-inertial waves were stalled in upper layers of cyclonic circulations, which strengthened vertical shears and entrainment cooling. Upgoing near-inertial energy propagation dominated inside a geostrophic cyclone that interacted with Katrina; the salient characteristics of these upward propagating waves were: (i) radiated from the ocean interior due to geostrophic adjustment following the upwelling and downwelling processes; (ii) rather than with the buoyancy frequency, they amplified horizontally as they encountered increasing values of  $\zeta_g$  during upward propagation; (iii) produced episodic vertical mixing through shear-instability at a critical layer underneath the OML. To improve the prediction of TC-induced OML cooling, models must capture geostrophic features; and turbulence closures must represent near-inertial wave processes such dispersion and breaking between the OML base and the thermocline. Oceanic response models must capture this variability to get the correct entrainment in cold and warm oceanic features. For the first time, these effects of the near-inertial wave wake in the presence of a background eddy field are now being explored in this study using these measurements and results from analytical theory.

To examine the observed levels of cooling in the WCE ( $\sim 0.5$  to  $1^\circ\text{C}$ ) and CCE ( $\sim 4^\circ\text{C}$ ), we used the predecessor of the HYCOM model (e.g, Miami Isopycnic Coordinate Ocean Model, or MICOM) to reduce spurious vertical mixing in a highly idealized configuration. Isopycnic coordinate models suppress the spurious numerical dispersion of material and thermodynamic properties. MICOM consists of four prognostic equations for the horizontal velocity vector, mass continuity or layer thickness tendency, and two conservative equations for salt and heat (Bleck and Chassignet, 1994). A modified version of MICOM (Chérubin *et al.*, 2006) is used to include a fourth-order scheme for the non-linear advective terms in the momentum equations and biharmonic horizontal diffusion. This modified version reduces numerical noise associated with dispersive effects and the development of shocks in frontal regimes. The model approach used in Jaimes *et al.* (2011) is:

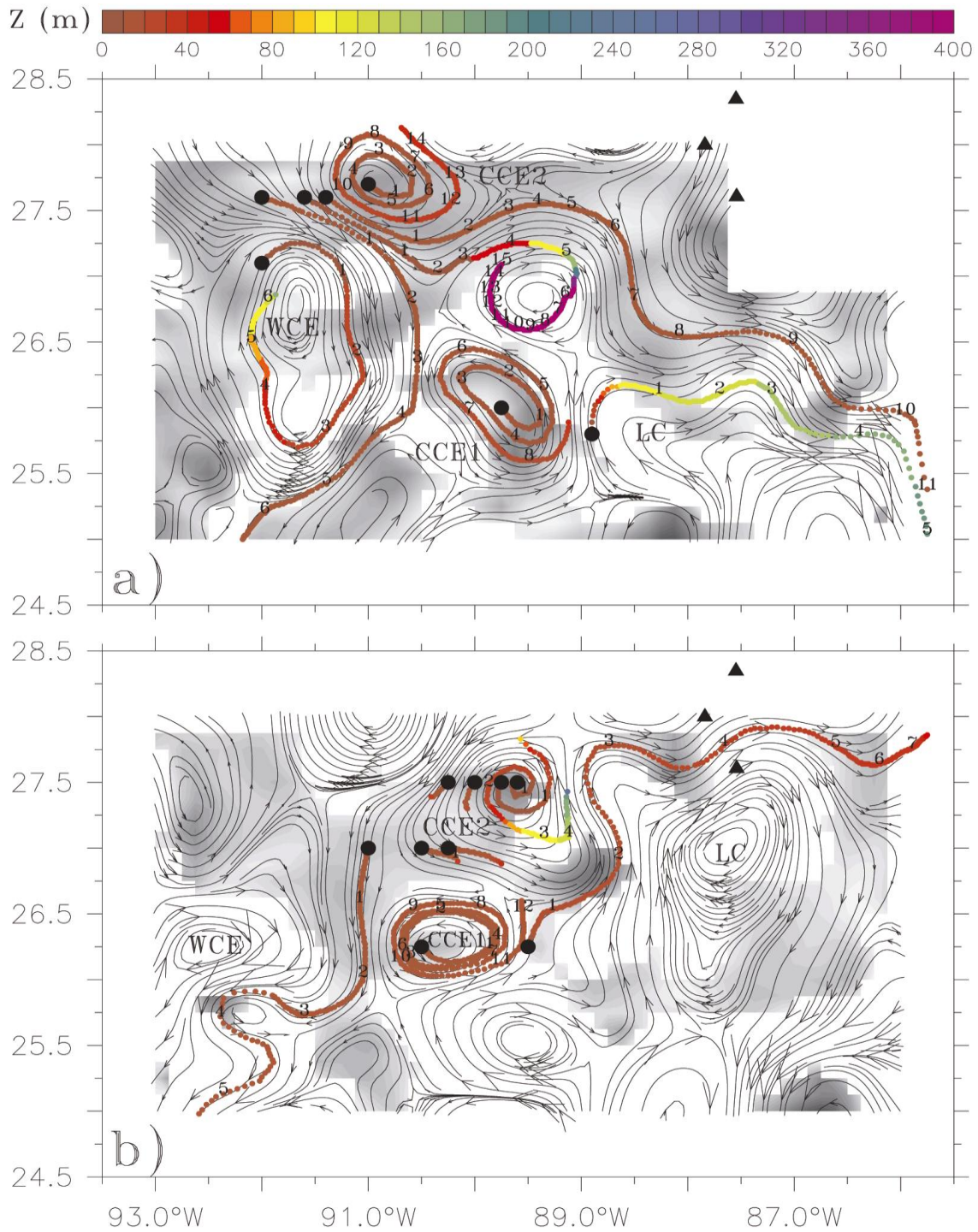


**Figure 13:** Near-inertial wave ray-tracing based on Kunze's (1985) model, for (a) Katrina and (b) Rita. The numbers along the wave rays indicate inertial periods (one inertial period is  $\sim 25.5$  hr), dots are hourly positions, color is the ray's depth level, and the flow lines are from geostrophic flow fields derived from (a) post Katrina (15 Sept.) and (b) post Rita (26 Sept.) airborne-based data. The gray shades represent regions where the effective Coriolis parameter exceeds  $> 0.2$ . This ratio and the flow lines were calculated from depth-averaged velocity fields.

- 1) Buoyancy fluxes are ignored both in the density equation and in the turbulent kinetic energy (TKE) equation (for consistency) because the interest is to isolate the OML response due to internal oceanic processes, which have been proven to drive most of the TC-induced OML cooling (Price, 1981; Greatbatch, 1984; Shay *et al.*, 1992; Jacob *et al.*, 2000; Hong *et al.*, 2000; Shay and Brewster, 2010).
- 2) The turbulence closure for the OML only considers: (i) instantaneous wind erosion by the wind-driven frictional velocity (Kraus and Turner, 1967:KT); and, (ii) vertical shear-driven entrainment at the OML base and over the stratified ocean below (Price *et al.*, 1986: PWP). These turbulence closures were chosen by reason of their mathematical simplicity, and because they provide direct physical insight on important mixing process observed over the thermocline inside a CCEs impacted by Katrina (JS09; JS10).
- 3) Idealized vortices (WCEs and CCEs) are initialized with an analytical model and density structures from direct measurements obtained during Katrina and Rita; these vortices satisfy the QG approximation.
- 4) An  $f$ -plane is used to prevent self-propagation of the QG vortices, which facilitates analyzing the near-inertial response at fixed points inside the stationary vortex. This approach cancels horizontal dispersion of near-inertial oscillations (NIOs) by meridional gradients in planetary vorticity (Gill, 1984). Any resulting horizontal wave dispersion is purely driven by  $\zeta_g$ .

The computational domain is a 2000×2000 km square ocean with an initially circular QG vortex (WCE or CCE) of ~150 to 300 km in diameter located at the center. The vertical extension of the vortex is 950 m, representative of Gulf of Mexico’s WCEs and CCEs. The vortex is located on top of an initially quiescent layer of 4000 m in thickness. The bottom is flat, and lateral boundary conditions are closed. The central latitude of the domain is 26.9°N, which allows reproducing near-inertial responses at the latitude of moorings used in JS09 and JS10. The horizontal grid resolution is 10 km that allows the resolution of horizontal wavelengths larger than 20 km. Horizontal resolutions of ~10 km are adequate for these investigations (Halliwell *et al.*, 2011).

Three vertical resolutions were used: 12, 23, and 47 isopycnic layers (Figure 14). In every case, the model’s top layer represents the OML. The initial OML thickness is the same for every vertical resolution, and it is determined by the analytical model as a function of the radius of the vortex, the target maximum azimuthal velocity, and density profiles from observational data. Given that experiments with higher vertical resolution improve the representation of the stratified ocean below the OML, OML cooling, and vertical dispersion of near-inertial energy, the discussion focus on the 47-layer numerical experiments that have vertical resolution of 10 m between the OML and the thermocline, allowing the model to resolve vertical wavelengths larger than 20 m. (The vertical sampling grid in the moorings used in Jaimes and Shay (2009, 2010) is ~8 m.)

**Table 3:** Characteristics of geostrophic features in the Gulf of Mexico where LC represents a clockwise-rotating ocean feature where  $U$ ,  $L$ , OML and  $Ro$  represent current, diameter, ocean mixed layer depth, and Rossby number of the warm and cold eddies, respectively.

Parameter	Observed		Modeled			
	LC/WCE	CCE	WCE1	WCE2	CCE1	CCE2
$U$ [ $\text{m s}^{-1}$ ]	1–2	0.5–0.8	0.95	1.5	0.6	0.8
$L$ [km]	200–400	100–150	250	300	150	150
OML [m]	~80	~30	~65	~80	~30	~25
$Ro$ ( $U/fL$ )	0.05–0.1	0.05–0.08	0.06	0.08	0.06	0.08

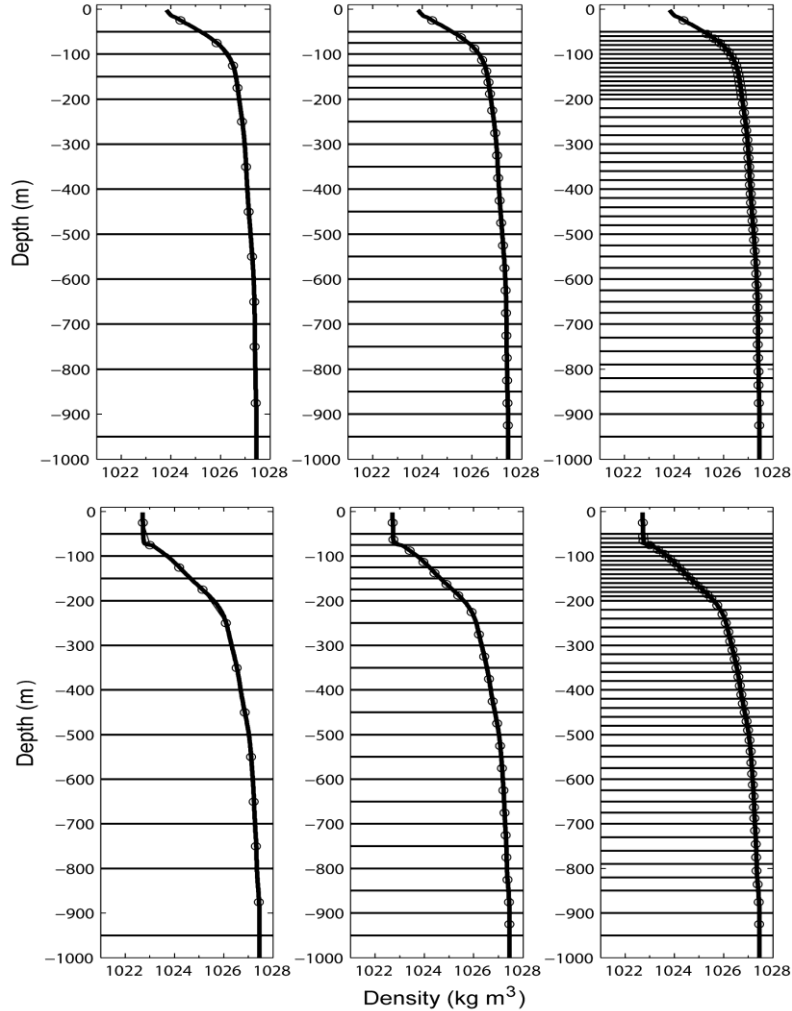


**Figure 14:** Model isopycnic layers: 12, 23, and 47, from left to right panels. Upper (lower) panels are for CCEs (WCEs). The circles represent the model density, and the bold line is the observed density profile (smoothed via polynomial fit). The horizontal lines represent the initial layer thickness outside the QG vortex. The top layer is the OML, and the bottom layer is not shown.

Based on observed characteristics of Gulf of Mexico’s WCEs and CCEs, four eddies are reproduced (Table 3): WCE1 ( $Ro=0.06$ ), WCE2 ( $Ro=0.08$ ), CCE1 ( $Ro=0.06$ ), and CCE2 ( $Ro=0.08$ ). These vortices are initialized in model runs with parameters summarized in Table 3. The main focus is on CCE2 and WCE1, because these model vortices are similar to eddy features that interacted with Katrina (CCE) and Rita (LC bulge). For these cases, the incorporation of vertical shear-driven mixing parameterization ( $R_b=1$  in PWP), reproduced additional average OML cooling of about  $0.1^\circ\text{C}$  on the right side of the storm track inside WCE1 (Fig. 15a, c). Maximum cooling of about  $0.7^\circ\text{C}$  was reproduced by KT+PWP in the vicinity of the moorings, compared with maximum cooling of  $\sim 0.5^\circ\text{C}$  by KT. The small difference between KT and KT+PWP indicates that in this warm anticyclone most of the cooling was driven by instantaneous wind erosion, and near-inertial vertical shear was not an important cooling mechanism, in accord with observational evidence presented elsewhere (Shay and Uhlhorn, 2008; JS09; JS10). In the case of CCE2, PWP caused additional cooling of more than  $1.2^\circ\text{C}$  that confirms the importance of near-inertial vertical shears for OML cooling in this oceanic cyclone (Fig. 15b, d). Inside CCE2, near-inertial vertical shear instability impacted both the magnitude of the cooling, and the horizontal extension of the region of cooling. These results are consistent with the observed cooling during Katrina and Rita in the LC and WCE (Jaimes and Shay 2009, 2010).

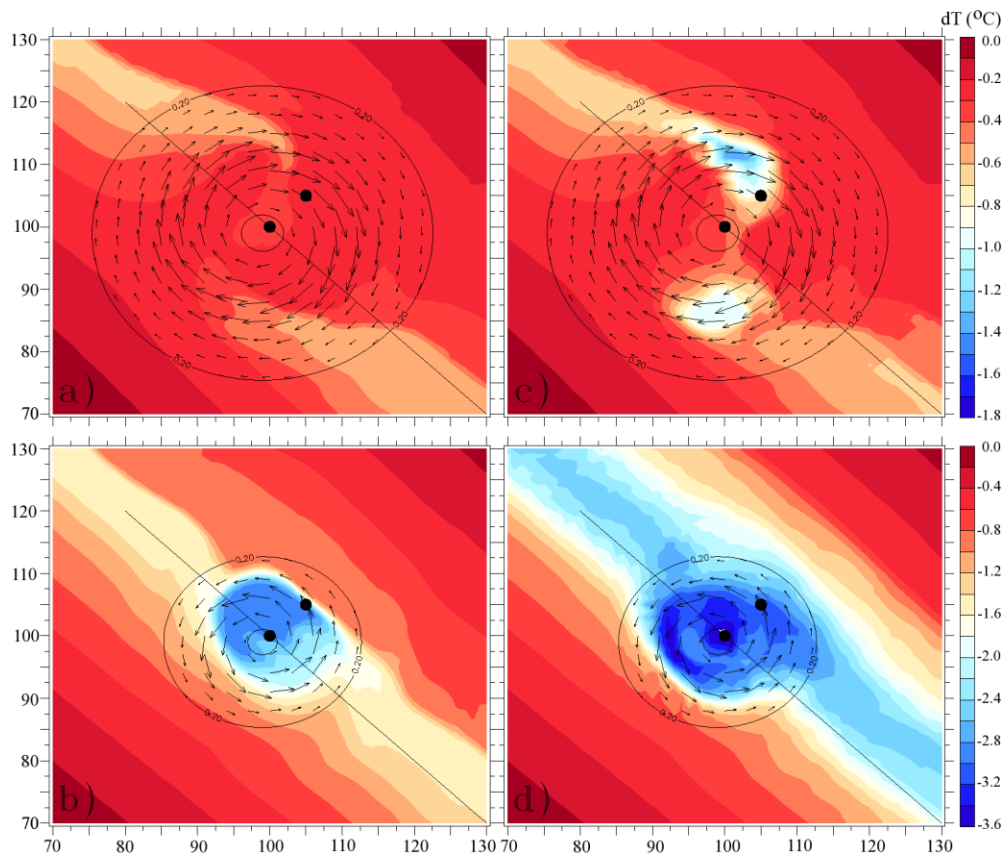


**Figure 15:** OML cooling  $dT$  ( $^{\circ}\text{C}$ ) in WCE1 (upper panels) and CCE2 (lower panels), in terms of the KT turbulence closure (a and b), and KT+PWP (c and d), where  $dT = T(\text{IP} = 3) - T(\text{IP} = -1.5)$ . Notice the difference in temperature scale between upper and lower panels. Vectors represent pre-storm currents in the OML and black line is trajectory of an idealized storm moving at  $6 \text{ m s}^{-1}$  (from Jaimes *et al.*, 2011).

**Gustav and Ike:** Hurricanes Gustav and Ike moved over the Gulf of Mexico and interacted with the LC and the eddy field in August and September 2008 (Meyers, 2011). As part of the NCEP tail Doppler Radar Missions, oceanic and atmospheric measurements were acquired on sixteen NOAA WP-3D research flights for pre, during and post-storm flights. In total, over 400 AXBTs and 200 GPS sondes were deployed to document the evolving atmospheric and oceanic structure over warm and cooler ocean features in these two hurricanes (Table 4). In addition, forty-five GPS sondes were deployed on 1 Sept over the float and drifter array deployed by the United States Air Force WC-130J north and west of the Loop Current. Similar to CBLAST observations, the float array also included the EM/APEX floats that measure the horizontal velocities as well as temperature and salinity structure (Sanford *et al.*, 2007). However, this effort significantly improved upon the CBLAST effort in that the forcing is better documented with the combination of GPS sondes and the Stepped Frequency Microwave Radiometer (Uhlhorn *et al.*, 2007) directly over the float and drifter array. In addition, each research flight carried AXBTs to document the evolving upper ocean thermal structure across the entire Gulf of Mexico for the first time. Note that the AXBTs were deployed to document pre- and post-storm oceanic variability in the Loop Current and its periphery where float and drifter measurements would be advected away from the storm track by the energetic ocean current. This is precisely why we need current profilers to deploy from the research aircraft on a routine basis. As stated above, for Katrina and Rita, modeling studies of Gustav and Ike were also delayed until the new Navy ocean analysis product becomes available for initialization.

**Table 4:** Summary of atmospheric (GPS) and oceanic (AXBT) profiler measurements from sixteen flights acquired in hurricanes Gustav and Ike in 2008. Numbers in parentheses represent profiler failures.

Hurricane Gustav				Hurricane Ike			
Date	Flight	GPS	AXBT	Date	Flight	GPS	AXBT
(2008)				(2008)			
28 Aug	RF43	0	49(2)	08 Sep	RF43	0	47(2)
29 Aug	RF42	12(4)	16(0)	09 Sep	RF42	19	6(0)
30 Aug	RF43	9	19(2)	10 Sep	RF42	17(1)	10(2)
31 Aug	RF42	24	16(1)	10 Sep	RF43	11	20(7)
31 Aug	RF43	17(2)	19(1)	11 Sep	RF42	16	10(1)
01 Sep	RF43	44	19	11 Sep	RF43	10	22(3)
03 Sep	RF43	4	54(4)	12 Sep	RF42	21(2)	10(4)
				12 Sep	RF43	8	20(4)
				15 Sep	RF43	0	61(5)
Total	7	111(6)	191(10)		9	111(3)	216(28)

**Tropical Storm/Hurricane Isaac:** Profiler measurements were acquired during its passage over the Gulf of Mexico from both NOAA WP-3D and USAF WC-130 aircraft in August 2012. In total, the NOAA WP-3D deployed 218 AXBTs, AXCTDs, and AXCPs from six flights including pre and post in the north central part of the Gulf. These data have been processed and are undergoing final quality control checks. As part of a US Navy sponsored AXBT demonstration project, approximately 125 AXBTs were deployed from the USAF aircraft and ten drifting buoys equipped with thermistor strings were deployed normal to Isaac track as part of a NOAA climate program conducted by scientists at AOML. Atmospheric sondes were also deployed from the NOAA WP-3D with oceanographic profilers that provide the lower part of the atmospheric boundary layer and the upper ocean simultaneously. Thus, we are in the process of combining these data sets to provide a more complete data set for subsequent analysis and modeling.

During Isaac's movement across the Gulf, it was characterized as a broad, fast storm moving between 7 to 8 m s<sup>-1</sup> with a radius of maximum winds of more than 90 km and decreasing to about 60 km. As Isaac approached the coast, the storm speed decreased to about 2 m s<sup>-1</sup> over Sigsbee Escarpment when Isaac became a category-1 hurricane due south of Louisiana. Thus, a key objective of these oceanographic measurements was to observe the level of upwelling across the Gulf since isopycnal displacements scale as the inverse translation speed ( $U_h^{-1}$ ). Based on scaling arguments, these displacements were less than 10 m in the central Gulf, increasing to more than 20 m just along the Escarpment.

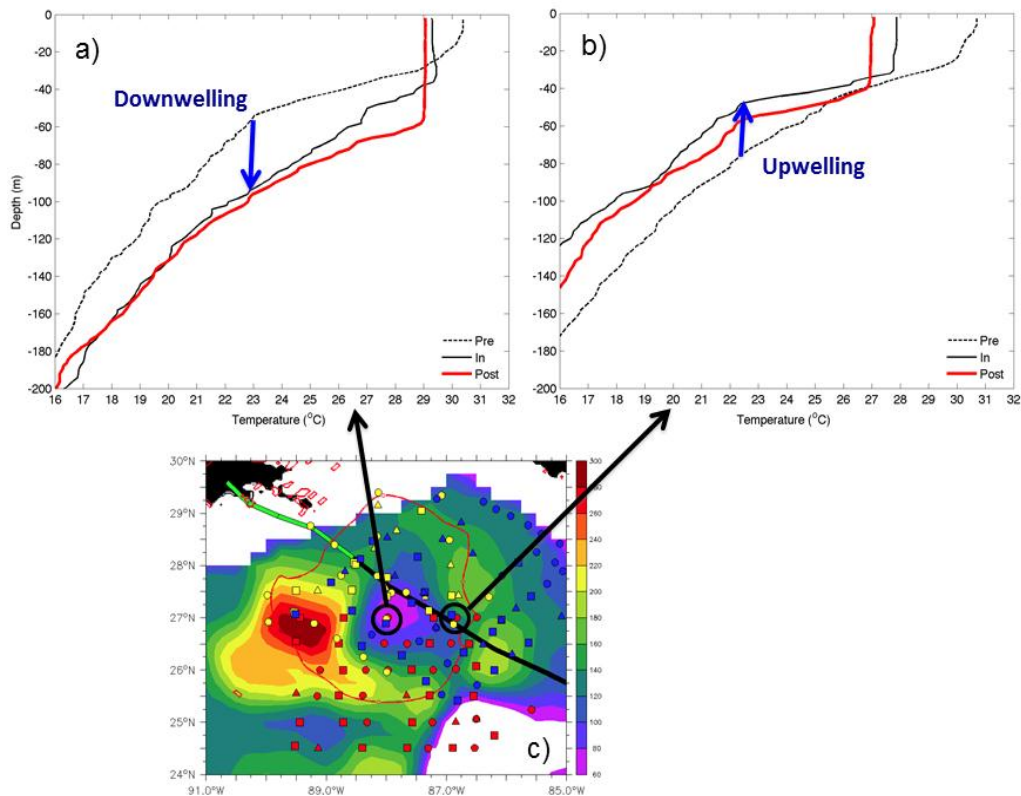


**Figure 16:** Thermal profiles ( $^{\circ}\text{C}$ ) comparisons on a) left and b) right side of hurricane Isaac from pre, during and post flights profiler measurements emphasizing downwelling and upwelling processes in the c) depth of the  $20^{\circ}\text{C}$  isotherm determined from the pre-storm flight in mid August. The red contour represents the positive cyclonically rotating wind stress curl.

As suggested in recently published studies (Jaimes *et al.*, 2011), these vertical displacements of isopycnals are also a function of the curl of geostrophic currents, rather than just a function of the wind stress alone. In this context, surface wind stress was estimated from the NOAA HRD HWIND product using the Donelan *et al.* (2004) surface drag coefficient. During intensification to hurricane (28 Aug), the cyclonically rotating wind stress curl extended over a region of more than 300 km in diameter ( $\sim 5R_{max}$ ). The wind stress curl scaled well with the local Coriolis parameter. The broad wind stress curl induced strong upwelling and downwelling signals on the right and left side of the track, respectively (Figure 16). These processes were enhanced in the cold core eddy on the right side of Isaac's track. That is, divergent wind-driven ocean currents in the surface mixed layer were  $0.6$  and  $0.8 \text{ m s}^{-1}$ , which were less than those predicted with scaling arguments. As in other documented cases in the Gulf, the upper ocean modulated Isaac's intensity. Moreover, the deeper isopycnal displacements show the oceanic response is not limited to just the upper ocean as upwelling tends to get enhanced along steep bottom slopes and strong background geostrophic currents. This is also consistent with the Ivan data where the response was observed at 950 m along the northern rim of the DeSoto Canyon. Such 3-D observations of the response must be captured by the oceanic models that are part of the coupled model strategy at NCEP to eventually forecast hurricane intensity.

Hurricane Forecast Improvement Project (HFIP)-Sponsored Workshop: In September 2012, a workshop was convened at NCEP to review progress on Air-Sea Interactions During Tropical Cyclones since the inaugural meeting in May 2005 (Shay *et al.*, 2006). There were about 15 attendees (Table 5)

compared to the larger earlier meeting in 2005. In a similar format to that used in the earlier meeting, the breakout group was structured to be atmospheric boundary layer, upper ocean and air-sea interfaces all addressing key cross-cutting questions aimed at improving the operational oceanic and coupled models at NCEP in support of HFIP objectives. A report is currently being drafted by Drs. Halliwell (AOML) and Kim (NCEP), the co-conveners of the workshop. The report will emphasize the next steps that must be taken to evaluate and improve the performance of coupled forecast models beyond the current practice of focusing almost entirely on errors in forecast track and intensity, and beyond focusing solely on SST in evaluating the ocean model response. Once that report is complete it will be available for wider dissemination to the HFIP community.

**Table 5:** *Invited Participants at an HFIP-sponsored Workshop on Ocean-Atmosphere Coupling at NCEP on 19 and 20 September 2012 that included federal, academic and private sector scientists from across the country. The Co-conveners are bold-faced in the table.*

Name	Affiliation	Attendance (I = in person; R = remote)
Jian-Wen Bao	NOAA/ESRL	I
Shaowu Bao	NOAA/ESRL	I
Pete Black	SAIC / NRL-MRY	I
Sue Chen	NRL-MRY	R
Joe Cione	NOAA/AOML/HRD	I
Chris Fairall	NOAA/ESRL	I
Isaac Ginis	URI/GSO	I
<b>George Halliwell</b>	NOAA/AOML/PhOD	I
<b>Hyun-Sook Kim</b>	NOAA/NCEP/EMC	I
Frank Marks	NOAA/AOML/HRD	R
Daniel Melendez	NOAA/NWS	I
Elizabeth Sanabia	USNA	I
Nick Shay	UM/RSMAS	I
Hendrik Tolman	NOAA/NCEP/EMC	I
Eric Uhlhorn	NOAA/AOML/PhOD	I

**Summary:** Since JHT support commenced in 2007, this study has been very productive in combining both basic and applied research aimed at operational forecast models. At NCEP, this effort sought to evaluate “coupled” modeling efforts that have not been systematically (and carefully) addressed with respect to key scientific issues related to the ocean models used to eventually couple to HWRF—a topic recently discussed at the NCEP meeting in 2012. In addition, there has not been appropriate development of metrics to assess oceanic model performance within a consistent fluid dynamical framework such as Taylor (2001) diagrams discussed herein. Using data as our guide to modeling, we have emphasized the need for high quality ocean data to perform these evaluations. For example, we made significant progress on this grant from numerical simulations with complex oceanic conditions observed during hurricane Ivan’s passage (Halliwell *et al.*, 2011), hurricane’s Katrina and Rita (Jaimes *et al.*, 2011), DWH Oil Spill disaster (Shay *et al.*, 2011) and now Hurricane Isaac (Jaimes *et al.*, 2013).

With respect to oceanic impacts, intensity changes over warm and cold eddies represent regimes of less and more negative feedback, respectively, to the atmosphere. Thus, the ocean is important in the coupled forecast problem. Accordingly, we have completed the analysis of Ivan within the context of mixing and upwelling and downwelling processes by comparing simulations of the currents and shears to *in situ* measurements from the SEED moorings (Teague *et al.*, 2007). In addition, we have analyzed pre- Katrina and Rita observations including detailed ray-tracing techniques (Kunze, 1985) to demonstrate the markedly different character of the forced near-inertial motions (Jaimes and Shay, 2010). As well as mixing processes from idealized MICOM simulations (Jaimes *et al.*, 2011). We will conduct a similar analysis on the HYCOM simulations when realistic ocean conditions are available from the Navy reanalysis to assess the impact on the mixing schemes via shear-instability. Over the past four years, these combined numerical and observational efforts here have benefitted from students (E. Uhlhorn, B. Jaimes, P. Meyers) to examine model sensitivities and comparing these simulations to the various data sets.

During the summer of 2010, several near weekly flights in support of Deep Water Horizon Oil Spill certainly improved ocean model initialization through advanced data assimilation methods as a warm eddy was shed from the LC over that three month period (Shay *et al.*, 2011). This is a regime where hurricanes can rapidly weaken or deepen as they interact with both warm and cold ocean features. Even under quiescent conditions, these data sets represent a challenge to the model to get the 3-D temperature, salinity and current structure accurately through vertical projection of the altimetry data. Processed profiler data from Gustav and Ike flights are being synthesized with drifter and float data to provide a clearer description of the cold wake northeast of the Loop Current where cooling exceeded 3°C compared to the Loop Current of about 1°C. Finally, we note that the Navy is now in the process of running a HYCOM global ocean reanalysis from 1993 to the present using the new vertical projection method. The reduced errors and biases expected with this reanalysis (see Figure 8) will enable us to evaluate model performance for earlier storms (time permitting) without the large negative impact of the cold bias that previously limited our ability to evaluate and improve ocean model parameterizations. Efforts to transition these results to EMC for improving ocean model initialization must continue.

The analysis will also benefit from the 5-year BOEMRE Loop Current Dynamics Study that includes extensive *in situ* measurements. Finally, in addition to the aircraft-based measurements from Isaac in August 2012, the modeling study will also benefit from the moored data acquired across the northern GoM acquired in support of the various Gulf of Mexico Research Institute consortia. Thus, we have an opportunity to put together a fairly complete data set for analysis and for both research modelers and the operational community at NCEP to assess their model performance.

*Acknowledgments:* This study has benefited from the interactions with Mr. William Teague in the Oceanography Department at the US Naval Research Laboratory at Stennis Space Center, Dr. Alexis Lugo-Fernandez at BOEMRE who provided ADCP moorings. This project has also benefited from support from the NSF, NASA, BOEMRE and NOAA (OR&R and OAR) in the acquisition and analysis of *in situ* and satellite measurements acquired during hurricanes and Deep Water Horizon oil spill in collaboration with NOAA's Hurricane Research Division (Drs. Frank Marks, Rob Rogers, Eric Uhlhorn) and Aircraft Operations Center (Dr. James McFadden, Capt. Brad Kearse). Dr. Benjamin Jaimes has also contributed to this effort. The Isaac data were acquired as part of a project sponsored by the Deep-C Gulf of Mexico Research Institute consortium project to Shay at UM/RSMAS in collaboration with ongoing NOAA HRD efforts such as IFEX field work.

## References (\* Represents Publications from Support 2007-2012)

- Bleck, R., and E. P. Chassignet, 1994: Simulating the oceanic circulation with isopycnic-coordinate models. *The Oceans: Physical-Chemical Dynamics and Human Impact*, S. K. Majumdar et al., Eds., The Pennsylvania Academy of Science, 17-39.
- Chérubin, L. M., Y. Morel, and E. P. Chassignet, 2006: Loop Current ring shedding: The formation of cyclones and the effect of topography. *J. Phys. Oceanogr.*, **36**, 569–591.
- Donelan, M. A., B. K. Haus, N. Reul, W. J. Plant, M. Stiassine, H. Graber, O. Brown, and E. Saltzman, 2004: On the limiting aerodynamic roughness of the ocean in very strong winds. *Geophys. Res. Letters.*, **31L18306**, doi:1029/2004GRL019460.
- Falkovich, A., I. Ginis, and S. Lord, 2005: Implementation of data assimilation and ocean initialization for the coupled GFDL/URI hurricane prediction system. *J. Atmos. and Ocean. Tech.*, **22**, 1918–1932.
- \*Halliwell, G., L. K. Shay, S. D. Jacob, O. Smedstad, and E. Uhlhorn, 2008: Improving ocean model initialization for coupled tropical cyclone forecast models using GODAE nowcasts. *Mon. Wea. Rev.*, **136 (7)**, 2576–2591.
- \*Halliwell, G. R., L. K. Shay, J. Brewster, and W. J. Teague, 2011: Evaluation and sensitivity analysis to an ocean model response to hurricane Ivan. *Mon. Wea. Rev.*, **139**, 921-945.
- Hong, X., S. W. Chang, S. Raman, L. K. Shay, and R. Hodur, 2000: The interaction between Hurricane Opal (1995) and a warm core ring in the Gulf of Mexico. *Mon. Wea. Rev.*, **128**, 1347–1365.
- Jacob, S. D., L. K. Shay, A. J. Mariano, and P. G. Black, 2000: The 3D mixed layer response to Hurricane Gilbert. *J. Phys. Oceanogr.*, **30**, 1407–1429.
- \*Jaimes, B., 2009: On the oceanic response to tropical cyclones in mesoscale ocean eddies. PhD Dissertation. Division of Meteorology and Physical Oceanography, Rosenstiel School of Marine and Atmospheric Science, University of Miami, Coral Gables, FL 33134, 143 pp.
- \*Jaimes, B. and L. K. Shay, 2009: Mixed layer cooling in mesoscale eddies during Katrina and Rita. *Mon. Wea. Rev.*, **137**, 4188–4207.
- \*Jaimes, B. and L. K. Shay, 2010: Near-inertial wave wake of hurricanes Katrina and Rita in mesoscale eddies. *J. Phys. Oceanogr.*, **40**, 1320-1337.
- \*Jaimes, B., L. K. Shay, and G. R. Halliwell, 2011: The response of quasi-geostrophic oceanic vortices to tropical cyclone forcing. *J. Phys. Oceanogr.*, **41**, 1965-1985.
- Jaimes, B., L. K. Shay, J. Brewster, R. Schuster, M. Powell, and F. Marks, 2012: Observed upwelling processes during hurricane Isaac. 67<sup>th</sup> Interdepartmental Hurricane Conference, Office of the Federal Coordinator, Silver Spring, MD, (Abstract)
- Jarosz, E., D. A. Mitchell, D. W. Wang, and W. J. Teague, 2007: Bottom-up determination of air-sea momentum exchange under a major tropical cyclone. *Science*, **315**, 1707-1709.

Kraus, E. B., and J. S. Turner, 1967: A one-dimensional model of the seasonal thermocline. II: The general theory and its consequences, *Tellus*, **19**, 98-105.

\*Mainelli, M., M. DeMaria, L. K. Shay and G. Goni, 2008: Application of oceanic heat content estimation to operational forecasting of recent category 5 hurricanes, *Wea and Forecast.*, **23(1)**, 3-16.

\*Meyers, P. C., 2011: Development and analysis of the Systematically Merged Atlantic Regional Temperature and Salinity (SMARTS) climatology for satellite-derived ocean thermal structure. M. S. Thesis, University of Miami, Coral Gables, FL, 33134, 99 pp.

Murphy, A. H., 1988. Skill scores based on the mean square error and their relationships to the correlation coefficient. *Mon. Wea. Rev.*, **116**, 2417-2424.

Nowlin, W. D. Jr., and J. M. Hubertz, 1972: Contrasting summer circulation patterns for the eastern Gulf. In: Contributions on the Physical Oceanography of the Gulf of Mexico, *Texas A&M Oceanogr. Stud.*, vol. **2**, edited by L. R. A. Capurro and J. L. Reid, pp. 119-138, Gulf Pub. Co.

Price, J. F., R. A. Weller, and R. Pinkel, 1986: Diurnal cycling: Observations and models of the upper ocean response to diurnal heating, cooling, and wind mixing. *J. Geophys. Res.*, **91(C7)**, 8411-8427.

Powell, M. D., P. J. Vickery, and T. A. Reinhold, 2003: Reduced drag coefficient for high wind speeds in tropical cyclones. *Nature*, **422**, 279-283.

Reynolds, R. W., T. M. Smith, C. Liu, D. B. Chelton, K. S. Casey, and M. G. Schlax, 2007: Daily high-resolution blended analyses for sea surface temperature. *J. Climate*, **20**, 5473-5496.

Rogers, R., S. Aberson, M. Black, P. Black, J. Cione, P. Dodge, J. Dunion, J. Gamache, J. Kaplan, M. Powell, L. K. Shay, N. Surgi, E. Uhlhorn, 2006: The intensity forecasting experiment (IFEX), a NOAA multiple year field program for improving intensity forecasts. *BAMS*, **87(11)**, 1523-1537.

\*Rappaport, E. N., J. L. Franklin, M. DeMaria, A. B. Shumacher, L. K. Shay and E. J. Gibney, 2010: Tropical cyclone intensity change before U. S. Gulf coast landfall. *Wea. and Forecast.*, **25**, 1380-1396.

Sanford, T B., J. F. Price, J. Girton, and D. C. Webb, 2007: Highly resolved observations and simulations of the oceanic response to a hurricane. *Geophys. Res. Lett.*, **34**, L13604, 5 pp.

\*Shay, L.K., 2009: Upper Ocean Structure: a Revisit of the Response to Strong Forcing Events. *In: Encyclopedia of Ocean Sciences*, ed. John Steele, S.A. Thorpe, Karl Turekian and R. A. Weller, Elsevier Press International, Oxford, UK, 4619-4637, doi: 10.1016/B978-012374473-9.00628-7.

\*Shay, L. K., 2010: Air-Sea Interactions in Tropical Cyclones (Chapter 3). In *Global Perspectives of Tropical Cyclones*, 2nd Edition, Eds. Johnny C. L. Chan and J. D. Kepert, *World Scientific Publishing Company*: Earth System Science Publication Series, London, UK, 93-131.

\*Shay, L. K., 2010: Air-sea interface and oceanic influences (Chapter 1.3). *Topic Chairman and Rapporteurs Report for Tropical Cyclone Structure and Structure Change of the 7<sup>th</sup> WMO International Workshop on Tropical Cyclones (IWTC-7) 15-21 Nov 2010 in St. Denis, La*

*ReUnion*, France, World Meteorological Organization Tropical Meteorology Research Series, **WMO TD-1561**, Eds. C. Velden, and J. Kepert, Geneva, Switzerland, 48pp.

\*Shay, L. K., B. Jaimes, J. K. Brewster, P. Meyers, C. McCaskill, E. W. Uhlhorn, F. D. Marks, G. R. Halliwell, O. M. Smedsted and P. Hogan, 2011: Airborne surveys of the Loop Current complex from NOAA WP-3D during the Deep Water Horizon oil spill. Eds, Y. Liu and D. Streets, AGU Monograph Special Issue, Monitoring and Modeling Deep Water Horizon Oil Spill, (*In Press*)

Shay, L. K., A. J. Mariano, S. D. Jacob, and E. H. Ryan, 1998: Mean and near-inertial response to hurricane Gilbert. *J. Phys. Oceanogr.*, **28**, 858–889.

Shay, L. K., N. Surgi, and J. Cione. 2006: Air-Sea interactions in tropical cyclones, *Proceedings from a National Center for Environmental Prediction Workshop*, Camp Springs, Maryland, 24-25 May 2005, 34pp.

\*Shay, L. K. and E. Uhlhorn, 2008: Loop Current Response to hurricanes Isidore and Lili, *Mon. Wea. Rev.*, **137**, 3248-3274.

\*Shay, L. K., and J. Brewster, 2010: Oceanic heat content variability in the eastern Pacific Ocean for hurricane intensity forecasting. *Mon. Wea. Rev.*, **138(6)**, 2110-2131.

Taylor, K. E., 2001: Summarizing multiple aspects of model performance in a single diagram. *J. Geophys. Res.*, **106**, 7183-7192.

Teague, W. J., E. Jarosz, D. W. Wang, and D. A. Mitchell, 2007: Observed oceanic response over the upper continental slope and outer shelf during Hurricane Ivan, *J. Phys. Oceanogr.* **37**, 2181-2206.

Uhlhorn, E. W., P. G. Black, J. L. Franklin, M. Goodberlet, J. Carswell and A. S. Goldstein, 2007: Hurricane surface wind measurements from an operational stepped frequency microwave radiometer. *Mon. Wea. Rev.*, **135**, 3070-3085.

\*Uhlhorn, E. W., 2008: Gulf of Mexico Loop Current mechanical energy and vorticity response to a tropical cyclone. PhD Dissertation. RSMAS, University of Miami, Coral Gables, FL 33143, 148 pp.

\*Uhlhorn, E., and L. K. Shay, 2011: Loop Current mixed layer response to hurricane Lili, 2002: Part I: Observations. *J. Phys. Oceanogr.* **42**, 400-419.

\*Uhlhorn, E., and L. K. Shay, 2013: Loop Current mixed layer response to hurricane Lili, 2002: Part II: Modeling results. *J. Phys. Oceanogr.* (*Accepted subject to minor revision*)

Walker, N., R. R. Leben, and S. Balasubramanian, 2005: Hurricane forced upwelling and chlorophyll a enhancement within cold core cyclones in the Gulf of Mexico. *Geophys. Res. Letter*, **32**, L18610, doi: 10.1029/2005GL023716, 1-5.

## ***Studies of Cloud, Drizzle, Turbulence, and Boundary Layer Variability over the Eastern Pacific in Support of the VOCALS Regional Experiment-2012 Report***

**Principal Investigator:** B. Albrecht (UM/RSMAS)

**NOAA Funding Unit:** OAR/CPO

**NOAA Technical Contact:** Jin Huang

### **Results and Accomplishments:**

This project is designed to contribute to our understanding of the dynamical, turbulence, microphysical, and drizzle properties of extensive boundary layer cloud decks in the southeasterly trade winds. Specifically, we are working to contribute to key elements of the observational and modeling studies designed to address the VOCALS (VAMOS Ocean-Cloud-Atmosphere-Land-Study) science hypotheses involving aerosol-cloud-drizzle interactions within these climatically critical cloud systems (Wood et al, 2011).

As part of this research project we analyzed observations from the CIRPAS Twin Otter (TO) research aircraft that was deployed in support of VOCALS. The CIRPAS Twin Otter aircraft made 19 research flights off the coast of Northern Chile during VOCALS-REx from Oct. 15 to Nov. 15. Cloud conditions were excellent during this deployment. The flight strategy involved operations at a fixed point (20 °S; 72 °W; reference point alpha) that allowed for a definition of the temporal evolution of boundary layer structures, aerosols, and cloud properties. Each flight included 3 to 4 soundings and near-surface, below-cloud, cloud base, in cloud, cloud top, and above inversion observations along fixed-height legs. This study used the aerosol, cloud, boundary-layer thermodynamics and turbulence data from those 18 flights to investigate the boundary layer, and aerosol-cloud-drizzle variations in this region.

A major effort of this project focused on the use of *in situ* and remote sensing observations from systems operating on the R/V Ron Brown (RB) in support of VOCALS REx during the Oct-Nov. 2008 cruises along with the observations made during previous cruises in the vicinity of the WHOI buoy along with observations from the buoy. Specifically, we used radar and lidar observations to define the cloud microphysical, drizzle and turbulence characteristics in clouds associated with both coupled and decoupled boundary layers and relating these characteristics to the larger-scale variability associated with pockets of open cells (POCs), rifts and other aerosol/cloud variations observed from the ship, nearby research aircraft, or inferred from satellite observations. Turbulence and drizzle retrieval techniques that have been developed and applied to radar data sets collected previously are being applied to the Doppler moments and spectra from the stabilized W-Band radar that was operated by NOAA ESRL/ETI. Doppler observations from the NOAA stabilized lidar are also being used to characterize the turbulence structure in the subcloud layer for cases where the retrieval of turbulence in the clouds has been made. These observations and analyses provide an unprecedented description of cloud, drizzle, and turbulence properties with high temporal and vertical resolution from sampling of clouds and drizzle observed over the ship. We continued our long-term collaborative efforts with Dr. Chris Fairall and other scientists as NOAA ESRL and with Dr. Virendra Ghate (Rutgers University) on this work and associated publications.

### ***Pre-VOCALS—Cloud and Meteorology Climatology from Buoy Observations at 20°S;85°W***

A 5-year climatology of the meteorology, including boundary layer cloudiness, for South-East Pacific region was developed using observations from a buoy located at 20°S and 85°W. This study was completed and results published under this current NOAA grant. The sea surface temperature and surface air temperature exhibit sinusoidal seasonal cycle that is negatively correlated with surface pressure. The relative humidity, wind speed and wind direction show little seasonal variability. But the advection of cold and dry air from the southeast varies seasonally and is highly correlated with the latent heat flux variations. A simple model was used to estimate the monthly cloud fraction using the observed surface downwelling longwave radiative flux and surface meteorological parameters. The annual cycle of cloud fraction is highly correlated to that of Klein lower tropospheric stability parameter (0.87), latent heat flux (-0.59) and temperature and moisture advection (0.60) but shows negligible correlation with the large-scale vertical velocity (-0.09). The derived cloud fraction compares poorly with the ISCCP derived low cloud cover, but compares well (0.86 correlation) with ISCCP low plus middle cloud cover. The monthly averaged diurnal variations in cloud fraction show marked seasonal variability in the amplitude and temporal structure. The mean annual cloud fraction is lower than the mean annual night-time cloud fraction by about 9%. Annual and diurnal cycles of surface longwave and shortwave cloud radiative forcing were also estimated. The longwave cloud radiative forcing is about  $45 \text{ Wm}^{-2}$  year round, but due to highly negative shortwave cloud radiative forcing, the net cloud radiative forcing is always negative with annual mean of  $-50 \text{ Wm}^{-2}$ . This work is published in Ghate et al. (2010).

### ***VOCALS—Boundary Layer, Cloud and Aerosol Variability at 20°N; 72°W***

The observations made from the VOCALS CIRPAS Twin deployment provide a unique characterization of the cloud and aerosol variability in the coastal environment of the Southeast Pacific. The marine atmospheric boundary layer structures observed showed relatively little variability and indicated little influence from meso-scale and large-scale systems. The aerosol and cloud properties demonstrate clear variations over this region during the study with accumulation mode aerosols in the boundary layer varying from  $200 - 700 \text{ cm}^{-3}$ . Aerosol number concentrations above the boundary layer were substantially smaller than those below ( $50 - 250 \text{ cm}^{-3}$ ) except for a two cases where these values were elevated. Cloud droplet concentration varied from  $50-400 \text{ cm}^{-3}$  over the 18 flights. Drizzle water content varies from  $10^{-5}$  to  $0.05 \text{ g m}^{-3}$  and 6 flights out of 18 flights have mean drizzle water content larger than  $0.0015 \text{ g m}^{-3}$ . Since the boundary layer conditions at this fixed point are so steady, the observations provide a unique data set for the evaluation of models operating at a variety of scales—from LES to large scale.

The boundary layer structures observed on several of the VOCALS flights were remarkably similar, although the observed aerosol concentrations in the boundary layer and the cloud water content and the liquid water path of the clouds topping the boundary layer varied considerably. On 10 of the flight days, the boundary layer was well mixed, the clouds sampled were non-precipitating, and conditions at the top and the bottom of the mixed layer were very similar. Calculated boundary layer back trajectories for the 72 hours prior to the observations at 20°N and 72°W remained mostly over coastal ocean areas and indicate that advective effects were generally small during this time. Thus the boundary layer, cloud and aerosol structures sampled on the individual days were likely to be steady and close to equilibrium. Despite the constancy of the thermodynamic structures of the boundary layers studied on these 10 flights, the subcloud CCN varied substantially and was closely coupled to the cloud droplet concentrations as well. CCN in the boundary layer for these cases ranged from 180-

580  $\text{cm}^{-3}$  in the relatively thin capping clouds. The liquid water path in these clouds ranged from 22 to 73  $\text{g m}^{-2}$  and was positively correlated with the aerosol and cloud droplet concentrations (Fig. 1) as described in a GRL and ACP papers (Zheng et al., 2010; 2011). Processes that may link the aerosol concentrations and the liquid water path and explain the observed positive correlation are currently under study using satellite observations along low-level trajectories and LES to study the effects of aerosols. Observations from the TO were also used in to develop the 20 °S boundary layer, cloud, and aerosol cross section developed from the VOCALS observations by Bretherton, et al. (2012). The observations were also used to study the effects of wind shear on the boundary layer. The aircraft observations have been used for evaluation of a real-time regional forecast model (Wang et al., 2011) and for investigating the role of shear in the boundary layer on the cloud and boundary layer structure (Wang et al, 2012).

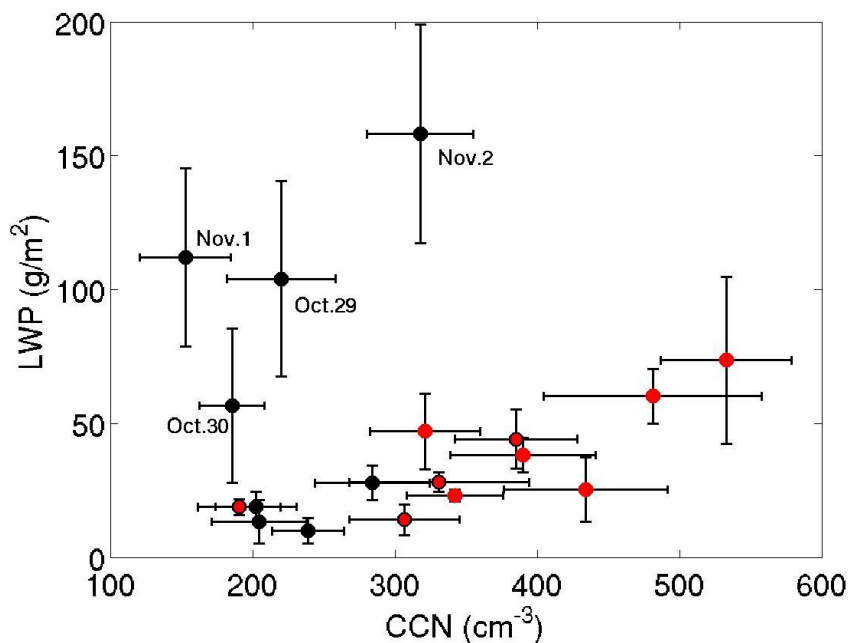


**Figure 1:** LWP as a function of sub-cloud CCN concentrations for all flights during VOCALS at Point Alpha. The error bars through these symbols indicate the standard deviation of CCN and estimates of LWP uncertainty (from Zheng et al, 2011).

### **VOCALS— Turbulence and Radiation in Stratocumulus Layers**

Observations made during a 24 hour period as part of the VOCALS-Rex from the Ron Brown are analyzed to study the radiation and turbulence associated with stratocumulus topped marine boundary layer (BL). The first fourteen hours exhibited a well-mixed BL with an average cloud top radiative flux divergence of  $\sim 130 \text{ W m}^{-2}$ ; the BL was decoupled during the last 10 hours with negligible radiative flux divergence. The averaged radiative cooling very close to the cloud top was  $-9.04 \text{ K hour}^{-1}$  in coupled conditions and  $-3.85 \text{ K hour}^{-1}$  in decoupled conditions. Data from the vertically pointing NOAA ESRL Doppler cloud radar and Doppler lidar were combined to yield the vertical velocity structure of the entire BL. The averaged vertical velocity variance and updraft mass-flux during coupled conditions were higher than those during

decoupled conditions at all levels by factor of 2 or more. The vertical velocity skewness was negative in the entire BL during coupled conditions, while it was weakly positive in the lower third of the BL and negative above during decoupled conditions. A formulation of velocity scale is proposed which includes the effect of cloud top radiative cooling in addition to the surface buoyancy flux. When scaled by the velocity scale, the in-cloud values of vertical velocity variance, updraft mass-flux and coherent downdrafts had similar magnitude during the coupled and decoupled conditions. The coherent updrafts which exhibited a constant profile in the entire BL during both the coupled and decoupled conditions scaled well with the convective velocity scale to a value of 0.6. These observations provide unprecedented observations of the turbulence structure of marine stratocumulus during coupled and uncoupled boundary layer conditions. Results are presented in Ghate et al (2012).

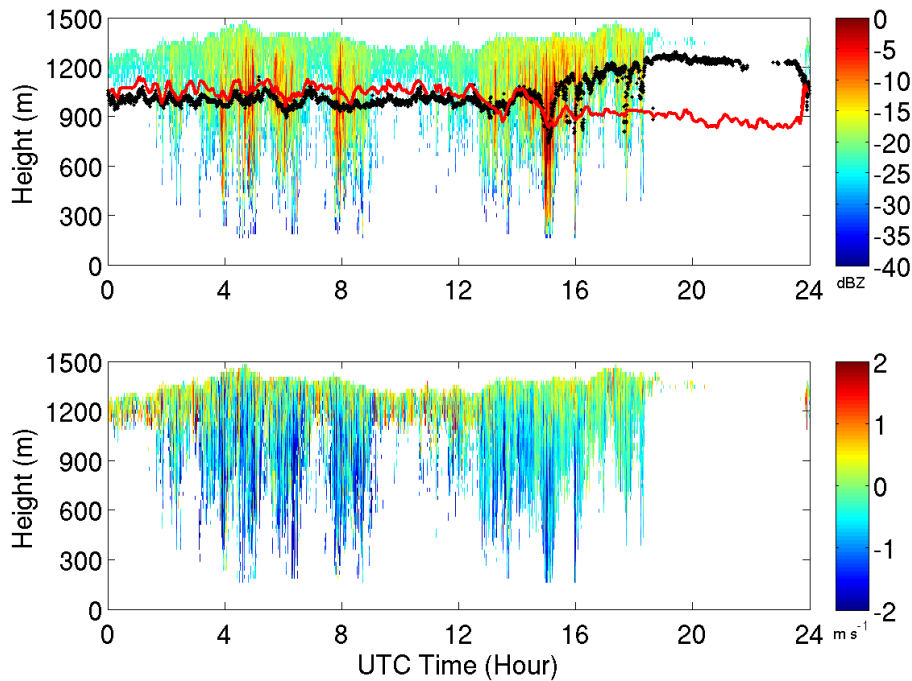


**Figure 2:** Reflectivity (top) and mean Doppler velocity (bottom) as recorded by the vertically pointing 95 GHz Doppler Cloud radar on 27 November 2008. The ceilometer recorded cloud base height is shown in black while the lifting condensation level calculated using surface measurements is shown in red. The local time is six hours behind UTC (from Ghate et al, 2012)

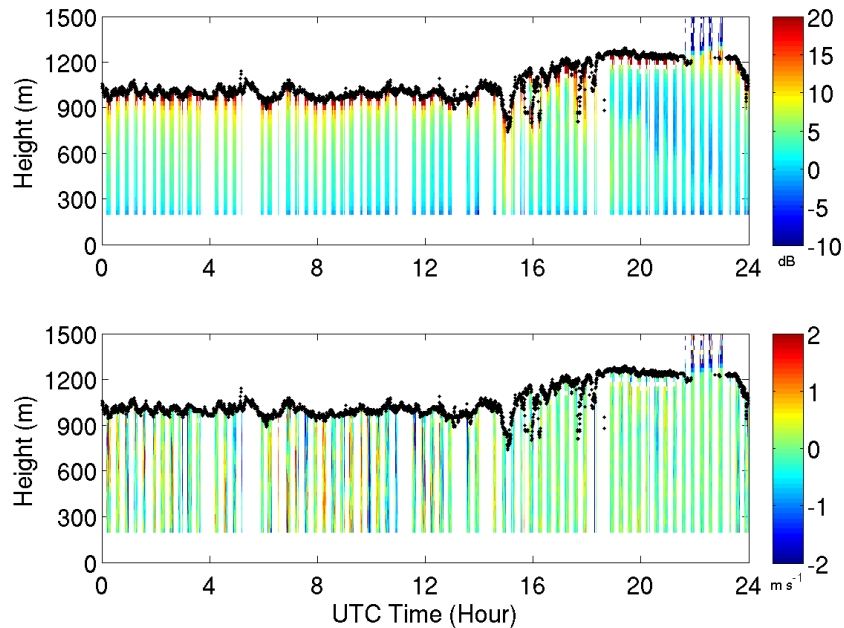


**Figure 3:** The signal to noise ratio (top) and Doppler velocity (bottom) as recorded by the HRDL when it was pointing vertically upwards on 27 November 2008. The ceilometer recorded cloud base height is shown in black. The local time is six hours behind UTC (from Ghate et al, 2012).

### Highlights of Accomplishments:

- Application of techniques to ship-based Doppler cloud radar and lidar observations is made to characterize the in-cloud and sub-cloud turbulence structure observed for 24-hr case obtained during the VOCALS cruise.
- Characterization of the cloud, aerosol, and boundary variability in the coastal environment of the VOCALS study area at 20°S; 72°W
- Publication of a 5-year climatology of the meteorology and surface fluxes including boundary layer cloudiness, for South-East Pacific region was developed using observations from the WHOI buoy located at 20°S and 85°W.

### Graduate Students:

Xue Zheng; Ph. D. 2012: University of Miami. Dissertation Title: “Observational and Numerical Studies of the Boundary Layer, Cloud and Aerosol, Variability in the Southeast Pacific Coastal Marine Stratocumulus”

### Publications (referred):

Bretherton, C. S., Wood, R., George, R. C., Leon, D., Allen, G., and Zheng, X, 2011: Southeast Pacific stratocumulus clouds, precipitation and boundary layer structure sampled along 20°S, during VOCALS-REx, *Atmos. Chem. Phys.*, **10**, 10639–10654, doi:10.5194/acp-10-10639-2010, 2010.

- Ghate, V., B. Albrecht, C. Fairall, and R. Weller, 2009: Climatology of Surface Meteorology, Surface Fluxes, Cloud Fraction, and Radiative Forcing over the Southeast Pacific from Buoy Observations. *J. Climate*, 5527-5540.
- Ghate, V., B. Albrecht, M. Miller, A. Brewer, C. Fairall, 2012: Turbulence and Radiation in Stratocumulus Topped Marine Boundary Layer: A Case Study from VOCALS-REx 2. (J. Appl. Meteo. Clim (accepted). Wang, S., O'Neill, L. W., Jiang, Q., de Szoeke, S. P., Hong, X., Jin, H., Thompson, W. T., and Zheng, X.: A regional real-time forecast of marine boundary layers during VOCALS-REx, *Atmos. Chem. Phys.*, **11**, 421–437, doi:10.5194/acp-11-421-2011, 2011.
- Wang, S., Zheng, X., and Jiang, Q.: Strongly sheared stratocumulus convection: an observationally based large-eddy simulation study, *Atmos. Chem. Phys.*, **12**, 5223-5235, doi:10.5194/acp-12-5223-2012, 2012.
- Wang, S., O'Neill, L. W., Jiang, Q., de Szoeke, S. P., Hong, X., Jin, H., Thompson, W. T., and Zheng, X.: A regional real-time forecast of marine boundary layers during VOCALS-REx, *Atmos. Chem. Phys.*, **11**, 421–437, doi:10.5194/acp-11-421-2011, 2011.
- Wood, R., Bretherton, C. S., Mechoso, C. R., Weller, R. A., Huebert, B., Straneo, F., Albrecht, B. A., Coe, H., Allen, G., Vaughan, G., Daum, P., Fairall, C., Chand, D., Gallardo Klenner, L., Garreaud, R., Grados Quispe, C., Covert, D. S., Bates, T. S., Krejci, R., Russell, L. M., de Szoeke, S., Brewer, A., Yuter, S. E., Springston, S. R., Chaigneau, A., Toniazzo, T., Minnis, P., Palikonda, R., Abel, S. J., Brown, W. O. J., Williams, S., Fochesatto, J., and Brioude, J., 2010: The VAMOS Ocean-Cloud-Atmosphere-Land Study Regional Experiment (VOCALS-REx): goals, platforms, and field operations. *Atmos. Chem. Phys. Discuss.*, **10**, 20769-20822, doi:10.5194/acpd-10-20769-2010.
- Zheng, X., Albrecht, B. A., Minnis, P., Ayers, K., and Jonsson, H. H., 2010. Observed aerosol and liquid water path relationships in marine stratocumulus., *Geophys. Res. Lett.*, **37**, L17803, doi:10.1029/2010GL044095, 2010.
- Zheng, X., B. Albrecht, B., Jonsson, H. H., Khelif, D., Feingold, G., Minnis, P., Ayers, K., Chuang, P., Donaher, S., Rossiter, D., Ghate, V., Ruiz-Plancarte, J., and Sun-Mack, S., 2011: Observations of the boundary layer, cloud, and aerosol variability in the southeast Pacific coastal marine stratocumulus during VOCALS-REx, *Atmos. Chem. Phys.*, **11**, 9943-9959.

# *Atmosphere-Ocean Interactions and Summer Rainfall Variability and Predictability in the Intra-Americas Region*

**Principal Investigator:** B. Kirtman (UM/RSMAS)

**NOAA Funding Unit:** OAR/CPO

**NOAA Technical Contact:** Jin Huang

*The following progress report includes the documentation from the previous report and final papers covered as part of the no-cost extension.*

## **Introduction**

This report describes the progress of the project entitled “Atmosphere-Ocean Interactions and Summer Rainfall Variability and Predictability in the Intra-Americas Region” during the period of May 1, 2011-April 30, 2012. The results are described in the following areas:

- (a) Evaluation of the prediction skill and predictability of rainy season precipitation in the intra-Americas region in the CFS and influence of ENSO
- (b) Comparison of rainfall variability between CFS global coupled simulation and the CFS simulation with Pacific Ocean SST specified as climatology
- (c) Coupled high resolution air-sea feedbacks in the Inter-American Seas region

## **Results and Accomplishments**

*(a) Evaluation of the prediction skill and predictability of rainy season precipitation in the intra-Americas region in the CFS and influence of ENSO*

In the previous report period, the simulations of Climate Forecast System (CFS) of National Centers for Environmental Prediction (NCEP) were analyzed to determine the nature of the leading mode of rainfall variability in the intra-Americas seas. It was found that this mode is an intrinsic mode that is independent of ENSO although ENSO can modify its amplitude. During the past year (the current report period), the forecast skill and predictability of the CFS in predicting seasonal precipitation in the intra-Americas region were assessed. The ensemble retrospective forecasts made by the CFS for the period 1981-2006 were analyzed, and the skill of CFS in predicting MJJ and ASO seasonal rainfall was assessed.

As seen from the correlations between the ensemble members of the forecast and observation for the ASO rainfall anomalies in Figure 1, the forecast skill is moderate for forecasts initiated in June while it is weak for those initiated in March. The predictability of the model (assuming the model to be perfect) is slightly higher for forecasts from June initial conditions. The signal-to-noise ratio has higher values in the southern part of the region. A similar analysis of the MJJ rainfall showed both the forecast skill and predictability of CFS to be lower. Further analyses showed that the skill is the lowest for the April rainfall in forecasts of all leads. The prediction skill is moderate for the ensemble mean for target months during August-January.

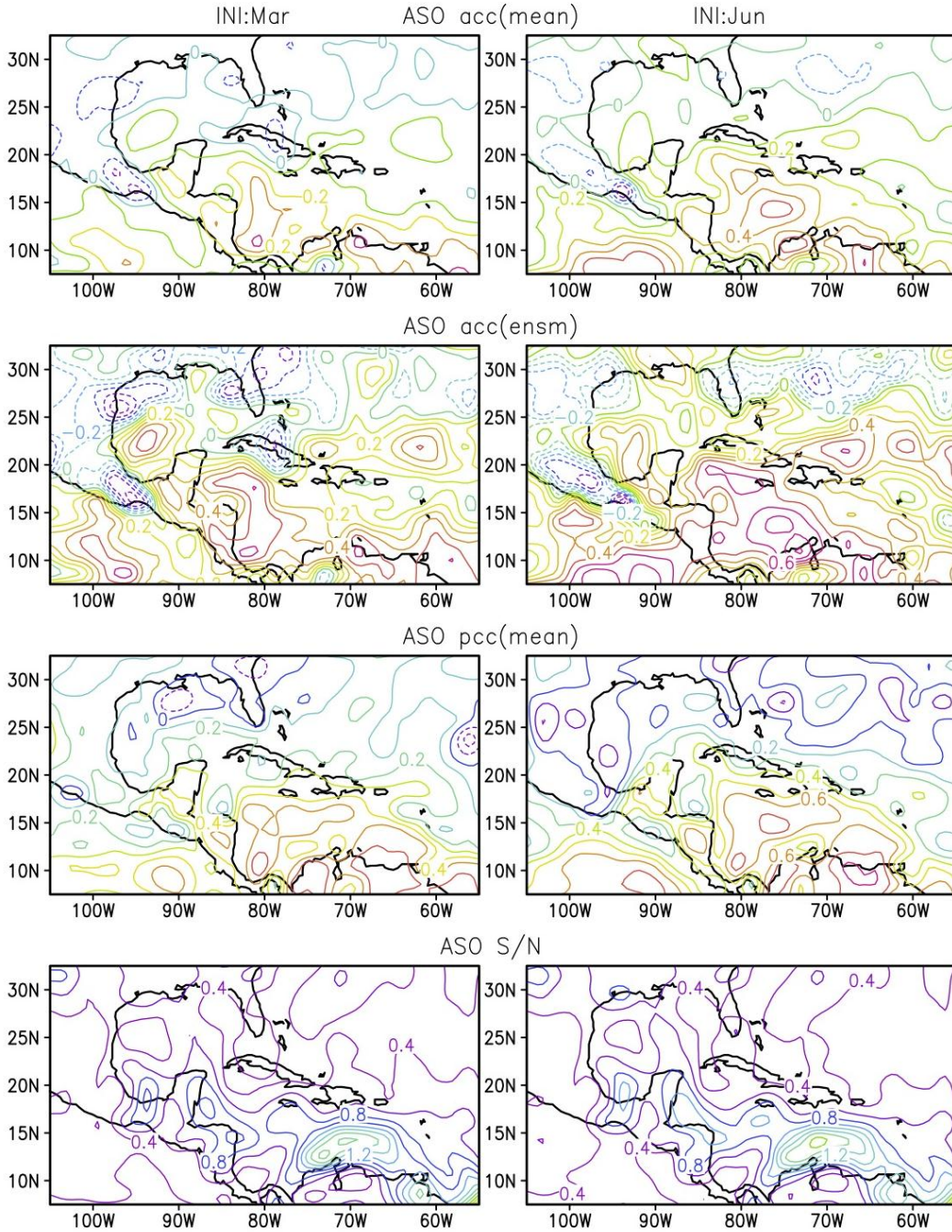


**Figure 1:** Anomaly correlation coefficient of MJJ rainfall based on individual members (shown is the mean of individual correlations) (upper row) and ensemble mean (second row), anomaly correlation coefficient calculated using the perfect model approach (third row), and the signal-to-noise ratio (lower row) for CFS ensemble forecasts initiated in December (left column) and March (right column). Interval is 0.1 for correlation coefficients and 0.2 for signal-to-noise ratio.

However, the CFS has higher skill in the prediction of tropical North Atlantic (TNA) SST and even higher skill in predicting the equatorial Pacific SST. This feature has an impact on the predictability of rainfall in CFS during ENSO and TNA events. The forecast errors in MJJ seasonal rainfall are

generally lower during both El Niño and La Niña years. However, for ASO seasonal rainfall, the errors are lower during El Niño years but higher during La Niña years. However, during the high TNA years, the errors in the rainfall forecasts are higher while they are relatively lower during the low TNA years.

*(b) Comparison of rainfall variability between CFS global coupled simulation and the CFS simulation with Pacific Ocean SST specified as climatology*

The influence of ENSO on the variability of rainfall in the intra-Americas Seas was examined by comparing the simulations of CFS with and without ENSO SST variability. In the first case (control run), the model is fully coupled over all the global oceans while in the second case (PACclim run) the model is run with climatological SST prescribed over the Pacific while the other oceans are coupled. Figure 2 shows the difference between the two runs in the simulation of MJJ and ASO seasonal rainfall. In the intra-Americas Seas, the variability (standard deviation) shows a very slight increase when the ENSO variability is absent. The EOF analysis of the seasonal rainfall was also performed for the two runs. It is found that the leading mode of the ASO seasonal rainfall in the PACclim run (ENSO absent) explains about 54% of the total variance while the leading mode in the control run (ENSO present) explains about 26%. These results further confirm the possibility that there is an intrinsic mode in the rainfall which may be influenced to some extent by the ENSO variability.

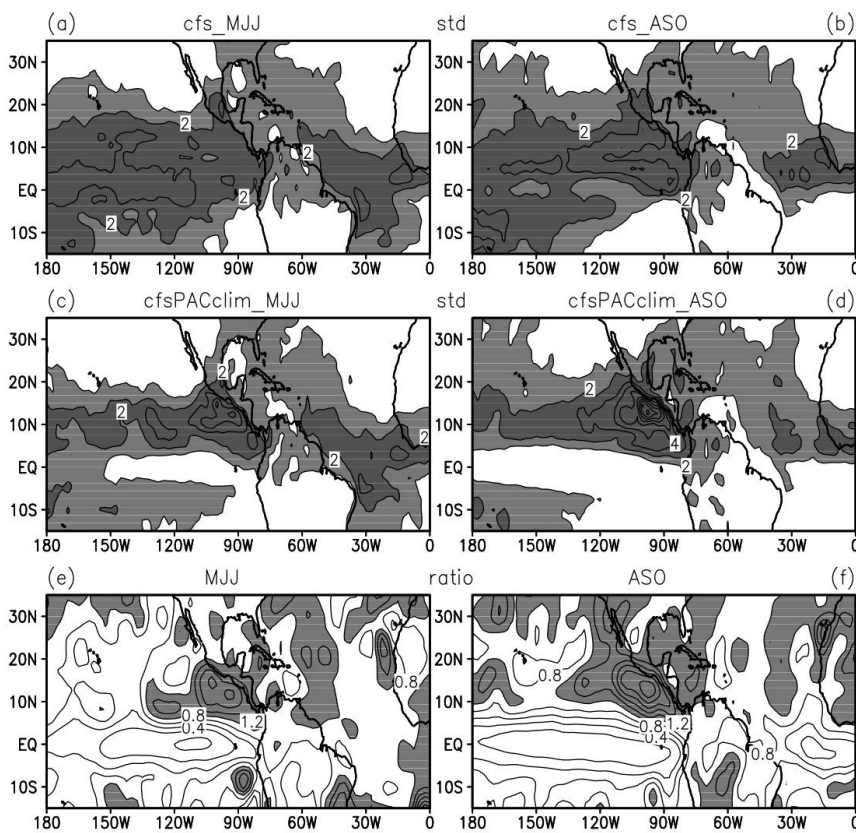


**Figure 2:** Standard deviation of MJJ and ASO rainfall in CFS control (upper panels) and climatological Pacific SST simulation (middle panels) and their ratio (lower panels). Interval is 1 mm/day for standard deviation and 0.2 mm/day for ratio.

*(c) Coupled high resolution air-sea feedbacks in the Intra-Americas Seas region*

There is a growing demand for environmental predictions that include a broader range of space and time scales and that include a more complete representation of physical processes. Meeting this demand necessitates a unified approach that will challenge the traditional boundaries between weather and climate science, and will require a more integrated approach to the underlying geophysical system science and the supporting computational science. One of the consequences of this unified or seamless approach is the need to explore much higher spatial resolution in weather and climate models. It is also recognized that interactions across time and space scales are fundamental to the climate system itself. The large-scale climate, for instance, determines the environment for microscale (order 1 km) and mesoscale (order 10 km) variability which then feeds back onto the large-scale climate. In the simplest terms, the hypothesis is that the statistics of microscale and mesoscale variability significantly impact the simulation of climate. In typical climate models at, say, 200 km horizontal resolution<sup>1</sup>, these variations occur on unresolved scales, and the micro- and mesoscale processes are parameterized in terms of the resolved variables. The motivation for our study is to determine how increased ocean model resolution impacts the simulation of climate variability and air-sea feedbacks in the Intra-Americas Seas (IAS) region. To this end, we report on two sets of numerical experiments that examine how resolved ocean fronts and eddies (the loop current in particular) affect the climate.

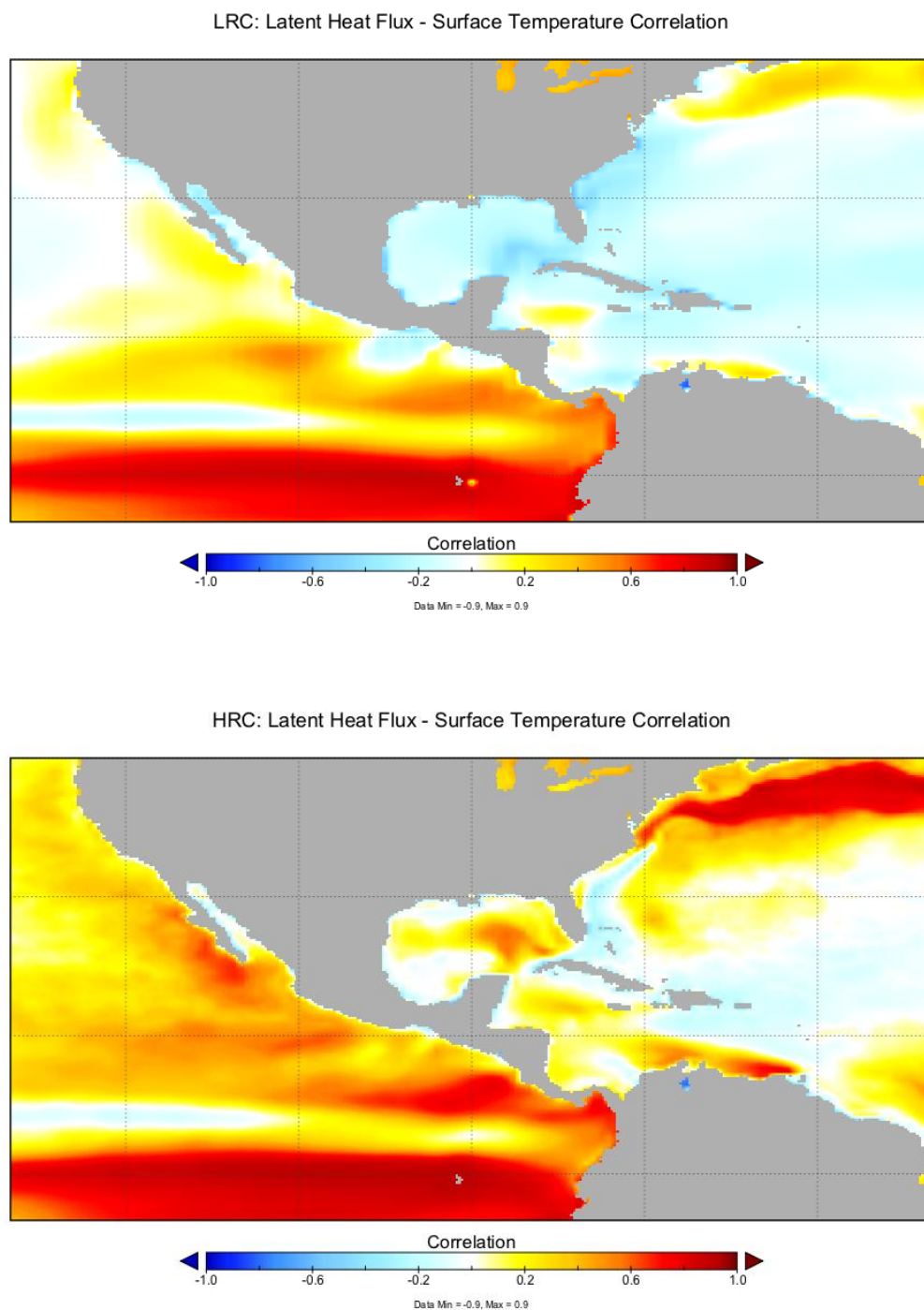
The experiments described here use two versions of CCSM4. The first version (referred to as LRC) uses the 0.5° atmosphere (zonal resolution 0.625°, meridional resolution 0.5°; the land component has the same resolution) coupled to ocean and sea-ice components with zonal resolution of 1.2° and meridional resolution varying from 0.27° at the equator to 0.54° in the mid-latitudes on a dipole grid. The second version the same atmosphere and land component models coupled to 0.1° ocean and sea-ice component models. This version of the model is referred to as HRC. In addition to the change in horizontal resolution from the control experiment, there are commensurate changes in the parameterization of horizontal sub-grid scale dissipation. The high-resolution model uses a biharmonic closure for both momentum and tracers. The hyper-viscosity and diffusivity are scaled with the cube of the local grid spacing. Multi-decadal simulations with LRC and HRC are described in detail Kirtman et al. (2012) and are briefly summarized here. The results presented in this here are based on the last 50 years of 150-year simulations of the LRC and HRC configurations of CCSM4.

Figure 3 shows the local correlation between the latent heat flux (LHF) and the SST from the LRC (top panel) and the HRC (bottom panel) simulations, respectively. Positive values of this correlation suggest that the ocean is “forcing” the atmosphere and negative values suggest that the atmosphere is forcing the ocean. There are a number of noteworthy differences between the two simulations throughout the IAS region. For example, the correlation is negative almost everywhere in the LRC simulation, whereas the HRC simulation has large positive correlations in the Gulf of Mexico (GoM) and the southern Caribbean. Analysis of the surface currents in the HRC simulation show that the center of positive correlation in the GoM are associated with the loop current which sheds eddies that propagate westward into the Text/Mexico coastal zone. Conversely, the LRC simulation has a stationary surface jet (i.e., no shedding eddies) between the Yucatán Peninsula and Cuba which weak negative correlations between the LHF and the SST. The southern Caribbean also has relatively strong eddy activity in the HRC simulation with similarly strong positive correlation. In these regions the LRC

---

<sup>1</sup> Throughout this discussion, model “resolution” refers to the spacing of model grid elements.

simulation captures some sense of this interaction, but with much weaker correlations. There are also significant differences in the northern Caribbean – western sub-tropical Atlantic associated with the Florida current merging into the Gulf Stream.



**Figure 3:** Local correlation between surface latent heat flux and SST for the LRC (top panel) and HRC (bottom panel). Positive correlations indicate ocean forcing atmosphere and negative correlations indicate atmosphere forcing ocean

## Highlights of Accomplishments

The project has been completed (except for one more paper submission). The main accomplishments are summarized below:

- The forecast skill and predictability of CFS in predicting the seasonal rainfall are weak to moderate for MJJ and ASO seasons. The skill is slightly higher for MJJ season during both El Niño and La Niña years. For the ASO season, the skill is higher during El Niño years but lower during La Niña years.
- During La Niña years, MJJ season has higher skill whereas ASO season has lower skill.
- The leading mode of rainfall variability may be intrinsic to the intra-Americas region and its amplitude may be modified due to the influence of ENSO variability.
- The simulation of the climate of the region is drastically changed when a higher resolution ocean model is used showing increased eddy activity.

## Publications from the Project Including Results from No-Cost Extension

Wu, R., and B. P. Kirtman, 2011: Caribbean Sea rainfall variability during the rainy season and relationship to the equatorial Pacific and tropical Atlantic SST. *Climate Dynamics*, **37**, 1533-1550.

Kirtman, B. P., E. K. Schneider, D. M. Straus, D. Min, R. Burgman, 2011: How weather impacts the forced climate response. *Climate Dynamics*, DOI: 10.1007/s00382-011-1084-3.

Kirtman, B. P., C. Bitz, F. Bryan, W. Collins, J. Dennis, N. Hearn, J. L. Kinter III, R. Loft, C. Rousset, L. Siqueira, C. Stan. R. Tomas, M. Vertenstein, 2012: Impact of ocean model resolution on CCSM climate simulations. *Climate Dynamics*, DOI 10.1007/s00382-012-1500-3.

Kirtman et al, 2013: Prediction from weeks to decades, *Climate Science for Serving Society: Research, Modelling and Prediction Priorities*. G. R. Asrar and J. W. Hurrell, Eds. *Springer*, in press.

Infanti, J. M., and B. P. Kirtman, 2013: Southeast US rainfall prediction in the National Multi-Model Ensemble. *J. Climate* (to be submitted).

## ***Multi-Model Ensemble Climate Prediction with CCSM and CFS***

**Principal Investigator:** B. Kirtman (UM/RSMAS)

**NOAA Funding Unit:** OAR/CPO

**NOAA Technical Contact:** Dr. Jin Huang

*The following progress report includes the documentation from the previous report and final papers covered as part of the no-cost extension.*

### **Objectives**

The four objectives of this study are all related to expanding multi-model seasonal prediction capabilities. First, we document the ENSO predictive capability of the NCAR CCSM3.0 and more recently CCSM3.5. This model is a natural candidate for inclusion in the U.S. operational multi-model prediction strategy (Higgins, personal communication 2006). Second, we document how CCSM3.0 (and CCSM3.5) can be combined with the current operational CFS to produce intraseasonal to interannual forecasts that are superior to either model alone. Third, we demonstrate how an ocean initial state using a particular ocean component (i.e., the Geophysical Fluid Dynamics Laboratory Modular Ocean Model; MOM) can be used in a coupled system that uses a different ocean component model (i.e., the Parallel Ocean Program; POP). This demonstration has the potential to simplify and broaden the multi-model prediction strategy, because institutions that do not have an independent ocean data assimilation system can more easily participate in prediction research. Fourth, we seek to show how an improved land initialization strategy impacts the forecast skill. Kirtman and Min (2009) describe in detail the results from the first three objectives in terms of SST predictions in the eastern Pacific. Paolino et al. present results showing impact of land surface initialization.

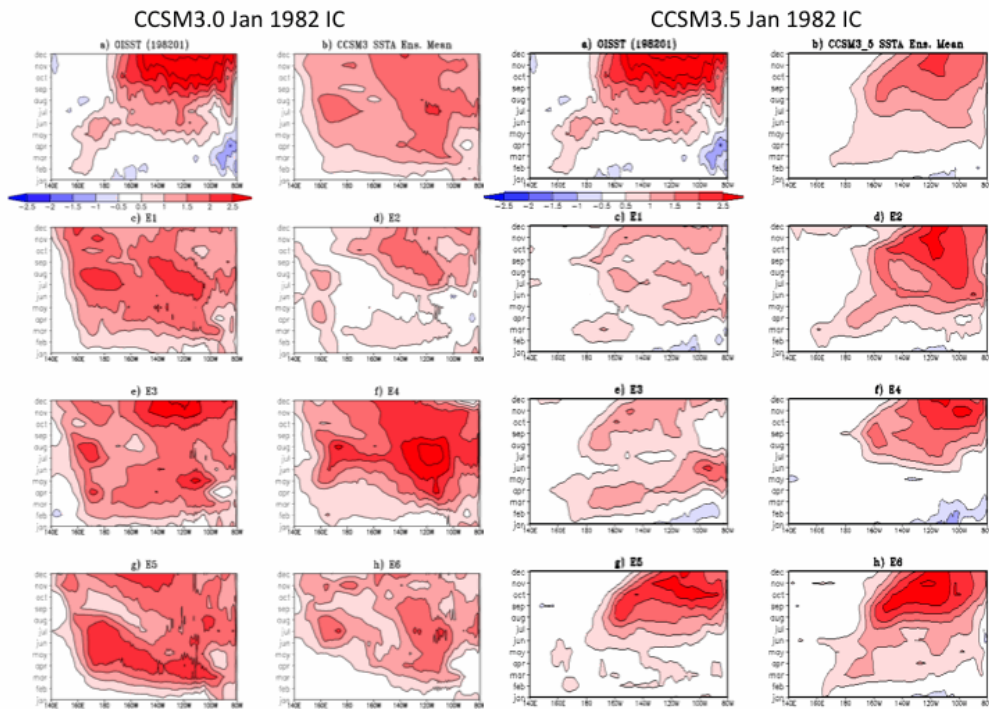
### **Results and Accomplishments**

#### **ENSO Forecast Skill CCSM3.0 vs. CCSM3.5**

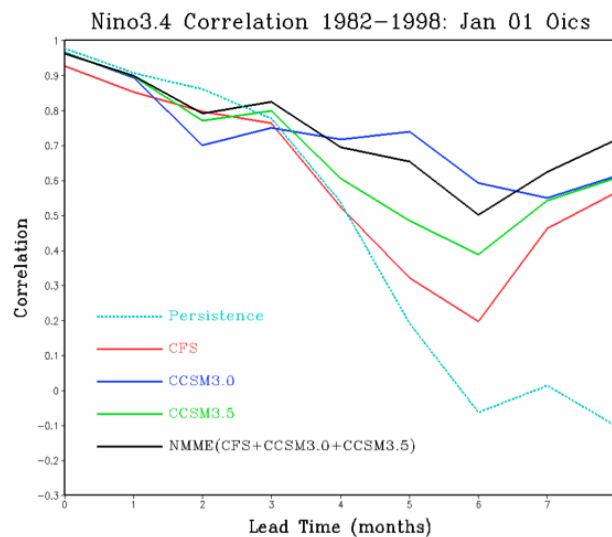
Figure 1 shows a specific example from forecasts initialized in January 1982. The plot shows Time–longitude equatorial Pacific SSTA cross sections for each CCSM3.0 and CCSM3.5. The first two columns correspond to the CCSM3.0 forecasts with (a) the observational estimate and (b) the ensemble mean. (c)–(h) Various CCSM3 forecast are denoted. Similarly, the last two columns [also labeled (a)–(h)] correspond to the CCSM3.5 forecast with (a) the observational estimate and (b) the ensemble mean. (c)–(h) The various CCSM3 forecasts are denoted. This particular case is an excellent example of how the improvement made to CCSM3.5 impact the systematic behavior of the forecasts. For example, typically CCSM3.0 predicts that the SSTA develops too early compared with observations and extend too far into the western Pacific. Both of these problems are significantly reduced with the CCSM3.5 forecasts.

Figure 2 shows the correlation coefficient for all retrospective forecasts initialized January 1982–1999 for CCSM3.0, CCSM3.5, CFS and the multi-model combination of all three models. For show lead time all three models indicate similar correlation with the observations, at longer leads the CCSM3.0 forecast are better correlated with the observations. More detailed statistical analysis indicates that multi-model forecast is statistically indistinguishable from the best model while which model is best model appears to be a function of lead time and initial month. Moreover, the multimodel forecast does appear to produce correlations that are significantly higher than the worst model, which again is a function of lead time and initial month. It is this fact that leads us to the conclusion that the multimodel

improves the “overall” forecast skill and emphasizes how the multimodel ensemble can conceptually be thought of as smoothing out the vagaries in skill associated with individual model differences. Figures 3 and 4 show maps of anomaly correlation as a function of lead time.



**Figure 1:** The plot shows Time–longitude equatorial Pacific SSTA cross sections for each CCSM3.0 and CCSM3.5. The first two columns correspond to the CCSM3.0 forecasts with (a) the observational estimate and (b) the ensemble mean. (c)–(h) Various CCSM3 forecast are denoted. Similarly, the last two columns [also labeled (a)–(h)] correspond to the CCSM3.5 forecast with (a) the observational estimate and (b) the ensemble mean. (c)–(h) The various CCSM3 forecasts are denoted. In this case the forecast were initialized in January 1982.



**Figure 2:** Nino3.4 (top) correlation coefficient for ensemble mean forecasts initialized in January.

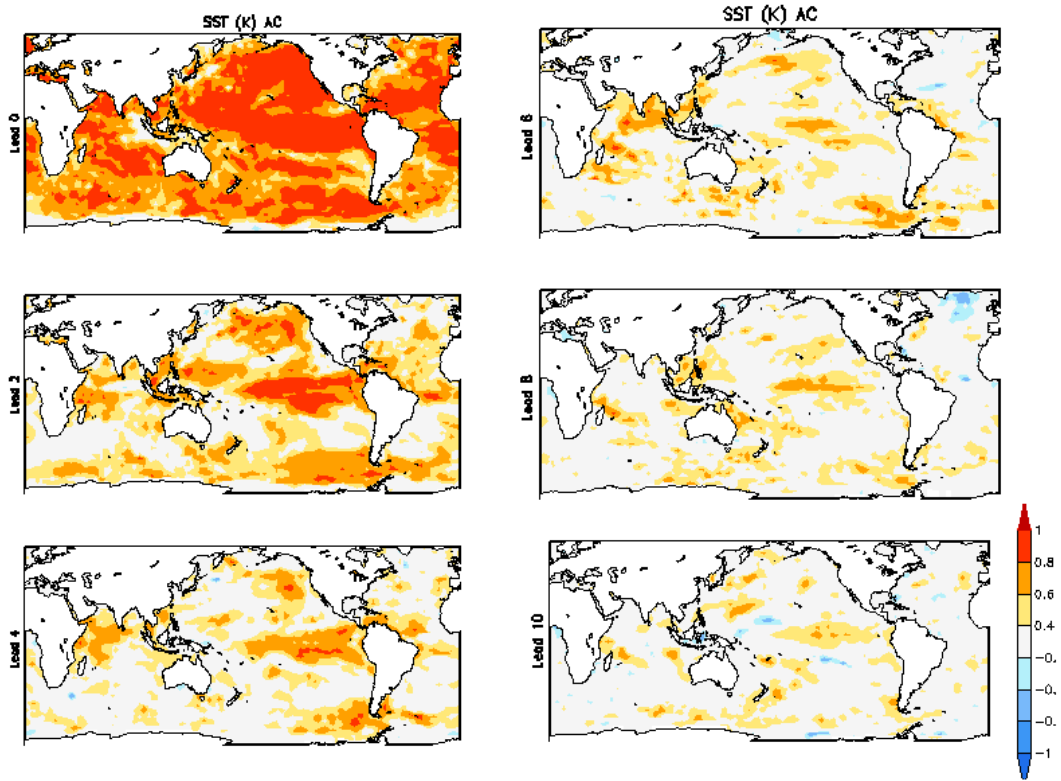


**Figure 3:** CCSM3.5 SST anomaly correlation as a function of lead-time.

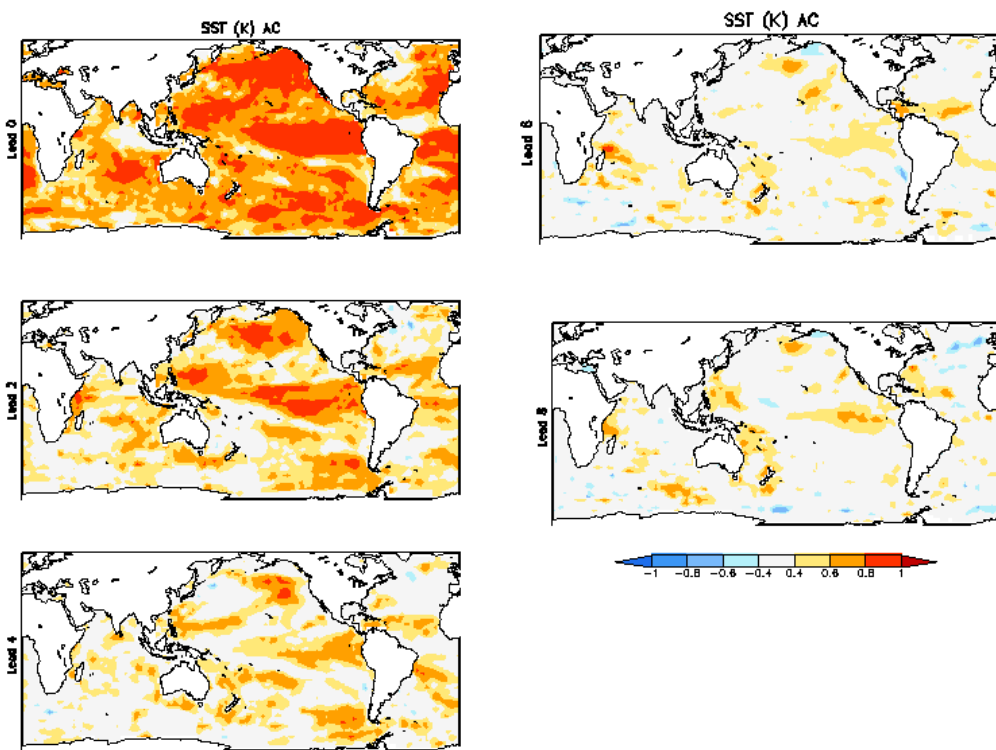


**Figure 4:** CFS SST anomaly correlation as a function of lead-time.

### Impact of Land Surface Initialization

The land surface initial conditions are initialized as follows: soil moisture and soil temperature are derived from the Second Global Soil Wetness Project (GSWP-2) daily data. GSWP-2 reports only soil wetness, so the initial soil moisture for a particular layer and column is considered to be either all liquid or all ice, depending on the corresponding soil temperature at that point. Profile data for different column types are restricted in the same manner as in the Common Land Model (CLM), which is the land surface component of the CCSM. We first compute the normalized anomalies of the GSWP-2 soil moisture from a 10-year climatology, and then combine those anomalies with the mean statistics from a 30-year CLM run, after a 100-year spin-up.

The GSWP-2 soil data are reported for six layers, from top to bottom, with depths of 10, 20, 20, 20, 30, and 50 cm, for a total depth of 1.5 m. The CLM soil column consists of 10 layers, and is 3.4 meters deep, with the bottom two layers spanning 2.0 meters. The initial soil data are created by imposing the GSWP-2 anomaly for the layer containing the depth of the CLM layer on the CLM climatology. Where the CLM layer overlaps two GSWP-2 layers, weighted anomalies are used. The bottom CLM layer is set to model climatology, and layer nine is relaxed to climatology. Initial soil data south of 60°S are set equal to the model climatology.

Initial values for the CLM vegetation variables are taken from a seven-day CAM only spin-up forecast, using the same atmospheric initialization as used in the fully coupled forecast. Initial snow depth and snow temperature are taken from daily values of the ERA-40 reanalysis. We have used the same formulation as the CLM in assigning initial snow depth for up to five snow layers. Snow is assigned to each column type according to the proper CLM formulation. Snow water equivalent is computed using the CLM formulation, after computing snow density from a mean of the ERA-40 skin temperature and 2 meter temperature.

In comparison with a previous set of forecast experiments which had initialized only the observed ocean state, there is firm evidence that we produce a much better representation of the interannual variability of the soil surface. The seasonal forecast of soil moisture is far superior, due in part to the ability of the CCSM3.0 to persist large-scale anomalies present in the initial soil state. The superior land surface forecast leads to a superior seasonal forecast of surface temperature. There is little evidence of an improved forecast of precipitation over land; although there is a suggestion of an improvement in the forecast over ocean. The improvement in the 2m surface temperature is shown in Figure 5 and described in more detail in Paolino et al. (2010).

### Intraseasonal Reforecasts

The focus of this part of the project is to assess the skill of a multi-model ensemble for *intraseasonal* prediction. In this phase of the project, the NCEP/Climate Forecast System (CFS) re-forecast experiments are used together with re-forecast experiments performed by the CO-Is (B. Kirtman and D. Paolino) using the NCAR/Community Climate System Model version 3.5 (CCSM3.5). The skill of the individual model forecasts and a multi-model ensemble forecast, formed by combining the two models, is assessed for a commonly used index of the Madden-Julian Oscillation (MJO).

The CCSM3.5 intraseasonal re-forecast experiments were initialized from 21-30 April, and 22-31 October for the years 1981-1999 and run for 1-year. The CFS re-forecast experiments (Saha et al. 2005) were initialized on the 1-3, 9-13, 19-23, and last two days of each month for the years 1981-2005

and run for 9-months. The overlapping years and initial dates between the two sets of re-forecasts are used to assess the skill in forecasting the MJO index. There are nine overlapping initial dates (Apr 21, 22, 29, 30; Oct 22, 23, 30, 31) over 19 overlapping years (1981-1999).

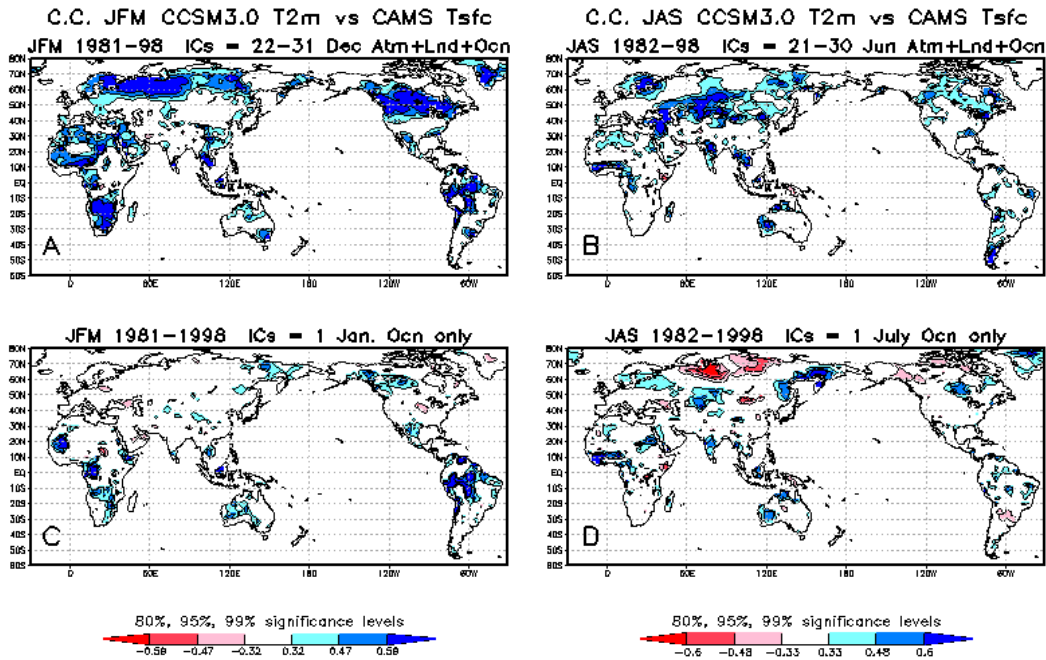


**Figure 5:** A) Correlation 2-meter temperature for CCSM3.0 *Full* forecast versus CAMS observed surface temperature for JFM 1981-1998. B) As in A), but for JAS 1982-1998. C) Correlation 2-meter temperature for CCSM3.0 *Ocean-only* forecast versus CAMS observed surface temperature for JFM 1981-1998. D) As in C), but for JAS 1982-1998. 80, 95 and 99% significance levels are shaded.

The real-time multivariate MJO index (RMM) of Wheeler and Hendon (2004) is the metric for the MJO that has been adopted by the Clivar MJO Working Group and is being used for their multi-model ensemble prediction efforts (Gottshalk 2008). The RMM index is determined from a combined empirical orthogonal function (CEOF) analysis of equatorially averaged zonal winds (200 hPa and 850 hPa) and outgoing longwave radiation (OLR). The index consists of the first two principal component time series of the combined EOFs and are in quadrature, describing an oscillation (Figure 6, top panels). The model fields are projected onto the observed CEOFs to calculate the model forecasted RMM indices. It is noted that for  $RMM1 > 0$  ( $RMM1 < 0$ ), the convection associated with the MJO is in the Maritime Continent (Western Hemisphere) regions. For  $RMM2 > 0$  ( $RMM2 < 0$ ), the maximum in convection is located in the Indian Ocean (Western Pacific). This index has been calculated for the CFS and CCSM.

The skill of RMM1 and RMM2 are compared for the individual models and a multi-model ensemble combination of the two. The multi-model ensemble is produced by averaging the RMM values of the two individual models. The average anomaly correlation skill for all of the overlapping cases as a function of lead-time is shown in Figure 6 (left panels) for RMM1 (top) and RMM2 (bottom). The skill of the individual models (CFS in red; CCSM in blue) is shown with the skill of the 2-member multi-model ensemble (black). Clearly, one of the models has significantly better skill than the other.

The CFS anomaly correlations fall below 0.5 around day-14 for RMM1 and around day-10 for RMM2, while the CCSM skill is above 0.5 up to about day-25 for RMM1 and day-20 for RMM2. The relatively poor skill by the CFS is likely due to a well-known issue related to the initialization of the CFS re-forecasts (A. Vintzileos, personal communication). It is noted that the two-member MME has similar skill to the CCSM and appears to have slightly better skill at longer lead-times for RMM1.

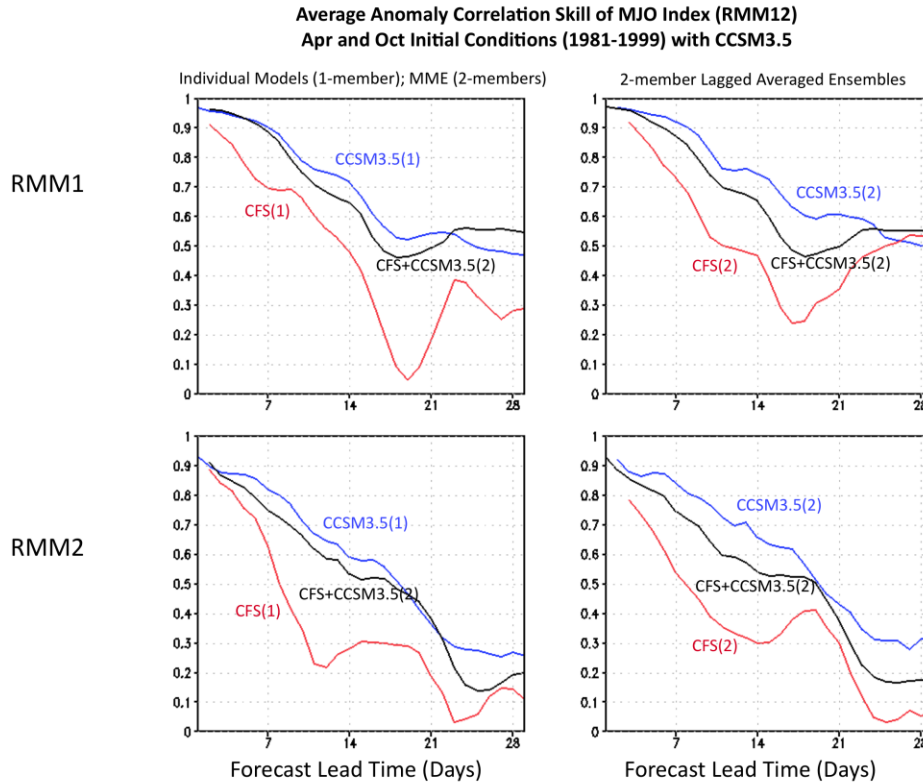


**Figure 6:** Average anomaly correlation skill of the RMM index (RMM1 top panels; RMM2 bottom panels) as a function of lead time for a set of re-forecast experiments with April and October initial conditions for the years 1981-1999 from the CFS (red), CCSM (blue), and a multi-model ensemble of the CFS+CCSM (black). Left panels show the skill of the individual models with a single ensemble member and the two-member MME. Right panels show the skill of two-member lagged average ensembles for the individual models and the MME

The skill comparisons described above are not completely fair comparisons since the skill of the individual models is shown for only a single ensemble member, while the MME is shown for two ensemble members. Therefore, all possible combinations of 2-member lagged average ensembles are generated for the overlapping cases. For example, ensembles are made by averaging the individual model forecasts initialized on Apr 21 and 22 for the same verifying calendar dates. For the multi-model ensemble, a lagged ensemble is produced for the case of Apr 21 from the CCSM and Apr 22 from the CFS and also Apr 21 from the CFS and Apr 22 from the CCSM. This is done for all possible combinations of 2-member lagged ensembles from the two models. The average anomaly correlation skill of these ensemble forecasts is shown in Figure 6 (right panels) for RMM1 (top) and RMM2 (bottom). Not surprisingly, the 2-member lagged average ensemble for each of the individual models has better skill than the single-member versions shown in the left panels. With this more realistic comparison, the skill of the multi-model ensemble is generally less skillful than the CCSM with the exception of lead-times greater than 22-days for RMM1. The key point to derive from these results is that the multi-model ensemble is able to provide skillful forecasts despite the fact that one of the

models has exceptionally poor skill. Although the less skillful model could have been identified a priori in these cases, this may not always be true.

This is the final project report. The research highlights and the publications are listed below.

### Highlights

- Intraseasonal skill in CFS and CCSM
- Improvements in land surface temperatures associated with land initialization
- Multi-model forecast skill

### Publications including work during the no-cost extension

- Achuthavarier, D., V. Krishnamurthy, B. P. Kirtman and B. Huang, 2012: Role of Indian Ocean in the ENSO-Indian summer monsoon teleconnection in the NCEP climate forecast system. *J. Climate*, doi: <http://dx.doi.org/10.1175/JCLI-D-11-00111.1>.
- Kirtman, B. P., T. Stockdale, R. Burgman, 2013: The Ocean's role in predicting seasonal to interannual climate. *Ocean Circulation and Climate*.
- Kirtman, B. P., C. Bitz, F. Bryan, W. Collins, J. Dennis, N. Hearn, J. L. Kinter III, R. Loft, C. Rousset, L. Siqueira, C. Stan. R. Tomas, M. Vertenstein, 2012a: Impact of ocean model resolution on CCSM climate simulations. *Climate Dynamics*, DOI 10.1007/s00382-012-1500-3.
- Kirtman et al, 2013: Prediction from weeks to decades, *Climate Science for Serving Society: Research, Modelling and Prediction Priorities*. G. R. Asrar and J. W. Hurrell, Eds. *Springer*, in press.
- Kirtman, B. P., E. K. Schneider, D. M. Straus, D. Min, R. Burgman, 2011: How weather impacts the forced climate response. *Climate Dynamics*, DOI: 10.1007/s00382-011-1084-3.
- Kirtman, B.P., and G. Vecchi, 2010: Why Climate Modelers Should Worry About the Weather, 511-523, The Global Monsoon System: Research and Forecast, 2nd Ed., World Scientific, Eds. C. P. Chang, Y. Ding, N.-C. Lau, R. H. Johnson, B. Wang, T. Yasunari.
- Kirtman, B. P., and D. Min, 2009: Multi-model ensemble ENSO prediction with CCSM and CFS. *Mon. Wea. Rev.*, DOI: 10.1175/2009MWR2672.1.
- Paolino, D. A., J. L. Kinter III, B. P. Kirtman, D. Min, D. M. Straus, 2012: The impact of land surface initialization on seasonal forecasts with CCSM. *J. Climate*, **25**, 1007-1021.
- Brunet, G., M. Shapiro, B. Hoskins, M. Moncrieff, R. Dole, G. N. Kiladis, B. Kirtman, A. Lorenc, B. Mills, R. Morss, S. Polavarapu and D. Rogers, 2010: Toward a seamless process for the prediction of weather and climate: the advancement of subseasonal to seasonal prediction. *Bull. Amer. Met. Soc.*, DOI:10.1175/2010BAMS3013.1.
- DiNezio, P. N., B. P. Kirtman, A. C. Clement, S.-K. Lee, G. A. Vecchi, A. Wittenberg, 2012: Diverging ENSO projection in response to global warming: The role of the background ocean changes. *J. Climate* doi: <http://dx.doi.org/10.1175/JCLI-D-11-00494.1>.
- Goddard, L., J. W. Hurrell, B. P. Kirtman, J. Murphy, T. Stockdale and C. Vera, 2012: Two timescales for the price of one (almost). *Bull. Amer. Met. Soc.*, doi: <http://dx.doi.org/10.1175/BAMS-D-11-00220.1>

## *Why do CGCMs have too much ENSO Variability in the Western Pacific?*

**Principal Investigator:** B. Kirtman (UM/RSMAS)

**NOAA Funding Unit:** OAR/CPO

**NOAA Technical Contact:** Jim Todd

Progress Report: 1 January 2012 – 31 August 2012

*The following progress report includes the documentation from the previous report and final papers covered as part of the no-cost extension.*

### **Abstract**

The local air-sea feedback diagnostic presented here shows that in many regions of the tropical ocean the atmosphere primarily drives interannual sea surface temperature variability. This diagnostic is applied to both uncoupled AGCM simulations and coupled simulations. The results support the claim that uncoupled AGCM simulations fail to capture the co-variability between the atmosphere and ocean particularly in warm regions of the Indo-Pacific. This has implications in terms of how well the model is able to reproduce the observed tropical teleconnections. In addition, the diagnostic reveals that the coupled models typically fail to capture the observed local air-sea feedbacks in the Western Pacific. Based on simple theoretical calculations the authors argue that: (i) this error leads to ENSO events that extend too far to the west and (ii) that to reduce this error addition stochastic forcing at the air-sea interface needs to be added to the coupled system. This second point is supported by CGCM experiments.

### **Introduction**

Changing oceanic conditions, as manifest through sea surface temperature (SST), can influence atmospheric circulation through a variety of processes, largely by changing enthalpy fluxes across the surface. Thus, sea surface temperature (SST) anomalies play an important role in atmospheric variability and predictability (Charney and Shukla 1981; Shukla 1998; Trenberth et al. 1998; Kang et al 2002, Wang and Zhang 2002, Wang et al 2004). However, atmospheric variability exists that is independent of SST forcing. Both forced and internal aspects of atmospheric climate variability impact oceanic conditions, both through local momentum, freshwater and enthalpy fluxes, and through the remote response of oceanic circulation via wave modes – some of these oceanic changes further impact atmospheric conditions – including those in the monsoon regions (e.g., Vecchi and Harrison 2000; Vecchi et al. 2006). Describing, understanding and representing the coupled interactions between the two fluid systems is a major focus of the scientific community, both as a source of predictability of climate conditions around the world, on a variety of time- and space-scales, and as a basic scientific research problem. For example, Hendon (2003) showed that seasonally varying air-sea interactions, particularly associated with latent heat flux were critical to interannual Indian Ocean SST anomalies and Indonesian rainfall. The importance of air-sea heat exchanges in the Indo-Pacific region in terms of capturing the monsoon variability was also noted by Krishna Kumar et al. (2005), Wu and Kirtman (2007), Wu and Kirtman (2005), Wu et al. (2006), Wang et al. (2003, 2005), Kucharshki et al. (2007), Bracco et al. 2007, Vecchi and Harrison 2004, and Lau and Nath (2000, 2003, 2004). Observed and simulated Indian Ocean SST variability and its relationship with the monsoon has also received considerable attention in recent years (e.g., Krishnamurty and Kirtman 2003, Xie et al 2002, Annamalai

et al 2003, Behera et al 2000, Huang and Kinter 2002, Song et al 2007, Izuka et al 2000, Jin and An 1999, Li et al 2002, Murtugudde and Busalacchi 1999, Murtugudde et al 2000, Saji et al 1999, Webster et al. 1999). There have also been simulations and observational studies demonstrating the role of Atlantic and Pacific Ocean variability on the Indian Ocean monsoon system (e.g., Kucharski et al. 2008; Shinoda et al. 2004). A detailed discussion of Indo-Pacific variability and its relationship with the monsoon can be found in the review article by Webster et al. (1998).

Simulations of atmospheric general circulation models (AGCMs) forced by prescribed SSTs (either observed or idealized in order to isolate particular mechanisms) allow us to assess aspects of the SST control on climate variability, and exploit this atmospheric response to SST anomalies for predictive purposes and to increase our understanding of the climate system. However, AGCM experiments forced by observed SST show both consistencies with and discrepancies from observations (e.g., Sperber and Palmer 1996; Kumar and Hoerling 1998; Kang et al. 2002; Wang et al. 2004). In addition to fundamental predictability limitations arising directly from internal atmospheric dynamics, two major reasons for the model-observation discrepancies are: (1) the biases in the model physics and (2) the lack of air–sea coupling in the forced simulations. The discrepancies due to (1) are model dependent and can be reduced with the improvement in the representation of atmospheric physical processes in the model. The discrepancies due to (2) are fundamental and common to all of the forced simulations, and arise because some SST features are actually the result of atmospheric conditions that arise due to either remote SST forcing or internal atmospheric dynamics independent of SST changes: the SST used as a forcing in some conditions is actually a response. In turn, using these SST anomalies that are forced by the observed atmosphere as prescribed SST in uncoupled atmospheric model simulation can result in improper local air–sea relationships in some regions resulting in unrealistic atmospheric variability (Saravanan 1998; Saravanan and McWilliams 1998; Bretherton and Battisti 2000; Wang et al. 2004, 2005; Krishna Kumar et al. 2005; Trenberth and Shea 2005; Wu et al. 2006). Some discrepancies due to the lack of air–sea coupling have been demonstrated in previous studies (Roebber et al. 1997; Barsugli and Battisti 1998; Wittenberg and Anderson 1998; Wu and Kirtman 2005).

To illustrate an aspect of discrepancy (2), Figure 1 shows that even the interannual correlation of seasonal SST and evaporation anomalies can differ in various regions around the tropics, when comparing SST-forced and coupled climate integrations using the same atmospheric component. There are substantial regions of negative correlation in the coupled climate model, indicating regions where enhanced evaporation is associated with cool conditions, while the correlation tends to be more positive in the AGCM, as warm conditions tend to favor evaporation in an SST-forced framework. The reader is also referred to Figure (top left panel) where we show the same correlation based on observational estimates. The observational estimates indicate significant regions of negative correlation that are either complete absent on the AGCM forced simulation or are weaker than observed in the CGCM simulations.

When and where the discrepancies due to the lack of air–sea coupling occur depends on what causes the SST anomalies. In the case that the local SST anomalies are primarily due to internal oceanic processes, it is likely that the forced simulations can capture the observed atmospheric variability. This is the case in the tropical central and eastern Pacific where the observed SST anomalies are mainly due to oceanic processes with surface heat fluxes mainly acting as a damping effect (e.g., Jin and An 1999; Kang et al. 2001) and SST forced simulations perform well (e.g., Kumar and Hoerling 1998; Kang et

al. 2002; Wang et al. 2004). In the case that the observed SST anomalies are largely due to atmospheric forcing, erroneous atmospheric response can result in the specified SST simulations. This occurs in the extratropics and the tropical Indo-western Pacific Ocean regions where the atmospheric forcing plays an important role in inducing SST anomalies (e.g., Lau and Nath 1996; Alexander et al. 2002; Lau and Nath 2000, 2003; Wang et al. 2003; Krishnamurthy and Kirtman 2003). In these regions, the forced simulations deviate from observations (e.g., Sperber and Palmer 1996; Wang et al. 2004; Wu et al. 2006) and coupled model simulations (e.g., Kitoh and Arakawa 1999; Wu and Kirtman 2005; Wu et al. 2006). We focus on the western tropical Pacific in more detail below and show how the air-sea feedbacks in the western Pacific ultimately impact the remote ENSO variability in coupled models.

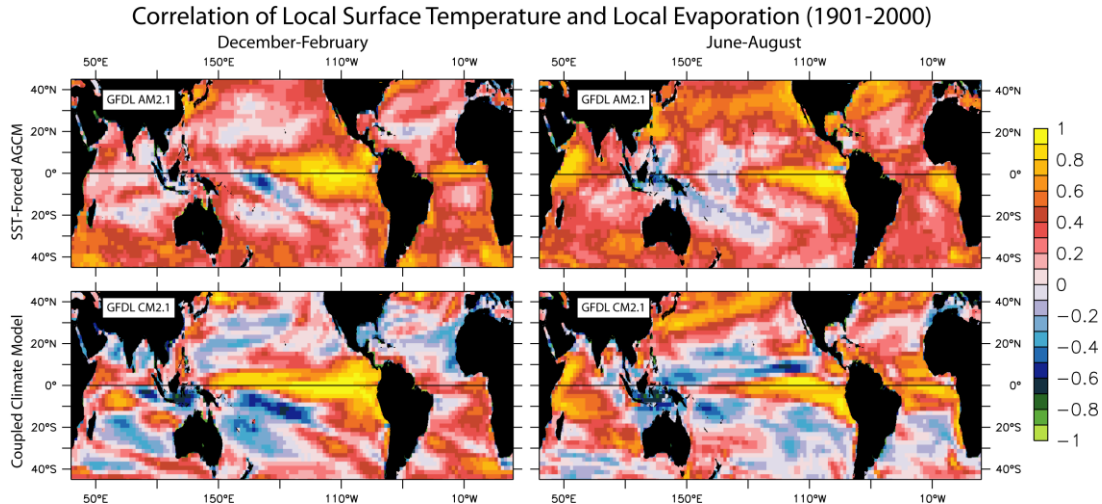


**Figure 1:** Correlation of seasonal-mean SST anomalies and evaporation anomalies from SST-forced AGCM (upper panels) and coupled climate model (lower panels) integrations over a 100-year period. The two model systems share the same atmospheric component. The atmospheric component is the finite volume version of the GFDL atmospheric model (AM2.1; GAMDT 2005, Lin et al 2006), and the coupled model is a version of the GFDL coupled climate model (CM2.1; Delworth *et al.* 2006, Gnanadesikan *et al.* 2006, Stouffer *et al.* 2006, Wittenberg *et al.* 2006, Song *et al.* 2006).

### Diagnosing Air-Sea Feedbacks

The nature of local air-sea interaction can be understood from the evolution of lag-lead correlation between the atmospheric variables and SST (von Storch 2000; Wu et al. 2006). Using a simple stochastic model, Barsugli and Battisti (1998) identified distinct lagged linear regression between sea and air temperature for coupled and uncoupled cases. von Storch (2000) provided a conceptual interpretation of how the different shapes of lag cross-correlations relate to different forcing-response relationships. The author identified very different evolution of the lag correlation between surface heat flux and SST in the mid-latitude North Pacific and the equatorial central Pacific. Wu and Kirtman (2005) demonstrated that the local lag-lead correlation between SST, rainfall, and surface evaporation can indicate an atmospheric negative feedback in the coupled model. The analysis of lag-lead correlations has been used to understand the atmosphere-ocean relationship in observations and models (Frankignoul et al. 1998; von Storch 2000; Frankignoul and Kestenare 2002; Frankignoul et al. 2002; Frankignoul et al. 2004; Kitoh and Arakawa 1999; Wang et al. 2005; Wu and Kirtman 2005; Wu et al. 2006). However, because atmosphere-ocean interactions are seasonally dependent (e.g., Hendon 2003; Wang et al. 2003), it is not so simple to analyze the lag-lead correlations.

Another way to reveal the air–sea relationship is to combine simultaneous atmosphere–SST and atmosphere–SST tendency correlations (Wu et al. 2006). SST anomalies can induce anomalous convection through surface evaporation and low-level moisture convergence. Because the atmospheric response to SST forcing is relatively fast, a large positive simultaneous correlation, for example, between rainfall and SST may indicate that the SST is forcing the atmosphere. On the other hand, anomalous atmospheric convection can change the SST through cloud-radiation and wind-evaporation effects and wind-induced oceanic mixing and upwelling. These atmospheric feedbacks can be detected in the SST tendency. Thus, the magnitude of simultaneous rainfall–SST and rainfall–SST tendency correlations can indicate the relative importance of SST forcing and atmospheric forcing. Wu and Kirtman (2005) showed that in regions where the atmosphere has a strong negative feedback on SST (e.g., tropical western North Pacific in boreal summer and tropical southwestern Indian Ocean in austral summer), the negative rainfall–SST tendency correlation is larger than the rainfall–SST correlation. This differs from the equatorial central-eastern Pacific where the positive rainfall–SST correlation is much larger than the rainfall–SST tendency correlation. Using simple model simulations, Wu et al. (2006) demonstrated that the surface turbulent heat flux–SST/SST tendency correlation displays marked differences for the case when atmospheric forcing dominates versus when SST forcing dominates. An analysis of heat flux–SST tendency correlation has been performed to identify the atmospheric forcing of SST in the North Pacific (e.g., Cayan 1992) and in the tropical Indo-western Pacific Ocean regions (e.g., Wu and Kirtman 2005; Wu et al. 2006).

The importance of accurately capturing the western Pacific air-sea feedbacks correctly (or the implications of failing to capture these feedbacks) is exemplified in Figure 2, which shows an example from several models participating in the Intergovernmental Panel on Climate Change (IPCC) Assessment Report four (AR4). In this figure we have plotted the spatial pattern of the first Empirical Orthogonal Function (EOF1) of the SST anomaly in the equator in the Pacific from five different state-of-the-art coupled models and observational estimates. All of the coupled models shown here have dominant ENSO modes that extend too far to the west. Often, but not always, the models have ENSO periodicities that are too fast compared to observations. The conventional wisdom is that the westward extension of the ENSO events and the fast periodicity is due to the cold tongue mean state errors. Simply, errors in the mean state are the cause for the errors in the anomalies. Here we suggest that the errors in the simulated ENSO are due to errors in the statistics of the tropical atmospheric weather and the associated air-sea feedback in the western Pacific. In other words, if there are large errors in the simulation of the weather statistics in the western Pacific and the associated air-sea feedbacks, then the climate simulation is seriously degraded.

### **Linking Theory with Simulation**

The theoretical coupled model presented in Wu et al. (2006) suggests that the source of the western Pacific problem is due to incorrect latent heat flux – SST feedbacks, and the theory suggest a potential solution. Wu et al. (2006) show that when the correlation between the latent heat flux (our convention here is that latent heat flux is positive upward) and SST anomalies is strongly negative, the SST variability can be viewed as strongly forced by atmospheric variability (noise). Conversely, when the ocean forcing dominates the correlation is positive. Figure 3 (in part taken from Wu et al. 2006) shows this correlation from satellite based observational estimates (top left) and the COLA anomaly coupled model (bottom left; Kirtman et al. 2002). Clearly, near the equator in the western Pacific the coupled model fails to capture the observed relationship. This is also true in significant regions of the tropical Indian and Atlantic Oceans. Similar errors have been identified with CFS (e.g., Wu et al. 2007) and

with CCSM3 (not shown). The theoretical model suggests two possible interpretations of this result: (a) the ocean is too strongly forcing the atmosphere or (b) the atmosphere is not forcing the ocean enough. Wu et al. (2006) describes the theoretical basis for these possible interpretations.

### The 1st EOF mode of SSTA

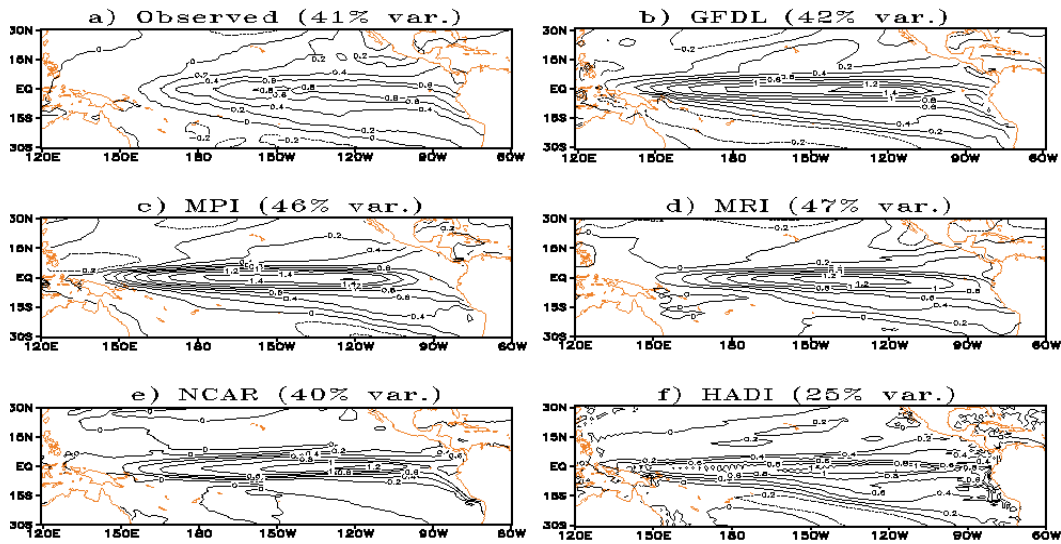
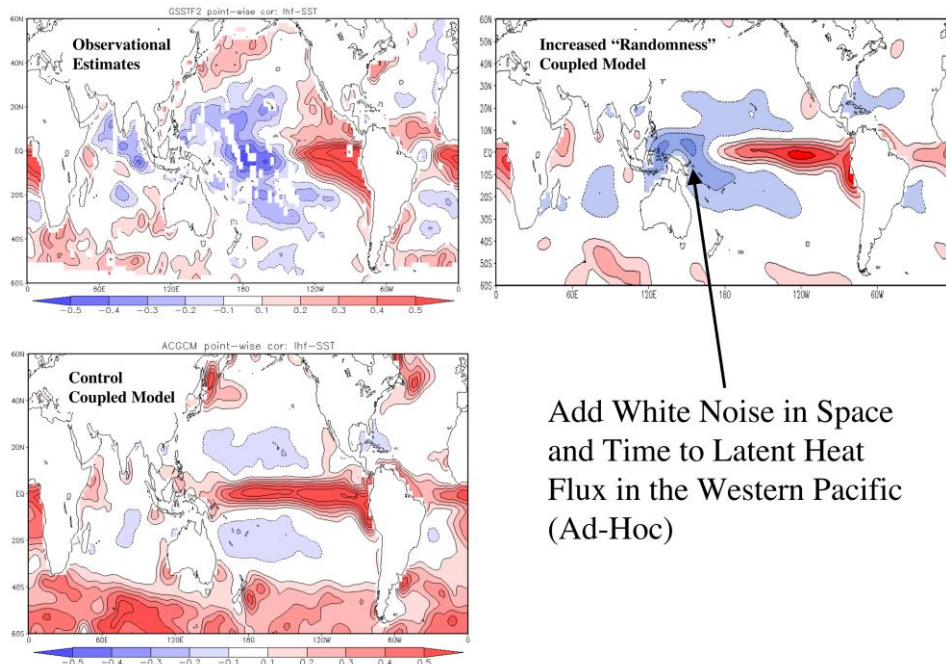


**Figure 2:** SSTA EOFs calculated from various coupled model intercomparison project simulations (CMIP3). The domain plotted corresponds to the domain of the EOF calculation. In each figure 100-years of data was used from simulation with fixed climate forcing at 1990 levels.

### Contemporaneous Latent Heat Flux - SST Correlation



Add White Noise in Space and Time to Latent Heat Flux in the Western Pacific (Ad-Hoc)

**Figure 3:** Contemporaneous correlation between latent heat flux anomalies (positive upward) and SST anomalies based on observational (top left) estimates from version 2 of the Goddard Satellite-Based Turbulence Fluxes (GFSST2) data, the COLA coupled model simulation (bottom left) and the COLA model forced with Gaussian white noise in the latent heat flux in the western Pacific (top right).

In the case of the atmosphere forcing the ocean, the theoretical model of Wu et al. (2006) adopted from Barsugli and Battisti (1998) is as follows:

$$\frac{dT_a}{dt} = \alpha(T_o - T_a) + N_a, \quad (1)$$

$$\frac{dT_o}{dt} = \beta(T_a - T_o) - \gamma_o T_o. \quad (2)$$

In the above,  $T_a$  and  $T_o$  refer to air and sea temperature, respectively. Air-sea heat flux (latent and sensible) is represented by the air-sea temperature difference,  $N_a$  represents atmospheric white noise forcing and  $\alpha$  and  $\beta$  are exchange coefficients. This theoretical model implies a negative contemporaneous correlation between the atmosphere and the ocean. In contrast, Wu et al. (2006) also present a simple theoretical model for the ocean forcing the atmosphere, e.g.,

$$\frac{dT_a}{dt} = \alpha(T_o - T_a), \quad (3)$$

$$\frac{dT_o}{dt} = \beta(T_a - T_o) - \gamma_o T_o + N_o. \quad (4)$$

In this case,  $N_o$  represent oceanic forcing of the atmosphere and the air-sea correlation is positive.

The theoretical model described above also suggests a possible solution to this air-sea feedback problem, namely we need to change the relative strength of the atmosphere forcing of the ocean or the ocean forcing of the atmosphere. In other words, we can simply modify  $N_a$  or  $N_o$  to change the air-sea correlation. We present here an ad-hoc preliminary attempt at modifying the relative forcing strength. Here we modify the effective  $N_a$  in the CGCM by simply add Gaussian white noise (in both space and time) to the latent heat flux that is used to force the ocean. In this test, the noise amplitude is arbitrarily chosen to be 15% of the day-to-day variance produced by a control run of the model and is only applied in the far western Pacific (5N-5S, 120E-160E). This Gaussian white noise forcing was applied to a 100-yr simulation of the COLA anomaly coupled model. The resulting correlation is also shown in Fig. 3 (top right). As predicted by the theoretical model, the correlation has changed sign in the western Pacific. We emphasize that this is more than simply reducing the amplitude of the correlation – it has actually changed sign. The entire ENSO system in this simulation has shifted further to the east with a consistent increase in the periodicity. This suggests the air-sea physics in the western Pacific can have a profound impact on the ENSO simulation. This impact is more than merely making the ENSO more irregular; it is shifting the system eastward modifying the oceanic time-scales (via wave dynamics) and even modifying the global teleconnections by shifting the region of maximum rainfall anomalies to the east. The changes in the periodicity and the eastward shift of the variability can easily be detected in Figure. 4, which shows the lag-lead regression of Nino3.4 SSTA onto equatorial Pacific SSTA. In essence, adding noise in the western Pacific heat flux has modified the coupled signal without explicit changes to either the atmospheric or oceanic component model.

Another possible solution to the problem is to restrict the uncoupled SST forcing of the atmospheric model to a region where SST can be largely be considered a local forcing (e.g., the eastern and central equatorial Pacific Ocean), and allowing the atmospheric model to couple to a thermodynamically or

dynamically active oceanic model elsewhere. Model configurations of this type have been used to explore the response of the monsoon and midlatitude climate systems to forcing from various tropical basins (*e.g.*, Alexander *et al* 2002, Lau and Nath 1996, 2000, 2003, 2004, Bracco *et al.* 2007), and to explore the impact of decadal oceanic variations in the Atlantic on global climate conditions (*e.g.*, Zhang *et al.* 2007).

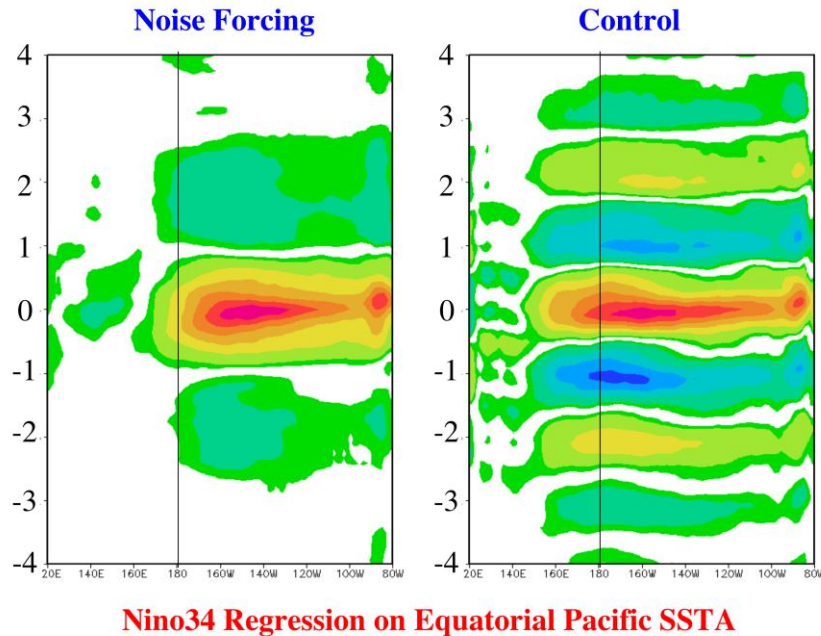


**Figure 4:** Lag-lead regression between Nino3.4 SSTA and equatorial Pacific SSTA. The left panel corresponds to the noise forcing experiment and the control is shown in the right panel. The contour interval is the same for both panels and starts at  $\pm 0.2$ . The lags and leads noted on the left of each panel are in years.

While the previous discussion has largely focused on large-scale errors arising from inadequate coupling – largely arising due to internal atmospheric variability, it is interesting to briefly consider the possibility of analogous issues on the oceanic mesoscale, arising from internal oceanic variability. There is now considerable evidence that the sharp SST gradients induced by oceanic mesoscale features (*e.g.*, upwelling filaments, eddies, tropical instability waves, sharp fronts, warm western boundary currents, etc) can drive changes in the atmosphere, through local air-sea interaction (*e.g.*, Chelton *et al.* 2001, 2004, 2005, 2007; Hashizume *et al.* 2001; Xie 2004; Vecchi *et al.* 2004; Seo *et al.* 2007, 2008; Minobe *et al.* 2008, Small *et al.* 2008). These atmospheric changes on the oceanic mesoscale result in variations to the enthalpy and momentum fluxes of sufficient magnitude to impact the oceanic structures that drove them (*e.g.*, Chelton *et al.* 2005, Vecchi *et al.* 2004, Seo *et al.* 2007, 2008). Thus, in order to correctly represent the physical processes behind these oceanic mesoscale features, one may be required to correctly represent the impact of this air-sea coupling. However, high-resolution ocean models are generally forced by winds from either global analysis products (like ECMWF and NCEP) or by winds derived from satellite scatterometry (such as NSCAT or QuickSCAT). Wind from the global analyses do not include features on the oceanic mesoscale, so the effects of this coupling will be absent from a forced experiment, while scatterometer winds include the impacts of coupling that correspond to the internal oceanic structures present in the real world, which need not correspond to those in the model. Thus, as eddy-permitting and eddy-resolving models

continue to be developed and implemented in climate-scale integrations, solutions to – perhaps analogous to those discussed above –the problem of inadequately representing air-sea interactions on the oceanic mesoscale must be explored and developed.

### **Final Remarks**

Dynamical numerical modeling systems are an essential tool in describing, understanding, representing and predicting the atmospheric and oceanic conditions of the global climate system, including those in the monsoonal regions of the world. Boundary-forced configurations of these models can represent many aspects of the variations of the ocean and atmosphere climate system, but discrepancies can arise from incorrectly specifying the boundary values as a forcing, when they are actually largely a response to variations in the system one is modeling. Solutions to this problem have been and should continue to be developed, and modelers should be keenly aware of these potential problems

### **Activities Associated with No-Cost Extension**

**Research Highlights:** Implemented Westerly Wind Burst (WWB) parameterizations in CCSM3 and CCSM4 and demonstrated how state dependent noise amplifies the ENSO signal and predictability. Moreover state dependent noise shifts the model ENSO from a damped regime to a self-sustained regime. Surprisingly, state independent noise has no impact on ENSO.

### **Publications**

- DiNezio, P. N., B. P. Kirtman, A. C. Clement, S.-K. Lee, G. A. Vecchi, A. Wittenberg, 2012: Diverging ENSO projection in response to global warming: The role of the background ocean changes. *J. Climate* doi: <http://dx.doi.org/10.1175/JCLI-D-11-00494.1>.
- Goddard, L., J. W. Hurrell, B. P. Kirtman, J. Murphy, T. Stockdale and C. Vera, 2012: Two timescales for the price of one (almost). *Bull. Amer. Met. Soc.*, doi: <http://dx.doi.org/10.1175/BAMS-D-11-00220.1>
- Kirtman, B. P., T. Stockdale, R. Burgman, 2013: The Ocean's role in predicting seasonal to interannual climate. *Ocean Circulation and Climate*.
- Kirtman, B. P., C. Bitz, F. Bryan, W. Collins, J. Dennis, N. Hearn, J. L. Kinter III, R. Loft, C. Rousset, L. Siqueira, C. Stan. R. Tomas, M. Vertenstein, 2012a: Impact of ocean model resolution on CCSM climate simulations. *Climate Dynamics*, DOI 10.1007/s00382-012-1500-3.
- Kirtman et al, 2013: Prediction from weeks to decades, *Climate Science for Serving Society: Research, Modelling and Prediction Priorities*. G. R. Asrar and J. W. Hurrell, Eds. *Springer*, in press.
- Kirtman, B. P., E. K. Schneider, D. M. Straus, D. Min, R. Burgman, 2011: How weather impacts the forced climate response. *Climate Dynamics*, DOI: 10.1007/s00382-011-1084-3.
- Kirtman, B.P., and G. Vecchi, 2010: Why Climate Modelers Should Worry About the Weather, 511-523, The Global Monsoon System: Research and Forecast, 2nd Ed., World Scientific, Eds. C. P. Chang, Y. Ding, N.-C. Lau, R. H. Johnson, B. Wang, T. Yasunari.

Lopez, H., B. P. Kirtman, E. Tzipperman, G. Gebbie, 2012: Impact of interactive westerly wind burst in CCSM. *Dyn. Atmos. Ocean.*, (in press).

Narapusetty, B., C. Stan, B. P. Kirtman, P. S. Schopf, L. Marx, and J. L. Kinter III (2012), The role of atmospheric internal variability on the tropical instability wave dynamics, *J. Geophys. Res.*, **117**, C00J31, doi:10.1029/2012JC007906.

Siqueira, L. S. P., and B. P. Kirtman, 2012: Predictability and uncertainty in a low order coupled model. *Nonlinear Process in Geophysics* doi:10.5194/npg-19-273-2012

Smith, D. M., A. A. Scaife and B. Kirtman, 2012: What is the current state of scientific knowledge with regard to seasonal and decadal forecasting. *Environ. Res. Lett.*, **7**, 015602, doi:10.1088/1748-9326/7/1/015602.

## References

Adler RF, Huffman GJ, Chang A, Ferraro R, Xie P, Janowiak J, Rudolf B, Schneider U, Curtis S, Bolvin D, Gruber A, Susskind J, Arkin P (2003) The version 2 global precipitation climatology project (GPCP) monthly precipitation analysis (1979-present). *J. Hydrometeor.* **4**, 1147–1167.

Alexander MA, Blade´ I, Newman M, Lanzante JR, Lau N-C, Scott JD (2002) The atmospheric bridge: the influence of ENSO teleconnections on air–sea interaction over the global oceans. *J. Clim.* **15**, 2205–2231.

Annamalai H, Murttugudde R, Potema J, Xie S-P, Wang B (2003) Coupled dynamics over the Indian Ocean: spring initiation of the zonal mode. *Deep Sea Res Part II Top Stud. Oceanogr.* **50**, 2305–2330.

Baquero-Bernal A, Latif M, Legutke S (2002) On the dipole like variability of sea surface temperature in the tropical Indian Ocean. *J. Clim.* **15**, 1358–1368.

Barsugli JJ, Battisti DS (1998) The basic effects of atmosphere-ocean thermal coupling on midlatitude variability. *J. Atmos. Sci.* **55**, 477–493.

Behera SK, Salvakar PS, Yamagata T (2000) Simulation of interannual SST variability in the tropical Indian Ocean. *J. Clim.* **13**, 3487–3499.

Bracco A, F. Kucharski, F. Molteni, W. Hazeleger, and C. Severijns (2007), A recipe for simulating the interannual variability of the Asian Summer Monsoon and its relation with ENSO. *Climate Dyn.*, **28**, 441-460, doi 10.1007/s00382-006-0190-0.

Bretherton CS, Battisti DS (2000) An interpretation of the results from atmospheric general circulation models forced by the time history of the observed sea surface temperature distribution. *Geophys. Res. Lett.* **27**,767–770.

Cayan, D.R. (1992) Latent and sensible heat flux anomalies over the northern oceans: driving the sea surface temperature. *J. Phys. Oceanogr.* **22**, 859–881.

- Chambers DP, Tapley BD, Stewart RH (1999) Anomalous warming in the Indian Ocean coincident with El Niño. *J. Geophys. Res.* **104**, 3035–3047.
- Charney J, Shukla J (1981) Predictability of monsoons. In: Lighthill J, Pearce RP (eds) *Monsoon dynamics*. Cambridge University Press, New York, pp 99–110.
- Chelton, D.B., M.G. Schlax and R.M. Samelson (2007) Summertime Coupling between Sea Surface Temperature and Wind Stress in the California Current System. *J. Phys. Oceanogr.*, **37**, 495-517. 641 642
- Chelton, D.B. and F.J. Wentz (2005) Global Microwave Satellite Observations of Sea Surface Temperature for Numerical Weather Prediction and Climate Research. *Bull. Amer. Meteor. Soc.*, **86**, 1097-1115.
- Chelton, D.B., M. Schlax, M.H. Freilich and R.F. Milliff (2004) Satellite measurements reveal persistent small-scale features in ocean winds. *Science*, 303, pp. 978–983.
- Chelton, D.B. and S.K. Esbensen, M.G. Schlax, N. Thum, M. H. Freilich, F. J. Wentz, 650 C.L. Gentemann, M. J. McPhaden and P.S. Schopf (2001) Observations of coupling between surface wind stress and sea surface temperature in the eastern tropical Pacific. *J. Climate*, **14**, 1479–1498.
- Chou S-H, Nelkin E, Ardizzone J, Atlas RM, Shie C-L (2003) Surface turbulent heat and momentum fluxes over global oceans based on Goddard satellite retrievals, version 2 (GSSTF2). *J. Clim.* **16**, 3256–3273.
- Chou S-H, Nelkin E, Ardizzone J, Atlas RM (2004) A comparison of latent heat fluxes over global oceans for four flux products. *J. Clim.* **17**, 3973–3989.
- Delworth, T. L., and Coauthors, 2006: GFDL’s CM2 global coupled climate models. Part I: Formulation and simulation characteristics. *J. Climate*, 19, 643–674. the Indo-Pacific sector during ENSO episodes. *J. Climate*, **16**, 3–20.
- Frankignoul C, Kestenare E (2002) The surface heat flux feedback. Part I: estimates from observations in the Atlantic and the North Pacific. *Clim. Dyn.* **19**, 633–647.
- Frankignoul C, Czaja Z, L’Heveder B (1998) Air–sea feedback in the North Atlantic and surface boundary conditions for ocean models. *J. Clim.* **11**, 2310–2324
- Frankignoul C, Kestenare E, Mignot J (2002) The surface heat flux feedback. Part II: direct and indirect estimates in the ECHAM4/OPA8 coupled GCM. *Clim. Dyn.* **21**, 21–51.
- Frankignoul C, Kestenare E, Botzet M, Carril AF, Drange H, Pardaens A, Terray L, Sutton R (2004) An intercomparison between the surface heat flux feedback in five coupled models, COADS and the NCEP reanalysis. *Clim. Dyn.* **22**, 373–388.

- Gill AE (1980) Some simple solutions for heat-induced tropical circulation. *Quart. J. Roy. Meteor.* **106**, 447–462.
- Gnanadesikan, A., and Coauthors, 2006: GFDL's CM2 global coupled climate models. Part II: The baseline ocean simulation. *J. Climate*, **19**, 675–697.
- Hashizume, H., S.-P. Xie, W.T. Liu and K. Takeuchi, 2001: Local and remote atmospheric response to tropical instability waves: A global view from the space. *J. Geophys. Res.-Atmos.*, **106**, 10 173-10 185.
- Hendon H (2003) Indonesia rainfall variability: impacts of ENSO and local air–sea interaction. *J. Clim.* **16**, 1775–1790.
- Huang B, Kinter III JL (2002) Interannual variability in the tropical Indian Ocean. *J. Geophys. Res.* **107**, 3199. doi:10.1029/2001JC001278.
- Iizuka S, Matsuura T, Yamagata T (2000) The Indian Ocean SST dipole simulated in a coupled general circulation model. *Geophys. Res. Lett.* **27**, 3369–3372.
- Jin F-F, An S-I (1999) Thermocline and zonal advective feedbacks within the equatorial ocean recharge oscillator model for ENSO. *Geophys. Res. Lett.* **26**, 2989–2992.
- Kalnay E, et al (1996) The NCEP/NCAR 40-year reanalysis project. *Bull. Am. Meteor. Soc.* **77**, 437–471.
- Kang I-S, An S-I, Jin F-F (2001) A systematic approximation of the SST anomaly equation for ENSO. *J. Meteor. Soc. Japan* **79**, 1–10.
- Kang I-S, et al (2002) Intercomparison of GCM simulated anomalies associated with the 1997–98 El Niño. *J. Clim.* **15**, 2791–2805.
- Kinter JL III, DeWitt DG, Dirmeyer PA, Fennessy MJ, Kirtman BP, Marx L, Schneider EK, Shukla J, Straus D (1997) The COLA atmosphere-biosphere general circulation model, vol. 1: formulation. COLA Technical Report 51, COLA, Calverton, 46 pp.
- Kinter JL III, Fennessy MJ, Krishnamurthy V, Marx L (2004) An evaluation of the apparent interdecadal shift in the tropical divergent circulation in the NCEP-NCAR reanalysis. *J. Clim.* **17**, 349–361.
- Kitoh A, Arakawa O (1999) On overestimation of tropical precipitation by an atmospheric GCM with prescribed SST. *Geophys. Res. Lett.* **26**, 965–2968.
- Klein SA, Sode BJ, Lau N-C (1999) Remote sea surface temperature variations during ENSO: evidence for a tropical atmospheric bridge. *J. Clim.* **12**, 917–932.

- Krishna Kumar K, Hoerling MP, Rajagopalan B (2005) Advancing dynamical prediction of Indian monsoon rainfall. *Geophys. Res. Lett.* **32**, L08704. doi:10.1029/2004GL021979.
- Krishnamurthy V, Kirtman BP (2003) Variability of the Indian Ocean: relation to monsoon and ENSO. *Quart J Roy Meteor Soc* 129:1623–1646
- Kucharski F., A. Bracco, J. H. Yoo, and F. Molteni, 2007: Low-frequency Variability of the Indian Monsoon-ENSO Relationship and the Tropical Atlantic: The “Weakening” of the 1980s and 1990s. *J. Climate*, **20**, 4255-4266.
- Kucharski F., A. Bracco, J. H. Yoo, and F. Molteni, 2008: Atlantic forced component of the Indian monsoon interannual variability. *Geophys. Res. Lett.*, **33**, L04706, doi:10.1029/2007GL033037.
- Kumar A, Hoerling MP (1998) Specification of regional sea surface temperatures in atmospheric general circulation model simulations. *J. Geophys. Res.* **103**, 8901–8907.
- Lau N-C, Nath MJ (1996) The role of the “Atmospheric Bridge” in linking tropical Pacific ENSO events to extratropical SST anomalies. *J. Clim.* **9**, 2036–2057.
- Lau N-C, Nath MJ (2000) Impact of ENSO on the variability of the Asian-Australian monsoons as simulated in GCM experiments. *J. Clim.* **13**, 4287–4309.
- Lau N-C, Nath MJ (2003) Atmosphere-ocean variations in the Indo-Pacific sector during ENSO episodes. *J. Clim.* **16**, 3–20.
- Lau N-C, Nath MJ (2004) Coupled GCM simulation of atmosphere-ocean variability associated with zonally asymmetric SST changes in the tropical Indian Ocean. *J. Clim.* **17**, 245–265,
- Li T, Zhang Y, Lu E, Wang D (2002) Relative role of dynamic and thermodynamic processes in the development of the Indian Ocean dipole: an OGCM diagnosis. *Geophys. Res. Lett.* **29**, 2110, doi:10.1029/2002GL015789.
- Matsuno T (1966) Quasi-geostrophic motions in the equatorial area. *J. Meteor. Soc. Japan* **44**, 25–42.
- Minobe, S., A. Kuwano-Yoshida, N. Komori, S.-P. Xie, and R.J. Small, 2008: Influence of the Gulf Stream on the troposphere. *Nature*, **452**, 206-209.
- Murtugudde R, Busalacchi AJ (1999) Interannual variability in the dynamics and thermodynamics of the tropical Indian Ocean. *J. Clim.* **12**, 2300–2326.
- Murtugudde R, McCreary JP Jr, Busalacchi AJ (2000) Oceanic processes associated with anomalous events in the Indian Ocean with relevance to 1997–1998. *J. Geophys. Res.* **105**, 3295–3306.
- Nicholls N (1978) Air–sea interaction and the quasi-biennial oscillation. *Mon. Wea. Rev.* **106**, 1505–1508.

- Nicholls N (1979) A simple air–sea interaction model. *Quart. J. Roy. Meteor. Soc.* **105**, 93–105.
- Reynolds RW (1988) A real-time global sea surface temperature analysis. *J. Clim.* **1**, 75–86.
- Reynolds RW, Marsico DC (1993) An improved real-time global sea surface temperature analysis. *J. Clim.* **6**, 114–119.
- Reynolds RW, Rayner NA, Smith TM, Stokes DC, Wang W (2002) An improved in situ and satellite SST analysis for climate. *J. Clim.* **15**, 1609–1625.
- Roebber PJ, Tsonis AA, Elsner JB (1997) Do climate simulations from models forced by averaged sea surface temperature represent actual dynamics? *Nonlin. Proc. Geophys.* **4**, 93–100.
- Saji NH, Goswami BN, Vinayachandran PN, Yamagata T (1999) A dipole mode in the tropical Indian Ocean. *Nature* **401**, 360–363.
- Saravanan R (1998) Atmospheric low-frequency variability and its relationship to midlatitude SST variability: studies using the NCAR climate system model. *J. Clim.* **11**, 1386–1404.
- Saravanan R, McWilliams JC (1998) Advective ocean-atmosphere interaction: an analytical stochastic model with implications for decadal variability. *J. Clim.* **11**, 165–188.
- Seo, H., M. Jochum, R. Murtugudde, A.J. Miller and J.O. Roads (2007a) Feedback of 813 Tropical Instability Wave - induced Atmospheric Variability onto the Ocean. *J. Climate*, **814**(20), 5842–5855.
- Seo, H. Mesoscale Couple Ocean-Atmosphere Interaction, Ph.D. Dissertation, University of California, San Diego, 2007.
- Shinoda T, Alexander MA, Hendon HH (2004) Remote response of the Indian Ocean to interannual SST variations in the tropical Pacific. *J. Clim.* **17**, 362–372.
- Shukla J (1998) Predictability in the midst of chaos: a scientific basis for climate forecasting. *Science* **282**, 728–731.
- Small, R.J., S. de Szoeko, S.-P. Xie, L. O'Neill, H. Seo, Q. Song, P. Cornillon, M. Spall and S. Minobe (2008) Air-sea interaction over ocean fronts and eddies. *Dynam. Ocean. & Atmos.*, in press.
- Song, Q., G.A. Vecchi, and A. Rosati (2007). Indian Ocean Variability in the GFDL CM2 Coupled Climate Model. *J. Climate*, **20**(13), 2895–2916.
- Sperber KR, Palmer TN (1996) Interannual tropical rainfall variability in general circulation model simulations associated with the atmospheric model intercomparison project. *J. Clim.* **9**, 2727–2750.

- Stouffer, R., and Coauthors (2006) GFDL's CM2 global coupled climate models. Part IV: Idealized climate response. *J. Clim.* **19**, 723–740.
- Trenberth KE, Shea DJ (2005) Relationships between precipitation and surface temperature. *Geophys. Res. Lett.* **32**, L14703. doi:10.1029/2005GL022760.
- Trenberth KE, Branstator GW, Karoly D, Kumar A, Lau N-C, Ropelewski C (1998) Progress during TOGA in understanding and modeling global teleconnections associated with tropical sea surface temperatures. *J. Geophys. Res.* **103**, 14291–14324.
- Vecchi, G.A., A.T. Wittenberg and A. Rosati (2006). Reassessing the role of stochastic forcing in the 1997-8 El Niño. *Geophys. Res. Lett.* **33**, L01706, doi:10.1029/2005GL024738.
- Vecchi, G.A. and D.E. Harrison (2000) Tropical Pacific sea surface temperature anomalies, El Niño and equatorial westerly wind events. *J. Climate*, 13(11), 1814-1830.
- Vecchi, G.A., and D.E. Harrison (2004) Interannual Indian rainfall variability and Indian Ocean sea surface temperature anomalies. In *Earth Climate: The Ocean-Atmosphere Interaction*, C. Wang, S.-P. Xie, and J.A. Carton (eds.), American Geophysical Union, Geophysical Monograph 147, Washington D.C., 247–260.
- Vecchi, G.A., S.-P. Xie and A.S. Fischer (2004) Ocean–atmosphere covariability in the 853 western Arabian Sea. *J. Climate*, **17**, 1213–1224.
- von Storch J-S (2000) Signature of air–sea interactions in a coupled atmosphere-ocean GCM. *J. Clim.* **13**, 3361–3379.
- Wang B, Zhang Q (2002) Pacific-East Asian teleconnection. Part II: how the Philippine Sea anomalous anticyclone is established during El Niño development. *J. Clim.* **15**, 1643–1658.
- Wang B, Wu R, Fu X (2000) Pacific-East Asian teleconnection: how does ENSO affect East Asian climate? *J. Clim.* **13**, 1517–1536.
- Wang B, Wu. R, Li T (2003) Atmosphere-warm ocean interaction and its impacts on the Asian-Australian monsoon variation. *J. Clim.* **16**, 1195–1211.
- Wang B, Kang I-S, Li J-Y (2004) Ensemble simulation of Asian-Australian monsoon variability by 11 AGCMs. *J. Clim.* **17**, 803–818.
- Wang B, Ding Q, Fu X, Kang I-K, Jin K, Shukla J, Doblas-Reyes F (2005) Fundamental challenge in simulation and prediction of summer monsoon rainfall. *Geophys. Res. Lett.* **32**, L15711. doi:10.1029/2005GL022734.
- Webster PJ, Magaña VO, Palmer TN, Shukla J, Tomas RA, Yanai M, Yasunari T (1998) Monsoons: processes, predictability, and the prospects for prediction. *J. Geophys. Res.* **103**, 14451–14510.

- Webster PJ, Moor AM, Loschnigg JP, Leben RR (1999) Coupled ocean-atmosphere dynamics in the Indian Ocean during 1997–98. *Nature* 401, 356–360.
- Witternberg AT, Anderson JL (1998) Dynamical implications of prescribing part of a couple system: results from a low-order model. *Nonlin. Proc. Geophys.* **5**, 167–179.
- Wittenberg, A. T., A. Rosati, N.-C. Lau, and J. J. Ploshay, 2006: GFDL’s CM2 global coupled climate models. Part III: Tropical Pacific climate and ENSO. *J. Climate*, **19**, 698–722.
- Wu R, Kirtman BP (2005) Roles of Indian and Pacific Ocean air–sea coupling in tropical atmospheric variability. *Clim. Dyn.* **25**, 155–170.
- Wu R, Kirtman BP, Pegion K (2006) Local air–sea relationship in observations and model simulations. *J. Clim.* **19**, 4914–4932.
- Wu, R., and B. P. Kirtman, 2007: Regimes of local air-sea interactions and implications for performance of forced simulations. *Climate Dynamics*, **29**, 393–410.
- Xie P, Arkin PA (1997) Global precipitation: A 17-year monthly analysis based on gauge observations, satellite estimates, and numerical model outputs. *Bull. Am. Meteor. Soc.* **78**, 2539–2558.
- Xie S-P, Annamalai H, Schott FA, McCreary JP (2002) Structure and mechanisms of South Indian Ocean climate variability. *J. Clim.* **15**, 864–878.
- Xie, S.-P. (2004) Satellite observations of cool ocean–atmosphere interaction. *Bull. Amer. Meteor. Soc.*, **85**, 195–209.
- Yu L, Reinecker MM (1999) Mechanisms for the Indian Ocean warming during the 1997–98 El Nino. *Geophys. Res. Lett.* **26**, 735–738.
- Yu L, Weller RA, Sun B (2004) Improving latent and sensible heat flux estimates for the Atlantic Ocean (1988–1999) by a synthesis approach. *J. Clim.* **17**, 373–393.
- Zhang, R., T. L. Delworth, and I. M. Held, 2007: Can the Atlantic Ocean drive the observed multidecadal variability in Northern Hemisphere mean temperature? *Geophysical Research Letters*, **34**, L02709, doi:10.1029/2006GL028683.
- Zhang Y, Rossow WB, Lacis AA, Oinas V, Mishchenko MI (2004) Calculation of radiative fluxes from the surface to top of atmosphere based on ISCCP and other global data sets: refinement of the radiative transfer model and the input data. *J. Geophys Res.* **109**, D19105. doi:10.1029/2003JD004457.

## *Climate Data Records of Sea-Surface Temperatures*

**Principal Investigator:** P. J. Minnett and E. Williams (UM/RSMAS)

**NOAA Funding Unit:** NOAA-OAR-CPO

**NOAA Technical Contact:** Dr. William L. Murray

### **Research Summary:**

We have continued the collection of ship-based radiometric measurements of the skin SST and deriving the matchups between these and the most recent version of the AVHRR Pathfinder SST retrievals.

### **Research Performance Measure:**

An ISAR has been mounted on the NYK Lines Ship *Andromeda Leader* throughout the performance period, with the second ISAR being installed on the M/V *Horizon Spirit*, in collaboration with colleagues in the DoE ARM program. Both ships provide measurements in the Pacific Ocean: the *Andromeda Leader* between Japan and the USA, and *Horizon Spirit* between Long Beach and Honolulu. The M/V *Horizon Spirit* deployment is particularly important as the measurements from the other instruments from the ARM Mobile Facility will provide an unprecedented determination of the marine atmosphere at the times of the matchups between the satellite radiometers and the ship-board measurements of the ocean skin SST.

Skin SST retrievals from VIIRS on the Suomi-NPP satellite have been included in the matchup-data streams, and the initial comparison with the ISAR measurements is very promising: mean difference (VIIRS – ISAR): 0.029K, st dev = 0.416K, n = 267.

With funding from the International Space Science Institute in Bern, Switzerland, the PI has chaired two international workshops in Bern on the generation of Climate Data Records from satellite radiometers (see <http://www.issibern.ch/teams/satradio/index.html>). A third and final workshop will be held in 2013.

Discussions have begun with National Physical Laboratory (NPL) and the Rutherford Appleton Laboratory both in the UK about holding the next infrared radiometry workshop. The NPL is motivated to host the workshop as they would be able to use their reference radiometer, AMBER, to characterize the ship-board radiometers and laboratory blackbody calibrator, and the RAL is interested in hosting the workshop as they would offer the use of the blackbody target in their thermal-vacuum chamber that has been used for the pre-launch calibration of the AATSR, and will be used for the SLSTR to be launched on the ESA satellite Sentinel-3 in 2014. Either option would provide traceability to National SI Standards as required for the generation of Climate Data Records of SST.

**FORMAT for Annual Progress Report**

**A. Grant Number:** See Table 1.

**B. Amount of Grant:** See Table 1.

**C. Project Title:** Marine and Estuarine Goal Setting for South Florida (MARES)

**D. Grantee:** See Table 1. Note: this report also includes work conducted by NOAA Atlantic Oceanographic and Meteorological Laboratory in support of this project.

Table 1. Year 3 funding by grantee.

A. Grant Number	B. Amount of Grant Year 3 (FY11)	D. Grantee	
NA08OAR4320889	\$109,431	University of Miami	P. Ortner (lead)
NA09NOS4780227	\$17,001	Florida Gulf Coast University	M. Savarese
NA09NOS4780228	\$229,465	Florida International University	J. Boyer
NA09NOS4780226	\$38,945	National Audubon Society, Inc.	J. Lorenz
NA09NOS4780224	\$28,907	Nova Southeastern University	B. Riegl
NA09NOS4780225	\$14,689	University of MA, Amherst	D. Loomis

**E. Award Period:** From: 09/01/2009 To: 08/31/2012

**F. Period Covered by this Report:** From: 06/01/2011 To: 05/31/2012

**G. Summary of Progress and Expenditures to Date:**

- I. Work Accomplishments: (as related to project objectives and schedule for completion)**
  - a. Provide a brief summary of progress, including results obtained to date, and their relationship to the general goals of the grant; and**

The overall goal of MARES (MARine and Estuarine goal Setting) has been “to reach a science-based consensus about the defining characteristics and fundamental regulating processes of a South Florida coastal marine ecosystem that is both sustainable and capable of providing the diverse ecosystem services upon which our society depends.” The hypothesis advanced was that through participation in a systematic inclusive process of reaching consensus, scientists would be able to contribute more directly and effectively to the critical decisions being made by policy makers and by natural resource and environmental management agencies. In a very real sense, MARES has been an ambitious sociological experiment.

South Florida is the site of the world’s largest and most expensive ecosystem restoration effort through the Comprehensive Everglades Restoration Plan (CERP). While a great many natural system scientists have participated in CERP, it is difficult or impossible to determine whether their contributions have made any difference. Human dimension scientists (economists, sociologists, cultural anthropologist etc.) have never been given the opportunity to participate. Moreover, CERP has focused upon the South Florida peninsula

itself, not upon the surrounding coastal marine ecosystem. This is despite significant well documented deleterious environmental changes in the surrounding coastal ecosystem. NOS/CSCOR funded MARES to address these deficiencies and facilitate Ecosystem-Based Management (EBM) of South Florida's coastal marine ecosystem.

The first step in the MARES process was to convene relevant experts (both natural system and human dimensions scientists), stakeholders and agency representatives within each sub region (i.e., Florida Keys/Dry Tortugas, Southeast Florida coast, and the Southwest Florida Shelf) and charge them with developing a visual representation of their shared understanding of the fundamental characteristics and processes regulating and shaping the ecosystem (MARES diagrams). The second step was to build upon these diagrams to develop Conceptual Ecosystem Models (CEMs). This evolved into an effort to apply a model framework (DPSEER- Drivers/Pressures/States/Ecosystem Services/Responses) that explicitly incorporates information about the effects that people have upon and the benefits they gain from the ecosystem. Using this framework we have developed what we call Integrated Conceptual Ecological Models (ICEMs) to organize information about the relationship between people and the environment in a format that will help managers deal with the trade-offs they face by using "Attributes that People Care About" to focus attention upon "Who cares?" and "What do they benefit or lose from changes in their environment?"

MARES ICEMs are intended to serve not only as a basis for synthesizing information but also for identifying indicators (both societal and ecological) and knowledge gaps. The indicators will be combined into a set of less than twenty indices that can be incorporated into coastal ecosystem report cards. Implementing a report card process relying upon such a set of indices would rigorously document trajectories towards (or away) from a sustainable and satisfactory condition. Individual indices (or sets of indices) may be used by agencies to evaluate the consequence of specific management alternatives. Where specific critical indices cannot be calculated due to a lack of data, the information gaps thereby identified can be used by science agencies (like NOAA, NSF or USGS) to prioritize their external and internal allocation of research resources.

In the period covered by this report (06/01/11 through 05/31/12), the project continued the development of the sub-regional ICEMs; continued progress toward more explicit/effective representation of the human dimensions model elements; adopted a systematic approach toward defining a suite of total system indices based on a roll-up of sub- regional indicators themselves based on quantifiable metrics; and began to work with coastal managers and resource agencies in applying project results.

#### *Regional Integrated Conceptual Ecosystem Models (ICEMs)*

An all PIs meeting was held August 25-26, 2011 to review overall progress in the project on developing ICEMs and indicators, establish consensus on key elements of the ICEMs, and identify objectives, tasks and a timeline for year 3 of the project (ca. federal FY2012). Prior to the August 2011 PI meeting, development of ICEMs for each of the three sub-regions had progressed sufficiently that draft reports for all three sub-regions were compiled for review and discussion. Meeting participants reviewed and critiqued key elements of these models, i.e. the drivers, pressures and ecosystem services that are common to all of the models. Work to finalize these lists continued after the meeting and the consensus resulting is documented in a revised Whitepaper 7: Ecosystem Services and Whitepaper 10: Drivers and Pressures. Workshop participants also participated in an exercise to summarize the most important Drivers, Pressures, and Ecosystem Services for each individual ICEM sub-region. Results obtained were captured in concise briefing documents available on line through the MARES website and social media (see below).

### *Increased Representation of Human Dimensions Elements*

During the past 12 months, substantial effort has gone towards improving representation of the human dimensions of the coastal marine ecosystem, which has been facilitated by supplemental funding. Resource economists have largely completed work upon five regional indices that track the monetary value of ecosystem services provided to human society by the coastal marine ecosystem.

As work on the economic-based indicators progressed, it became evident that a complementary set of human dimensions indicators is needed that are not economic in nature. To this end, Susan Lovelace and Maria Dillard, of the National Centers for Coastal Ocean Science's Hollings Marine Lab, were recruited to join the project and work with Loomis and Peterson on this effort. The human dimensions non-economic working group (these four plus Ortner) was formed and met for a workshop in January 24-25, 2012 to explore potential avenues for development of non-economic indicators. This effort is currently working on a manuscript that will investigate human dimensions science within South Florida's coastal marine ecosystem and develop non-economic human dimensions indicators. Preliminary results of their collaborative work were presented at The Coastal Society conference, held in Miami, June 3-6, 2012 during which Loomis, Kelble and Ortner presented at a special session targeting natural resource management practitioners. In addition a manuscript was prepared and submitted for publication by Loomis et al. to a special issue of *Estuaries and Coasts: Human Dimension of our Coasts* entitled: "The Human Dimensions of Coastal Ecosystem Services: Management for Social Values".

A major additional aspect of project evolution over the past year that was stimulated by our human dimensions scientists is to utilize social media. In addition to the MARES website and Data Management System (DMS), MARES staff now also maintains a MARES blog and MARES Facebook page. This foray into social media has markedly increased public access to and awareness of MARES.

### *Indices and Indicators*

A Total System Workshop, held February 29-March 1 2012, reviewed progress on indicators and identified opportunities to interact with managers and stakeholders. With respect to indicators, workshop participants developed and agreed upon a systematic approach to move from the relatively large number of indicators, defined at the sub-region level within the ICEMs, to a smaller number of integrative indices applicable to the overall South Florida coastal marine ecosystem. Metrics, indicators and indices provide information at different levels of detail. Metrics are summaries of raw data; they are system attributes that we can directly measure. Using explicit assumptions, indicators integrate the information provided by metrics to assess the condition of key components of the ecosystem at specific locations within the South Florida coastal region. Within different sub-regions, metrics can be weighted differently in assembling the indicator. Indices (numerical combinations of multiple indicators) are not sub-regionally weighed and are intended to provide a simple overview of conditions in the overall ecosystem. A report card (see below) would therefore be a combination of indices not indicators or metrics and have comparatively few individual components. More information on this iterative integrating process has been made available on the MARES website.

With respect to managers and stakeholders the discussions focused upon how the information synthesized by the ICEM and indicators could be used to inform upcoming South Florida resource management decisions. This included identifying specific management agencies and individuals to be contacted and what types of products MARES could deliver to inform specific management decisions. With respect to products, the managers in the room argued that an overall system report card would not be useful to their own decision-making processes.

### *Targeted Interactions with Agency Stakeholders*

Based on information received at the February workshop, project leaders identified key organizations who have expressed interest in utilizing MARES products and results. At the sub-regional level, project staff and PIs are working with contacts at the Florida Department of Environmental Protection's (DEP) Coral Reef Conservation Program with respect to the Southeast Florida Shelf sub-region, with the Florida Keys National Marine Sanctuary with respect to the Florida Keys/Dry Tortugas sub-region, and with the Sanibel-Captiva Conservation Foundation with respect to the Southwest Florida Shelf sub-region.

Feedback from these organizations is being used to:

- Improve and finalize the MARES sub-regional MARES conceptual diagrams (pictorial representations the most important processes and parameters in the specific subregional environment and their spatial relationships) which these agencies are already employing in their internal processes;
- Refine the ICEMs for each sub-region;
- Assure the inclusion of indicators specific to each sub-region that are most relevant to their issues and concerns; and,
- Develop briefing documents, information materials and processes derived from MARES and its internal product stream that directly addresses agency concerns and issues.

At the level of the overall South Florida coastal marine ecosystem, project staff and the Leaders Group are working with Everglades National Park (ENP) to conduct a regional risk assessment and scenario analysis with respect to a specific management alternative under consideration within ENP jurisdiction in Florida Bay. This exercise will use the ICEMs developed by the MARES project as the basis for the analysis. The results of an exercise to be held in August 2012 will provide the MARES project with explicit feedback on the utility of its ICEMs and indicators. The exercise provides park staff the opportunity to explore what changes might be required to current management practices, if there is a shift to using goal and objectives framed by ecosystem services. It will specifically target management alternatives under consideration such as extending "poll and troll" zonation within ENP marine waters.

MARES has also been working with the ENP-funded "Synthesis of Everglades Research and Ecosystem Services" project (SERES, <http://everglades-seres-org.evergladesfoundation.org>). Early stages of the SERES project benefitted from concepts originating in the MARES project, and SERES and MARES staff and PIs have participated in each other's meetings. Each project is linking the condition (state) of the ecosystem to ecosystem services ("things that people care about"). The links are being made using different quantification tools in each project, and this difference will provide valuable information regarding how to further develop ecosystem assessment tools beyond the products of MARES, that integrate human dimensions and economic information. In future, potential links *between* the two projects may yield a more comprehensive view of the value of South Florida ecosystems that integrates both coastal and freshwater elements.

In addition to ENP, the US Army Corps of Engineers is interested in applying a similar MARES risk assessment to the latest project suite being considered within CERP. This project suite entitled the Central Everglades Planning Project (CEPP) is planning to use ecosystem services valuation to conduct cost-benefit analysis. They will specifically rely upon MARES efforts that have already defined ecosystem services and linked them to ecosystem state for the downstream coastal ecosystems affected by CEPP.

All the NOAA Marine Sanctuaries prepare "Condition Reports". These Condition Reports have relied upon the traditional Pressure-State-Response (PSR) model in which humans only explicit inclusion is that they can exert pressure upon natural resources and the environment. The message being given is negative: that human society and the natural environment are necessarily in conflict. The NMS Office wants to change

that conversation and proposes to do so by incorporating the Driving Forces-Pressures-State-Ecosystem Services-Response (DPSE) Model that we have developed in MARES for the Florida Keys National Marine Sanctuary, which fully incorporates humans into the ecosystem. By showing how humans benefit with improvements in environmental conditions or suffer costs when environmental conditions are degraded, we break the false dichotomy of the economy and the environment. Now the focus of the conversation turns to the trade-offs between drivers of the economy that put pressure on environmental resources and those drivers of the economy that are dependent on the quantity and quality of environmental resources. A mockup of a "Condition Report" for the Florida Keys National Marine Sanctuary is being developed relying upon the MARES model. The hope is this approach will become the model for how Condition Reports are prepared for the entire ONMS System of sites.

The Sanibel-Captiva Conservation Foundation (SCTF) executive board has expressed their interest in using the MARES Southwest Florida Shelf region tools in their discussions with elected officials and managers. They are particularly interested in the oyster, water quality and beaches sub-models and indicators. With respect to beaches they have asked us to develop an explicit comparison with the Southeast regional beach sub-models.

Non-governmental organizations may also use the products of MARES. The National Audubon Society recently completed a strategic planning process that has resulted in their conservation efforts focusing on bird migratory routes known as flyways. A major component of the Eastern Seaboard Flyway is the stopover habitat in South Florida. These habitats provide critical food and water resources as well resting and recuperating places for migrants before and after crossing open water habitats en route to the Antilles or the Yucatan. The waterbird ICEM and scorecard produced by MARES may be used to evaluate Audubon's efforts to conserve critical habitat for these migratory birds.

Last, in addition to working with agency partners within the South Florida region, results from the MARES project are being used in implementing Ecosystem-Based Management at the scale of the entire Gulf of Mexico (GoM) through NOAA's Integrated Ecosystem Assessment (IEA) project. The western part of the MARES domain is of course within the IEA domain and a MARES PI is one of the lead NOAA PI's in the GoM IEA project. The earliest evidence of the role MARES has played in advancing the GoM IEA, is that both the MARES DPSE model and its indices approach to integrating indicator information have been adopted by the GoM IEA. In addition, the GoM IEA funded a postdoc who will be a major contributor to the ENP workshop applying to both the GoM and MARES the same approach (see next section).

**b. Provide a brief summary of work to be performed during the next year of support, if changed from the original proposal; and indication of any current problems or unusual developments that may lead to deviation of research directions or delay of progress toward achieving project objectives.**

There are only two funded months left on the three year award. The project requires more time, thus each NOAA award will be requesting a one-year no-cost extension with the exception of CIMAS. CIMAS is funded under a Shadow Award whose termination date is June 30, 2013 and is not eligible for such an extension. Having said that, CIMAS intends to continue to work on the project along with the rest of the awards until August 31, 2013 when the no-cost extensions expire.

While its rationale and overall goal are unchanged, MARES has greatly evolved over the past three years and has been implemented very differently than described in the original proposal. Major changes already

remarked upon include the DPSER modeling framework, the substitution of ICEMs for CEMs and the increasing emphasis upon, inclusion of and funding for human dimensions science in addition to the biophysical sciences. The use and utility of conceptual diagrams in developing the ICEMs was also not originally envisioned. In addition we have eliminated development of a distinct and separate Total System ICEM which is no longer necessary due to the way we are now integrating sub-regional indicators (which may include weighted metrics) into regional indices that are sufficient to describe the Total System. Our targeted interactions with agency stakeholders was also not originally envisioned. This has become a centerpiece of our efforts to apply MARES to management issues. Last, as discussed at length at the February-March meeting, given the realities of reduced federal (including NOAA) and state agency environmental monitoring and the marked dearth of relevant human dimensions data, the “final” explicitly MARES product will not be report on South Florida ecosystem status but rather an ecosystem “scorecard”: essentially a template consisting of a set of indices that integrating ecological and human dimensions indicators (both economic and non-economic) that themselves may be combinations of metrics. Indices will be unweighted combinations of indicators but the indicators themselves will be weighted appropriately for the different subregions in the MARES domain. This scorecard will not (more accurately cannot) be populated with data at this time. It will be essentially a blank slate (a spreadsheet of quantitative equations and variable definitions), akin to the scorecard an avid fan fills in during a baseball game. Moreover the extent to which specific indices will be fully developed will vary depending upon the degree of present knowledge and data availability. Nonetheless the set will be logically comprehensive and the approach fully explicit (and therefore readily emulated) in a least a few of the indices. The use of such a template is flexible in that all or part of it could be adopted by agencies, regional authorities or natural resource managers as required for their own purposes. This scorecard will be the final MARES “white paper”. Rather than specifically producing a white paper that highlights major information gaps, the degree to which data is available to populate specific indices will serve to identify the most critical information gaps (from the perspective of what information is necessary to truly assess overall ecosystem status and trends).

This scorecard template, the completed set of three ICEMs, the complete set of “white papers” and a few peer reviewed publications (see section below) will constitute the set of MARES specific project products during the final funded months and the no cost extension. Shortly into the no cost extension period we will have no more access to paid MARES staff members, who will have completed their contract. That said, we anticipate no difficulty in completing this set of tasks nor in continuing our efforts to facilitate the decisions of key agency partners who have expressed specific interest in MARES (see above). We also (albeit beyond the no-cost extension period) are considering a MARES special issue journal publication to be submitted to *PLOS One* entitled “MARES: the development of tools to support Ecosystem Based Management in the South Florida coastal ecosystem.” One reason this forum has been selected is that it is entirely published online. The editors tell us that the individual manuscripts can be completed, reviewed and published when each is ready. Then, after all are accepted, the entire set would be made available on line as an integrated special subject volume.

The August workshop held with ENP will undertake a risk assessment modifying the approach of Altman et al. (2011) and conduct a scenario analysis to look at the impact of a potential management action within Florida Bay. This workshop will use the ecosystem services, pressures, and states defined by the MARES ICEMs to quantify the ecosystem services under the greatest risk due to the variety of pressures and the pressures causing the greatest risk in the production of a diversity of ecosystem services. The connections between pressures, states, and ecosystem services will also be defined and the strength of the connection weighted based upon expert opinion. This will turn the DPSER model into a network representation that can be explored in more detail and used to conduct scenario analyses that will be able to at least qualitatively describe how a proposed management action will influence ecosystem services and sustainability. The approach was tested in an earlier GoM IEA workshop, whose conveners included

MARES PIs.

**2. Applications:**

**This section should describe specifically the outputs and management outcomes achieved. Outputs are defined as products (e.g. publications, models) or activities that lead to outcomes (changes in user knowledge or action). In cases where proposed management outcomes are not fully achieved, indicate the progress made during the reporting period. Also, indicate expected outputs and management outcomes for the next year of support.**

**a. Outputs:**

**i. New fundamental or applied knowledge**

None

**ii. Scientific publications**

MARES whitepapers are intended to provide guidance and facilitate discussion within the project. All whitepapers are or will be available at <http://sofla-mares.org>. The list below includes six already as near final drafts and two more to be completed during the remaining funded months or early in the no-cost extension period.

Date	Title
Nov 17, 2009	Including human dimensions science in MARES conceptual ecological model framework
Mar 1, 2011	Developing quantitative ecosystem indicators of environmental State
Mar 1, 2011	Publication style guide for MARES project reports
Apr 12, 2011 (revised Feb 1, 2012)	Ecosystem services defined for the South Florida coastal marine ecosystem
May 1, 2012	Selecting Human Dimensions Economic Indicators for South Florida Coastal Marine Ecosystem
Nov 4, 2011	Drivers and Pressures Identified for the South Florida Coastal Marine Ecosystem
TBD	Selecting Human Dimensions Non-economic Indicators for

	the South Florida Coastal Marine Ecosystem
TBD	Scorecard of South Florida Coastal Marine Ecosystem Status

As earlier noted, one manuscript has already been submitted and is currently in review for a special issue of *Estuaries and Coasts* entitled: Loomis *et al.* “Human Dimension of our Coasts entitled: The Human Dimensions of Coastal Ecosystem Services: Management for Social Values”.

A manuscript on the DPSEER framework is in near final form and will soon be submitted by Kelble *et al.* entitled: The EBM-DPSEER model: Integrating Ecosystem Services into the DPSEER Framework.

A manuscript on the ICEM of the highly diverse habitats of the coastal wetlands along the southwestern coast of Florida is in near final form and will be submitted by Wingard and Lorenz entitled: An integrated conceptual ecological model for the wetland landscape of the southwest Florida coast.

The MARES regional ICEMs (FK/DT, SW Florida Shelf, and SE Florida Coast) are near completion and will become NOAA technical documents, to be released by AOML. At the time of this report, copy editing had begun on the FK/DT ICEM report. The SW Florida Shelf has since been delivered to the copy editor. It is anticipated that the SW Florida Shelf and SE Florida Coast reports will be finalized and submitted early in the no cost extension period.

An MSc thesis was accepted by ETH Zurich (their student worked with a MARES Nova Southeastern University PI who served as his co-advisor). The thesis provided a discrete mathematical formulation of the DPSEER process, thus providing a quantitative extension to the conceptual approach: Elmer F (2012) Identifying reef protection measure for the SE Florida shelf through a DPSEER model. MSc Thesis, ETH (Eidgenoessische Technische Hochschule) Zurich, 1-123.

**iii. Patents** - None are anticipated.

**iv. New methods and technology**

The DPSEER framework is sufficiently distinct from the more familiar DPSEER framework as to constitute a new method or approach. It improves upon the earlier framework in more explicitly capturing and representing human concerns and human resources.

The Risk Assessments being done by MARES (and MARES PIs in other contexts) are modifying the Altman *et al.* (2011) approach to include state variables and more realistically represent the linkage between pressures and ecosystem services.

**v. New or advanced tools (e.g. models, biomarkers)** - None are anticipated.

**vi. Workshops**

<b>Date</b>	<b>Title</b>
Oct 21-22, 2009	All PI Meeting: Rollout Workshop to kick off the project and ensure that everyone is on the same page.
Dec 9-10, 2009	Florida Keys and Dry Tortugas Reef Tract ICEM Technical Workshop at FIU
Mar 22-23, 2010	Florida Keys and Dry Tortugas Reef Tract QEI Workshop (Homestead)
Aug 19-20, 2010	Southwest Florida Shelf ICEM Technical Workshop at FGCU
Mar 29-30, 2011	Southeast Florida Shelf ICEM Technical Workshop at NSU
Aug 25-26, 2011	All PIs Workshop at FIU
Jan 24-25, 2012	Human Dimensions Non-economic Indicators Workshop (Homestead)
Feb 29-Mar 1, 2012	Total System Workshop (Homestead)

In addition, the MARES project was used as demonstration of a successful evaluation planning and management approach in an Integrated Coastal Zone Planning Workshop led by Berhard Reigl and hosted by the V.J. Raman College of Science and Technology in Bhubaneshwar, India, during March 2012. The workshop was attended by 10 coastal zone planners in various Indian government agencies.

#### **vii. Presentations**

<b>MARES Briefings and Conference Presentations</b>		
<b>Date</b>	<b>Description</b>	<b>PI</b>
Oct, 2009	CERP RECOVER Leadership Group	P. Ortner
Oct 20, 2009	Florida Keys National Marine Sanctuary Scientific Advisory Panel	J. Boyer
Nov 2009	South Florida Ecosystem Restoration Task Force Science Coordination Groups	C. Kelble
Nov 12, 2009	Southeast Florida Coral Reef Initiative	J. Boyer
Apr, 2010	NOAA's Gulf of Mexico Integrated Ecosystem Assessment Team*	C. Kelble
Jul, 2010	Greater Everglades Ecosystem Restoration Conference	W. Nuttle
Oct 3, 2010	Gulf of Mexico Fishery Management council	J. Boyer
Oct 19-22, 2010	Florida Keys Science Conference	E. Johns G. Johns C. Kelble W. Nuttle
Oct 20, 2010	Florida Keys National Marine Sanctuary Advisory Council	J. Boyer
Nov 1, 2010	Gulf Fishery Management Council's Scientific & Statistical Committee	J. Boyer
Nov, 2010	American Water Resources Association	P. Ortner
Feb 16, 2011	2011 ASLO Aquatic Sciences Meeting	P. Ortner
May 2011	Science Coordination Group, South Florida Ecosystem Restoration Task Force	C. Kelble
Aug 2011	National Academy Panel: Independent Scientific Review of Everglades Restoration Progress	J. Boyer
Aug 2011	Biscayne Bay Regional Restoration Coordination Team	W. Nuttle
Aug 2011	EMECS 9 (Environmental Management of Enclosed Coastal Seas) Conference	W. Nuttle
Oct 21, 2011	U. S. Coral Reef Task Force	J. Boyer

Nov 6-10, 2011	Coastal and Estuarine Research Federation Conference	J. Boyer G. Johns C. Kelble D. Loomis R. Magnien F. Marshall
May 2012	Technical Advisory Panel, Southeast Florida Coral Reef Initiative (SEFCRI)	J. Boyer
May 9-10, 2012	South Atlantic Fishery Management Council's Coral Advisory Panel	S. Blair
Jun 3-6, 2012	The Coastal Society Conference	C. Kelble D. Loomis G. Johns P. Ortner

**viii. Outreach activities/products (e.g. website, newsletter articles)**

An interactive website was developed for all PIs and public for the dissemination of documents and information, [www.sofla-mares.org](http://www.sofla-mares.org). All reports and brochures are available for downloading and comments can be contributed to this site. What is more significant (and timely) is that our human dimensions scientists indicated that to be effective we needed to make better use of social media.

The project launched a blog site, <http://www.maresblog.org/>, to facilitate dissemination of results from the MARES project and feedback from coastal managers and stakeholders, especially in winding up the project. The intent is to post digests of the technical products on the blog, e.g. the conceptual diagrams and short, easy to read briefings on indicators and elements of the ICEMs. The blog format means that readers can link to and forward links to each item posted. The blog also allows readers to provide suggestions and criticisms back to us via comments.

The project is also maintaining a Facebook page, <http://www.facebook.com/pages/Mares-Project/205172649499385>. The Facebook page serves as a portal for brief communications within the project on topics related to the MARES project, for sharing information with other coastal programs in South Florida, e.g. Seagrant, the FKNMS, etc., and to serve as a convenient and accessible entry point for the public into other online resources maintained by the project, e.g. the website and blog.

As noted earlier, the public and stakeholder response to these new social media approaches has been exceedingly positive. Although project funding will end in a few months and staff will no longer be under contract, the MARES website and blog will continue to be maintained through CIMAS.

**b. Management outcomes- I. Management application or adoption of:**  
**i. New fundamental or applied knowledge**

As noted above the Florida DEP is already relying upon our conceptual diagrams and the CSTF plans to utilize some of the state submodels for their region.

**ii. New or improved skills - None are anticipated.**

**iii. Information from publications, workshops, presentations, outreach products**

See above

**iv. New or improved methods or technology**

As earlier discussed the ONMS is evaluating our MARES DPSEER approach first for their mandated FKNMS Condition Report but thereafter as the model for all subsequent sanctuaries where there is substantial human utilization of the natural resources.

**v. New or advanced tools**

The ICEMs serve as the basis for synthesizing our scientific knowledge and help in identifying Quantitative Ecosystem Indicators (QEI, both societal and ecological). The QEIs are being combined into a parsimonious set of Ecosystem Indices (EI) which are incorporated into a overall system scorecard/template. When populated with data such a scorecard can provide information as to the trajectory of the SFCME towards (or away) from a sustainable and satisfactory condition. Individual EI (or smaller sets of indicators and metrics) may be used by different agencies with specific mandates or responsibilities to make explicit the benefits of (but also the tradeoffs between) alternative management options. Equally important, to the degree that such templates are agreed upon as necessary and sufficient to describe system trajectory, the lack of the data required to populate the template highlights information gaps.

**c. Management outcomes - II. Societal condition improved due to management action resulting from output; examples:**

None to date. The measure of ultimate benefit with respect to South Florida, however, will be if and when specific natural management decisions reflect the consensus reached by the MARES participants, when the participation of scientists and mid-level managers and administrators in MARES, is expressed in decisions made by those to whom they report. In other words, when decisions are truly being made by using adaptive management guided by the best-available-science.

**d. Partnerships established with other federal, state, or local agencies, or other research institutions (other than those already described in the original proposal).**

By including agency representatives within the MARES process (see Table 2 below), the task of delivering the most appropriate (and therefore effective) MARES products to individual management agencies has become a highly distributed activity, specific to each agency and its own management structure, mandate and requirements, and relying upon agency rather than MARES resources. Successful examples include the fact that Florida DEP is already using MARES infographics and the ICEM derived from it models to guide their implementation strategy for southeast coast marine protected areas, the FKNMS has decided to adopt the relevant ecosystem services analysis done by MARES human dimensions scientists in lieu of developing their own during their required development of a new management plan and the ENP workshop discussed just above.

<b>Participating Agency</b>	<b>Agency Employees/Representatives</b>
NOAA/NOS/Florida Keys National Marine Sanctuary (FKNMS)	Billy Causey
NOAA/National Marine Fisheries Service (NMFS)	Jim Bohnsack, Joan Browder, John Lamkin, Joe Serafy
NOAA/NOS/Coral Reef Conservation Prog.	Dana Wusinich-Menendez
NOAA/OAR/ AOML	Chris Kelble, Tom Carsey, Jack Stamates
U. S. Department of the Interior (DOI)/National Park Service (NPS)	Carol Mitchell (Leaders Group), Tylan Dean, David Rudnick, Bob Johnson, William Perry,
U. S. DOI/Fish & Wildlife Service (FWS)	Patrick Pitts, Todd Hopkins
U. S. Environmental Protection Agency	Pat Bradley
U.S. Army Corps of Engineers (Jacksonville District)	David Tipple, RECOVER Co-Chair
US Geological Service	Lynn Wingard
South Florida Water Management District (SFWMD)	Peter Doering, Patty Sime,
Florida Fish and Wildlife Conservation Commission (FWC)	John Hunt (Leaders Group), Gil McRae
Florida Department of Environmental Protection (FDEP)	Chantal Collier, Joanna Waldzak, Katherine Tzadik, Kent Edwards, Jamie Monty
Broward County	Ken Banks
Miami-Dade Department of Environmental Regulation and Management	Steve Blair, Susan Markley

**3. Expenditures:**

**a. Describe expenditures scheduled for this period.**

**b. Describe actual expenditures this period.**

<b>University of Miami</b>		
<b>Cost Category</b>	<b>Planned</b>	<b>Actual</b>
Personnel	\$61,785	\$100,117
Fringe Benefits	\$15,565	\$22,511
Supplies	\$815	\$0
Indirect	\$31,266	\$48,995
<b>Total</b>	<b>\$109,431</b>	<b>\$171,623</b>

**c. Explain special problems that led to differences between scheduled and actual expenditures, etc.**

Additional funds expended were carryover funding from Year 2 award.

<b>Florida Gulf Coast University</b>		
<b>Cost Category</b>	<b>Planned</b>	<b>Actual</b>
Personnel	\$8,726.12	\$6,254

Fringe Benefits	\$2,313.49	\$1,463
Indirects	\$5,961.39	\$3,842
<b>Total</b>	<b>\$17,001.00</b>	<b>\$11,559</b>

**c. Explain special problems that led to differences between scheduled and actual expenditures, etc.**

Delays in workshop and reporting responsibilities are currently being addressed.

<b>Florida International University</b>		
<b>Cost Category</b>	<b>Planned</b>	<b>Actual</b>
Personnel	\$32,169.62	\$24,009.78
Fringe Benefits	\$9560.81	\$7,677.73
Travel	\$1,000.00	\$3,198.77
Contractual	\$167,506	\$151,140.80
Indirects	\$19,228.70	\$15,245.22
<b>Total</b>	<b>\$229,465.13</b>	<b>\$200,264.30</b>

**c. Explain special problems that led to differences between scheduled and actual expenditures, etc.**

None

<b>National Audubon Society, Inc.</b>		
<b>Cost Category</b>	<b>Planned</b>	<b>Actual</b>
Personnel	\$17,651.44	\$17,651.44
Fringe Benefits	\$6,001.66	\$6,001.66
Contractual	\$15,291.90	\$15,291.90
<b>Total</b>	<b>\$38,945.00</b>	<b>\$38,945.00</b>

**c. Explain special problems that led to differences between scheduled and actual expenditures, etc.**

None.

<b>Nova Southeastern University</b>		
<b>Cost Category</b>	<b>Planned</b>	<b>Actual</b>
Personnel	\$14,424.00	\$20,525.42
Fringe Benefits	\$3,376.00	\$5,439.27
Indirects	\$11,107.00	\$15,804.50
<b>Total</b>	<b>\$28,907.00</b>	<b>\$41,769.19</b>

**c. Explain special problems that led to differences between scheduled and actual expenditures, etc.**

Additional funds expended were carryover funding from Year 2 award.

<b>University of Massachusetts, Amherst / East Carolina University</b>		
<b>Cost Category</b>	<b>Planned</b>	<b>Actual</b>
Personnel	\$8037.85	\$8037.85
Fringe Benefits	\$1318.20	\$1318.20
Indirects	\$5,332.95	\$5332.95
<b>Total</b>	<b>\$14,689.00</b>	<b>\$14,689.00</b>

**c. Explain special problems that led to differences between scheduled and actual expenditures, etc.**

None.

<b>AOML</b>		
<b>Cost Category</b>	<b>Planned</b>	<b>Actual</b>
Personnel	\$14,322	\$14,322
Fringe Benefits	\$4,583	\$4,583
Travel	\$42,966	\$42,966
Other	\$15,118	\$15,118
Indirects	\$4,915	\$4,915
<b>Total</b>	<b>\$81,904</b>	<b>\$81,904</b>

**c. Explain special problems that led to differences between scheduled and actual expenditures, etc.**

None.

Prepared By:



Signature of Principal Investigator

Date 06/30/2012

**NOAA COP Annual Progress Report Form**

**7/16/2007**